pmd*CRC

# F6 Project Final Report 2008

## Validation of spectral remote sensing data for geological mapping and detection of hydrothermal footprints in the Mount Isa Inlier

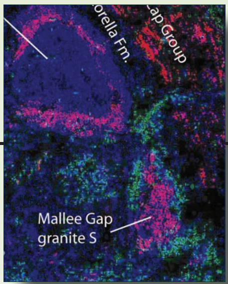


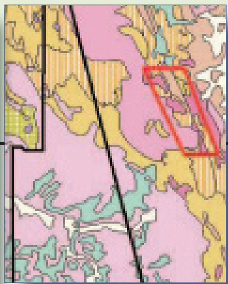

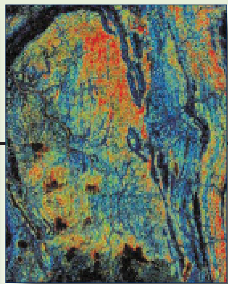

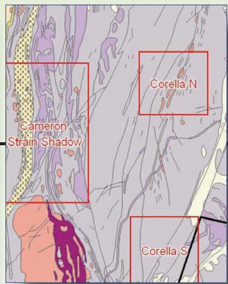


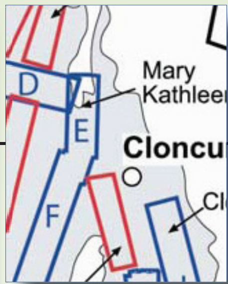


Compiled by C. Laukamp

pmd*CRC

# *Validation of spectral remote sensing data for geological mapping and detection of hydrothermal footprints in the Mount Isa Inlier (final report and database)*

C. Laukamp, J. Cleverley, T. Cudahy, R. Hewson, M. Jones, N. Oliver, M. Thomas

## *1. Introduction*

This report represents the database of former reports delivered in the F6 and I7 projects of the pmd*CRC (Laukamp, 2007a; Laukamp et al., 2008a; Laukamp, 2008; Thomas, 2008), partly published (Laukamp, 2007b) and presented at conferences (Laukamp et al., 2008b, Thomas et al., 2008). The aim of the overall project was the validation of spectral remote sensing data for the mapping of regional and small-scale hydrothermal alteration patterns in the Mount Isa Inlier, focussing on the Eastern Fold Belt (Cloncurry District, Selwyn Range) and the Mary Kathleen Fold Belt. Processed hyperspectral and ASTER images (geoscience products) were released by the collaborative Queensland NGMM project between GSQ and CSIRO (Fig. 1).
The presented paper gives an overview about the sampled areas and provides some interpretation of selected hyperspectral mineral maps. Further applications of the hyper- and multispectral data can be found in chapters 4 to 5, which include a hands on for the mapping of rock units occurring in the Eastern Fold Belt and a list of recommended HyMap and ASTER products for the exploration after selected deposit types occurring in the Mount Isa Inlier. For more detailed description of the mapping of hydrothermal alterations patterns in the Mount Isa Inlier the reader is referred to Laukamp et al. (2008). Similar studies were undertaken in the Yilgarn using the geoscience products for geological, alteration and regolith mapping based on a mineral systems approach (Cudahy et al., 2005).

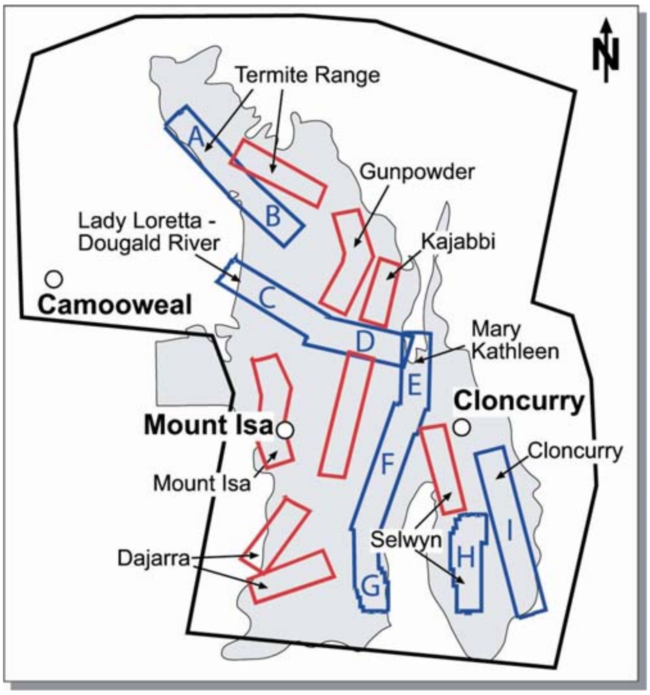


**Fig. 1. Coverage of ASTER and HyMap imagery in the Mount Isa Inlier (black frame: Satellite multispectral coverage (ASTER), blue & red frames: HyMap swaths, in grey: approximate outcropping areas of the Mount Isa Inlier).**

The key areas are shown on Fig. 2 and Fig. 3. Three of the key areas from Block H (N Kuridala, Young Australia, N Mount Elliott) are not discussed in this report, but sample data are provided in the Appendix.

### *1.1 Regional Geology*

The Eastern Fold Belt of the Mount Isa Inlier is well known for the occurrence of major IOCG-deposits. A combination of specific mineral maps, derived from hyperspectral imaging in the VNIR to SWIR-range was used to detect variations in mineral chemistry of Paleoproterozoic lithologies in the Cloncurry District (Block H, I; Fig. 1) and central to northern Mary Kathleen Foldbelt (Block E, F; Fig. 1) and mineralisation related alteration patterns.

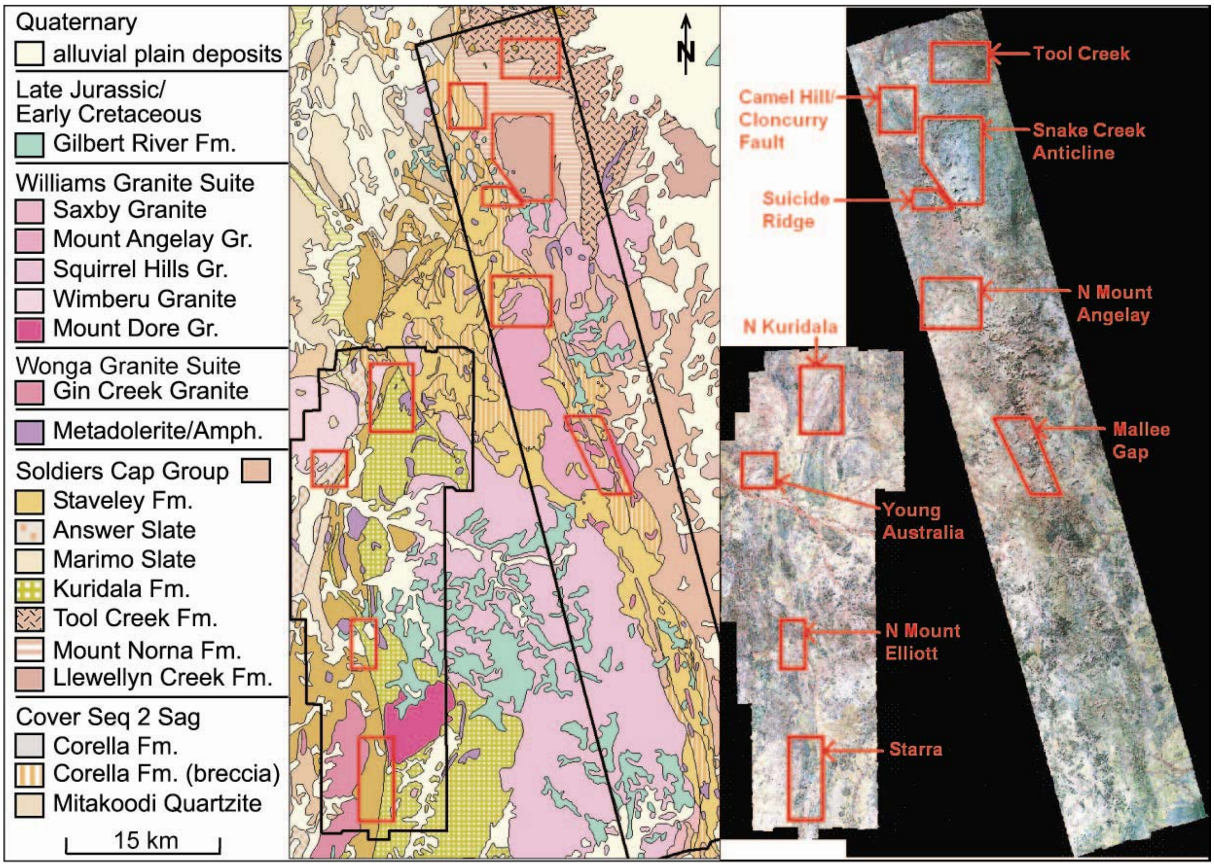


**Fig. 2. Geological map and false colour image of the Selwyn and Cloncurry District. HyMap swath as black frames with block H (Selwyn) on the left and block I (Cloncurry) on the right. Field areas of the 2007 and 2008 field campaigns in red.**

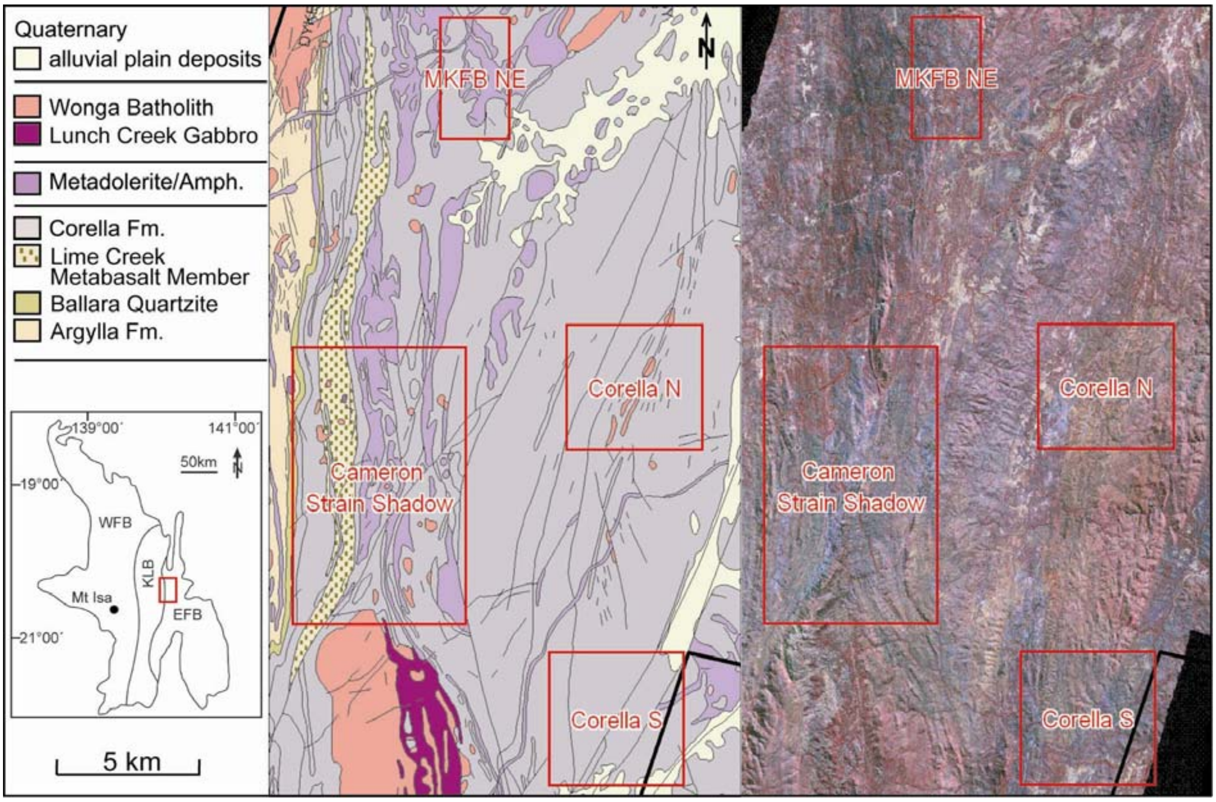


**Fig. 3. Geological map and false colour images of the central Mary Kathleen Fold Belt. Black lines indicate boundary of HyMap swaths E and F. Field areas of the 2008 field campaign in red.**

## *2. Methods*

### *2.1 Spectral images provided by CSIRO/NGMM*

F6 spectral techniques report: "The Advanced Spaceborne Thermal Emission and Reflectance Radiometer (ASTER) is an imaging instrument on board of Terra, the Earth Observing System (EOS) satellite. ASTER is a high resolution multispectral imaging device that records data in 14 spectral bands: 3 bands in VNIR with 15 meter spatial resolution, 6 bands in SWIR with 30 meter spatial resolution and 5 bands in TIR with 90 meter spatial resolution. Calibration of ASTER data using the new high resolution HyMap data and reprocessing improved the accuracy and usability of the data (Thomas, 2008). The new ASTER geoscience products were used to find mineral dispersion pathways in the regolith and to identify windows of basement geology in areas of extensive cover.

The HyMap® system was flown by HyVista Corporation Pty. Ltd. on a fixed wing aircraft typically at an altitude of about 2.5 km. The sensor collects reflected solar radiation in 128 bands covering the 0.440- to 2.500-µm wavelength range, including the VNIR and SWIR regions of the electromagnetic spectrum.

The theory of remote sensing spectral analysis is described in Laukamp (2008) and in more detailed in published literature (King et al., 2004). Additional to the processed HyMap and ASTER images provided by the collaborative Queensland NGMM project between GSQ and CSIRO, product descriptions of the respective images are available as download from www.em.csiro.au/NGMM. These product descriptions contain important details of the type of processing of the respective geoscience products, such as applied base algorithms, filters, stretching modes as well as an assessment of their accuracy (Appendix 8.1).

### *2.2 Ground-validation, lab work and database*

For the purpose of ground-truthing the accuracy of the HyMap and ASTER products four field campaigns in 2007/2008 were undertaken. About 335 samples were taken from the Blocks E, F, H and I and are listed in Appendix 8.2. A comprehensive collection of pictures from the field campaigns in 2007 and 2008 helped with the interpretation of the hyperspectral images (Appendix 8.3.1). Further 10 samples were provided for PIMA measurements by M. Rubenach and T. Blenkinsop. About 47 thin sections have been investigated for their mineral assemblages and alteration signatures. The thin sections are listed in Appendix 8.6.

*PIMA*

The portable infrared mineral analyser (PIMA) was used for ground validation of HyMap and ASTER data. PIMA can be used to analyse small sample areas of ca. 15 mm in diameter. The PIMA measures reflected radiation in the SWIR-range (1.3 -2.5µm) and can detect a limited range of minerals such as chlorite, mica, sulphates and carbonate. A single PIMA analysis took about 30 seconds when using a PIMA integration of 1. PIMA analyses were partly backed up with XRD/XRF analyses at the Advanced Analytical Centre of the James Cook University in Townsville and thin sections.

Results of about 950 PIMA analyses are partly shown in the results chapter, where the selected reflectance spectra are followed by tables with a description of the analysed surfaces (sample number, rock type, surface, cut) and interpretation of the absorption features either by using the auxmatch function of TSG Core or own interpretation (in italic). For the automated determination of the two major phases a suite of minerals, which are possibly contained in the respective rock types, was selected with the TSG Core software. These .tsg-files are enclosed in Appendix 8.4 and are viewable with the Spectral Geologist Software TSG Pro or TSG Core. The complete set of PIMA analyses (.fos-files) is listed in the sample list (Appendix 8.2) and can be uploaded into TSG Core or TSG Pro. Pictures from all PIMA samples are collected in Appendix 8.3.2.

*XRD/XRF*

A Siemens D5000 X-Ray Diffractometer (XRD) using a theta-2 theta goniometer and a copper anode x-ray tube, fixed slits, monochromator and a forty position sample changer was used to determine crystalline phases in the samples. Qualitative interpretation of the XRD analyses was done by Carsten Laukamp and/or people subcontracted to the AAC. Mineral assemblages derived from qualitative interpretation are shown in Tab. 2, Tab. 5, Tab. 8, Tab. 11, Tab. 14 and Tab. 17 and the original data files are attached to this report (Appendix 8.5.1).

A Bruker-AXS S4 Pioneer X-ray Fluorescence Spectrometer (XRF) was used for semi-quantitative elemental analysis of the samples. Semi-quantitative results are shown in Tab. 1, Tab. 4, Tab. 7, Tab. 10, Tab. 13 and Tab. 16 and in the original data files from the AAC (Appendix 8.5.2).

## *3. Results of geochemical analyses and interpretation of hyperspectral images*

This chapter includes a brief description of the studied and sampled areas and results of geochemical analyses (XRD/XRF) and selected reflectance spectra of the PIMA analyses. Furthermore selected hyperspectral images of the study areas are discussed. The full list of samples, XRD/XRF results, PIMA analyses and the MapInfo database can be found in the Appendix.

### *3.1 Snake Creek Anticline area*

The Snake Creek Anticline is located circa 25km SSE of Cloncurry, to the East of the Cloncurry Fault (Fig. 2). The main lithologies comprise the Llewellyn Creek Formation (Pol: Pelitic schist with garnet, staurolite and andalusite; phyllite, metagreywacke, quartzite and amphibolite) and interlayered amphibolites, metabasalts and metadolerites (Pol_d) (Fig. 4).

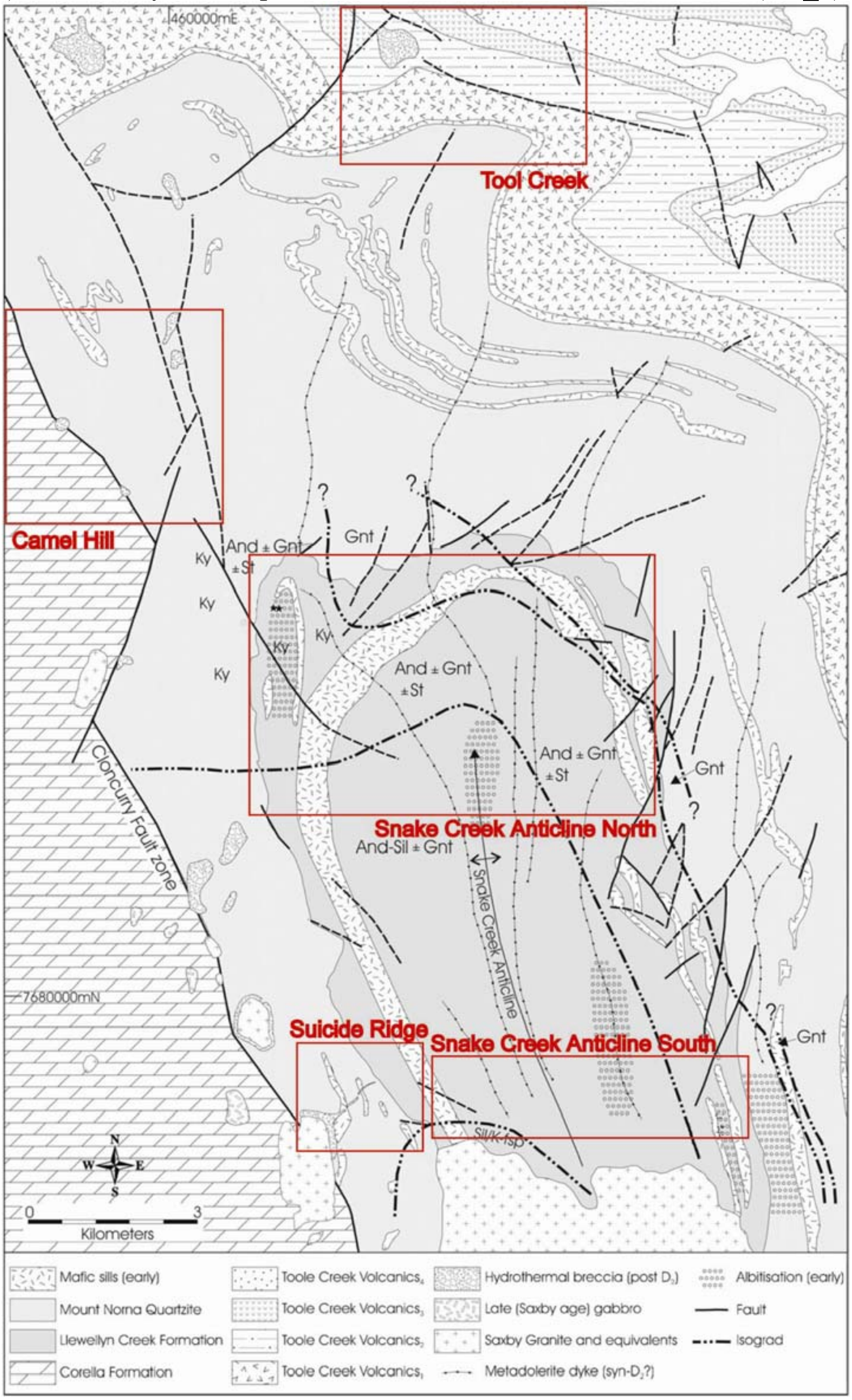


**Fig. 4. Geological Map of the Snake Creek Anticline, showing distribution of late, Saxby Granite related gabbros and index minerals related to the changes of metamorphic facies of the country rocks (Rubenach et al., 2008). In red are the key areas of the northern Cloncurry District, discussed in this report. For sample points see Appendix 8.1.3 (MapInfo workspace) and 8.2 (sample list and GPS-points).**

### *3.1.1 Geochemistry*

Results of the geochemical analyses with XRF/XRD are given in Tab. 1 and Tab. 2.

| rock type | and-schist | and-schist | and-schist | and-schist | meta-quarzite | albitite | andalusite-crystals | psammite | bt-fsp-rock | rock + bt-veins | and-schist | meta-psammite | and-schist | and-schist | dolerite-dyke | meta-quarzite | meta-quarzite | mica-schist | mica-schist |
|---|---|---|---|---|---|---|---|---|---|---|---|---|---|---|---|---|---|---|---|
| sample | 150S1 | 150S2 | 150S3 | 150S4 | 150S5 | 150S6 | 150S7 | 151S1 | 152S1 | 152S2 | 155S1 | 157S1 | 162S1a | 162S1c | 163S1 | 164S1a | 164S1b | 164S2 | 164S3 |
| **O** | 61,035 | 60,289 | 59,198 | 63,447 | 63,810 | 61,523 | 59,253 | 61,381 | 62,582 | 61,633 | 60,133 | 63,387 | 61,288 | 62,912 | 55,189 | 61,091 | 63,169 | 58,926 | 58,638 |
| **Na** | 1,044 | 0,600 | 0,589 | 1,898 | 1,594 | 6,984 | 1,025 | 4,048 | 2,366 | 4,710 | 1,048 | 1,311 | 0,561 | 0,603 | 2,003 | 2,242 | 3,682 | 0,509 | 0,350 |
| **Mg** | 0,967 | 0,926 | 1,750 | 2,069 | 0,563 | 0,038 | 1,638 | 1,463 | 0,831 | 0,404 | 0,938 | 0,822 | 0,366 | 0,584 | 2,158 | 1,243 | 0,297 | 0,923 | 0,824 |
| **Al** | 9,596 | 9,761 | 11,026 | 6,511 | 5,898 | 7,994 | 10,405 | 7,129 | 6,510 | 6,607 | 10,977 | 7,498 | 6,908 | 6,154 | 5,963 | 8,108 | 5,529 | 11,069 | 12,104 |
| **Si** | 19,421 | 19,627 | 17,418 | 17,790 | 24,083 | 22,306 | 17,279 | 21,399 | 22,678 | 24,699 | 19,101 | 21,225 | 24,273 | 24,851 | 18,278 | 20,500 | 24,958 | 19,396 | 17,752 |
| **P** | 0,069 | 0,092 | 0,052 | 0,058 | 0,096 | 0,118 | 0,080 | 0,089 | 0,059 | 0,052 | 0,063 | 0,056 | 0,092 | 0,085 | 0,094 | 0,262 | 0,178 | 0,106 | 0,053 |
| **S** | 0,013 | 0,005 | 0,006 | 0,005 | 0,028 | 0,003 | 0,007 | 0,017 | bd | bd | 0,005 | 0,004 | 0,005 | 0,005 | 0,024 | 0,008 | 0,008 | 0,005 | bd |
| **Cl** | 0,174 | 0,241 | 0,367 | 0,276 | 0,088 | 0,008 | 0,109 | 0,058 | 0,107 | 0,028 | 0,178 | 0,125 | 0,026 | 0,055 | 0,303 | 0,095 | 0,021 | 0,113 | 0,192 |
| **K** | 3,674 | 3,909 | 4,073 | 2,830 | 1,585 | 0,271 | 1,676 | 1,577 | 1,659 | 0,609 | 3,700 | 2,357 | 2,298 | 2,453 | 1,463 | 2,717 | 0,800 | 4,926 | 5,505 |
| **Ca** | 0,314 | 0,264 | 0,258 | 0,636 | 0,719 | 0,392 | 2,661 | 0,364 | 1,312 | 0,231 | 0,168 | 0,594 | 0,151 | 0,178 | 4,542 | 0,248 | 0,293 | 0,209 | 0,018 |
| **Ti** | 0,351 | 0,356 | 0,453 | 0,366 | 0,154 | 0,211 | 0,405 | 0,293 | 0,234 | 0,178 | 0,313 | 0,228 | 0,174 | 0,162 | 0,803 | 0,282 | 0,135 | 0,384 | 0,348 |
| **V** | 0,007 | 0,009 | 0,011 | 0,009 | bd | bd | 0,015 | 0,007 | bd | bd | 0,008 | bd | bd | bd | 0,038 | 0,009 | bd | 0,008 | 0,010 |
| **Cr** | 0,004 | 0,002 | 0,004 | 0,002 | 0,002 | 0,001 | 0,007 | 0,003 | 0,001 | bd | 0,001 | 0,001 | 0,002 | 0,001 | bd | 0,002 | | 0,003 | 0,001 |
| **Mn** | 0,011 | 0,024 | 0,020 | 0,020 | 0,008 | | 0,116 | 0,002 | 0,003 | 0,017 | 0,005 | 0,009 | 0,207 | 0,008 | 0,127 | 0,011 | 0,003 | 0,017 | 0,008 |
| **Fe** | 3,241 | 3,814 | 4,693 | 4,027 | 1,319 | 0,131 | 5,285 | 2,102 | 1,590 | 0,798 | 3,291 | 2,324 | 3,597 | 1,906 | 8,988 | 3,143 | 0,883 | 3,315 | 4,100 |
| **Ni** | 0,001 | bd | 0,001 | 0,001 | bd | bd | bd | bd | bd | bd | bd | bd | bd | bd | bd | bd | bd | bd | bd |
| **Ga** | bd | 0,002 | bd | bd | bd | bd | 0,002 | bd | bd | 0,001 | 0,002 | bd | bd | bd | bd | bd | bd | bd | bd |
| **Rb** | 0,014 | 0,016 | 0,020 | 0,016 | 0,005 | bd | 0,008 | 0,006 | 0,007 | 0,002 | 0,012 | 0,009 | 0,005 | 0,007 | 0,010 | 0,013 | 0,003 | 0,017 | 0,020 |
| **Sr** | 0,005 | 0,004 | 0,003 | 0,010 | 0,008 | 0,004 | 0,011 | 0,009 | 0,010 | 0,002 | 0,003 | 0,010 | bd | bd | 0,010 | 0,005 | 0,007 | 0,004 | 0,003 |
| **Zr** | 0,011 | 0,014 | 0,016 | 0,013 | 0,014 | 0,029 | 0,008 | 0,011 | 0,016 | 0,015 | 0,011 | 0,015 | 0,012 | 0,013 | 0,008 | 0,022 | 0,011 | 0,013 | 0,010 |
| **Ba** | 0,048 | 0,046 | 0,029 | 0,017 | 0,026 | bd | 0,030 | 0,030 | 0,026 | bd | 0,051 | 0,030 | 0,027 | 0,029 | bd | bd | bd | 0,060 | 0,082 |
| **W** | 0,015 | 0,012 | 0,015 | bd | 0,021 | 0,015 | bd | 0,013 | 0,022 | 0,039 | 0,012 | 0,014 | 0,027 | 0,019 | 0,016 | 0,015 | 0,031 | bd | bd |
| **Total** | 100,000 | 100,000 | 100,000 | 100,000 | 100,000 | 100,000 | 100,000 | 100,000 | 100,000 | 100,000 | 100,000 | 100,000 | 100,000 | 100,000 | 100,000 | 100,000 | 100,000 | 100,000 | 100,000 |

**Tab. 1. Semi-quantitative XRF analyses of samples from the Snake Creek Anticline area. All values in weight %. bd - below detection limit.**

| Snake Creek Anticline | | | | feldspars | | | micas | | | | | | chlorites | | septo-chlorites | | clay minerals | | amphiboles | | $Al_2SiO_5$-polymorphs | | | | | opaques | | |
|---|---|---|---|---|---|---|---|---|---|---|---|---|---|---|---|---|---|---|---|---|---|---|---|---|---|---|---|---|
| | | | quartz | K-feldspar | albite | calcian albite | *muscovite* | *sodic muscovite* | *Fe-mica (phengitic)* | phlogopite | biotite | *clinochlore* | *Mg-chlorite* | *cronstedtite (Fe-septochlori* | *serpentine mineral* | *kaolin-type phase* | *kaolinite* | *actinolite* | *sodic clinoamphibole* | sillimanite | andalusite | kyanite | *dolomite* | alunite | pyrope, ferrian | pyrite | magnetite |
| sample | rock type | unit | | | | | | | | | | | | | | | | | | | | | | | | | |
| 150S1 | and-schist | Pol | x | | | x | ~x | | | | | | | | | | | | | | x | | | | | | |
| 150S2 | and-schist | Pol | x | | x | | | | x | x | | | | | | x | x | | | | | | | | | | |
| 150S3 | and-schist | Pol | x | | | x | | | | x | | | | | | | x | | | | x | | | | | | |
| 150S4 | and-schist | Pol | x | | | x | | | | ~x | | | | | | | | | | | | | | | | | |
| 150S5 | metaquarzite | Pol | x | | ~x | | ~x | | | | | | | | | | | | | | | | | | | | |
| 150S6 | albitite | Pol | x | | x | | | | | | | | | | | | | | | | | | | | | | |
| 150S7 | andalusite-crystals | Pol | | | | | x | | | | x | | | | | | | x | | | xx | x | | | | | |
| 151S1 | metapsammite | Pol | x | | ~x | | | | | x | x | | | | | | | | | x | | | | | | | |
| 152S1 | bt-fsp-rock | Pol | x | (x) | ~x | | | | | x | | | | | | | | | | | | | | | | | |
| 152S2 | kfsp dom. rock + bt-ve | Pol | x | | x | | x | | | | | | | | | | | | | | | | | | | | |
| 155S1 | and-schist | Pol | x | | | x | ~x | | | | | | | | | | | | | | x | | | | | | |
| 157S1 | metapsammite | Pol | x | | ~x | | ~x | | | | | | x | | | | | | | | | | | x | | | |
| 162S1a | grt-schist, and-schist | Pol | x | | | | | | ~x | | | | | x | x | | | | | | | | x | | x | | |
| 162S1c | grt-schist, and-schist | Pol | x | | | | ~x | | | x | | x | | | | | | | | | | | | | | | |
| 163S1 | dolerite-dyke | Pol_d | x | x | x | | | | x | | | | | | | x | | | x | | | | | | | | x |
| 164S1a | metaquarzite | Pol | x | | ~x | | | x | | | | | | | | | | | | | | | | | | | |
| 164S1b | metaquarzite | Pol | x | | ~x | | | x | | | | | | | | | | | | | | | | | | x | |
| 164S2 | micaschist | Pol | x | | (x) | | ~x | | | | | | | | | | | | | | | x | | | | | |
| 164S3 | micaschist | Pol | x | | | | | | x | | | | | | | | | | | | | | | | | | |

**Tab. 2. Qualitative XRD results of samples from the Snake Creek Anticline area. Minerals in italic are critical in the interpretation of the HyMap data. Rock units: Pol - Llewellyn Creek Formation, Pol_d - Amphibolite, metabasalt, metadolerite. Mineral occurrences: xx - percentage ≥ 80%, x - major component, (x) - minor component.**

### *3.1.2 PIMA analyses*

Reflectance spectra of PIMA analyses of selected samples are shown in Fig. 5 and Fig. 6.

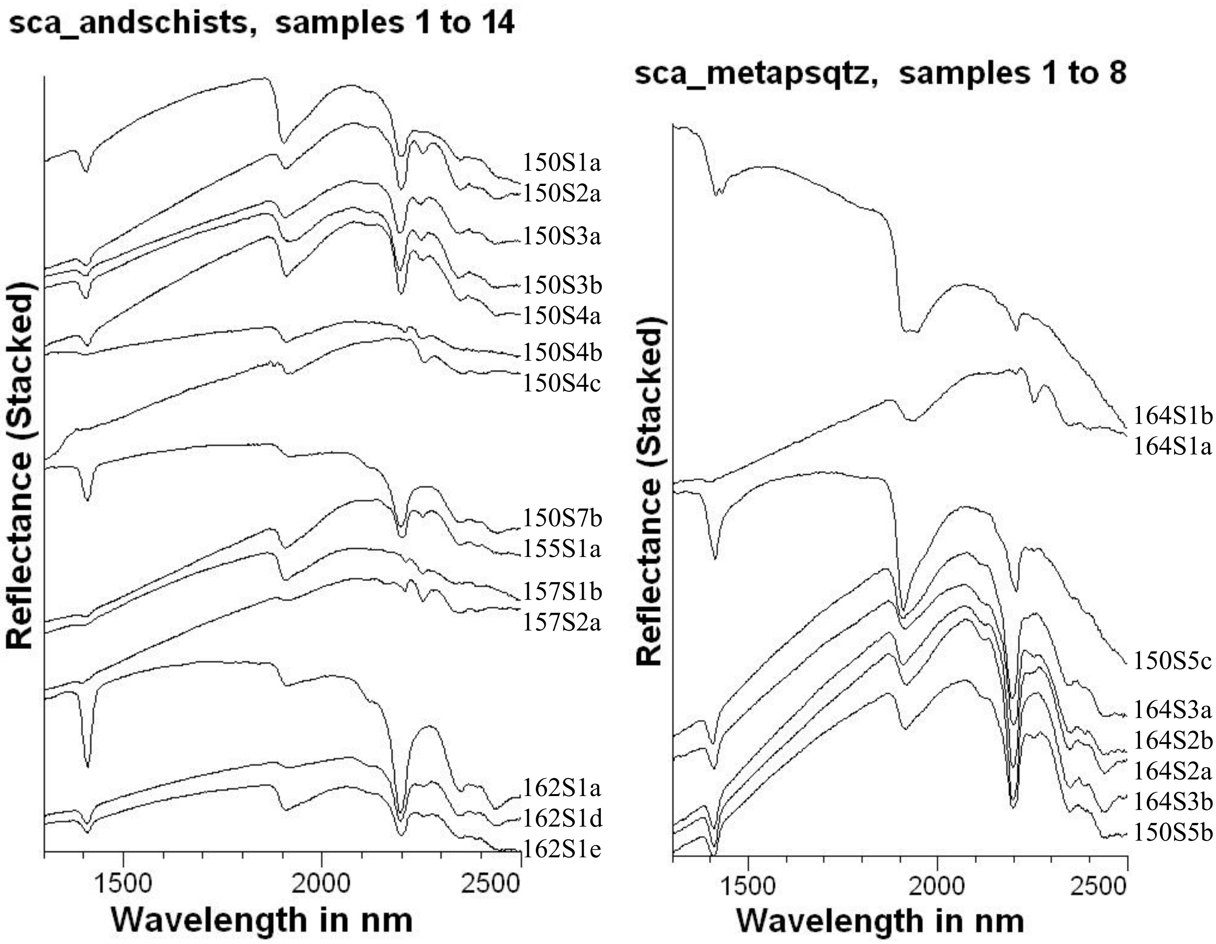


**Fig. 5. PIMA spectra of samples from the Snake Creek Anticline. Respective SSQ and interpretative results from XRD shown in Tab. 2 and Tab. 1. Left: Andalusite-bearing schists. Right: Micaschists and metaquartzites.**

| sample | rock type | surface | cut | spectra dominating minerals (acc. to TSG auxmatch or *own int.*) |
|---|---|---|---|---|
| 150S1a | metapsammite | weathered | parallel S1 | Ill, Mg-clays |
| 150S2a | metapsammite | weathered | parallel S1 | Bt, Ill |
| 150S3a | metapsammite | weathered | parallel S1 | Ill, Phl |
| 150S3b | metapsammite | fresh | parallel S1 | Ill, Bt |
| 150S4a | Andalusite | weathered | parallel S1 | Ill, Bt |
| 150S4b | Andalusite | fresh | perpendicular S1 | Bt, Hal |
| 150S4c | Andalusite | fresh | perpendicular S1 | *Bt* |
| 150S5b | metaquarzite | weathered | parallel S1 | Ill, Alu |
| 150S5c | metaquarzite | fresh | parallel S1 | Mnt, Hal |
| 150S6c | albitite | fresh | parallel S1 | Mnt, *Chl* |
| 150S6d | albitite | weathered | parallel S1 | Mnt, Hal |
| 150S7b | Andalusite | altered | parallel c | Ill |
| 151S1a | metapsammite | weathered | perpendicular S1 | Ill, Ep |
| 151S1b | metapsammite | fresh | perpendicular S1 | Ill, Bt |
| 152S1a | metapsammite | weathered, joint | perpendicular S1 | Ill, Mg-Chl |
| 152S1b | metapsammite | fresh | parallel S1 | Ill, Phl |
| 152S1c | metapsammite | fresh | perpendicular S1 | Int Chl, Mnt |

| | | | | |
|---|---|---|---|---|
| 152S2a | metapsammite | weathered | perpendicular S1 | Mnt, Ms |
| 152S2b | metapsammite | fresh | perpendicular S1 | Mnt, Ms |
| 152S2c | metapsammite | fresh | parallel S1 | Ms, Mg-Chl |
| 152S2d | metapsammite | weathered | parallel S1 | Ms, Mg-Chl |
| 155S1a | metapsammite | weathered | parallel S1 | Bt, Ill |
| 157S1b | metapsammite | weathered | | Bt, Mg-clays |
| 157S2a | Andalusite | weathered | | Bt, Kln |
| 162S1a | metapsammite | weathered | parallel S1 | Ill |
| 162S1d | metapsammite | fresh | perpendicular S1 | Ill, Bt |
| 162S1e | metapsammite | weathered | perpendicular S1 | Ill, Ep |
| 163S1a | dolerite | weathered | parallel S1 | Ill, Act |
| 164S1a | metaquarzite | weathered | perpendicular S1 | Bt, Alu |
| 164S1b | metaquarzite | weathered | parallel vein | Mnt, Alu |
| 164S2a | micaschist | weathered | parallel S1 | Ill, Phl |
| 164S2b | micaschist | weathered | parallel S1 | Ill, Phl |
| 164S3a | phyllonite | weathered | parallel S2 | Ill |
| 164S3b | phyllonite | weathered | perpendicular S1 | Ill |

**Tab. 3. Description of samples shown in Fig. 5 and Fig. 6. PIMA integration: 1. Mineral abbreviations after Kretz (1983). Other minerals: Alu - alunite, Hal - halloysite.**

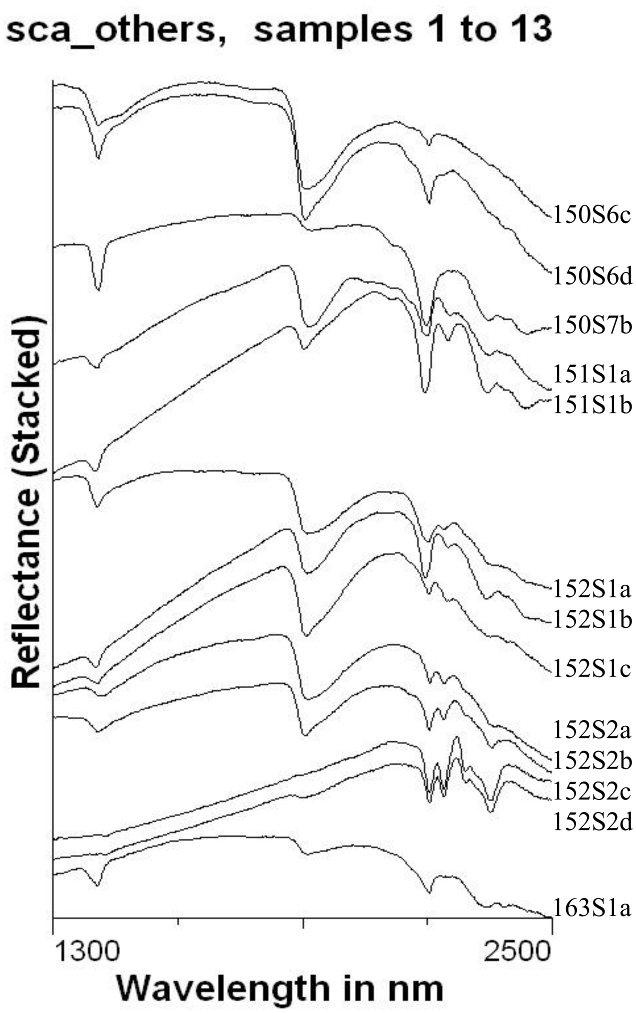


**Fig. 6. PIMA spectra of samples from the Snake Creek Anticline (metapsammites, dolerite). Respective SSQ and interpretative results from XRD shown in Tab. 2 and Tab. 1.**

*3.1.3 hyperspectral imaging*

The two main lithologies of the Snake Creek Anticline, the metasedimentary successions of the Llewellyn Creek Formation and the interlayered amphibolites can be displayed with the white mica products and the various MgOH products respectively. On Fig. 7a, showing the white mica abundance, the occurrence of the Llewellyn Creek Formation to the east of the Cloncurry Fault is clearly visible, due to its high white mica content. Major interferences are caused by the Snake Creek, running from the centre of the Snake Creek Anticline towards the NW, and hills, which are topped by Mesozoic sandstones of the Gilbert River Formation. The latter ones appear themselves as black spots on the "white mica abundance image", but are surrounded by high white mica abundance, due to better outcrops of Soldiers Cap Group.

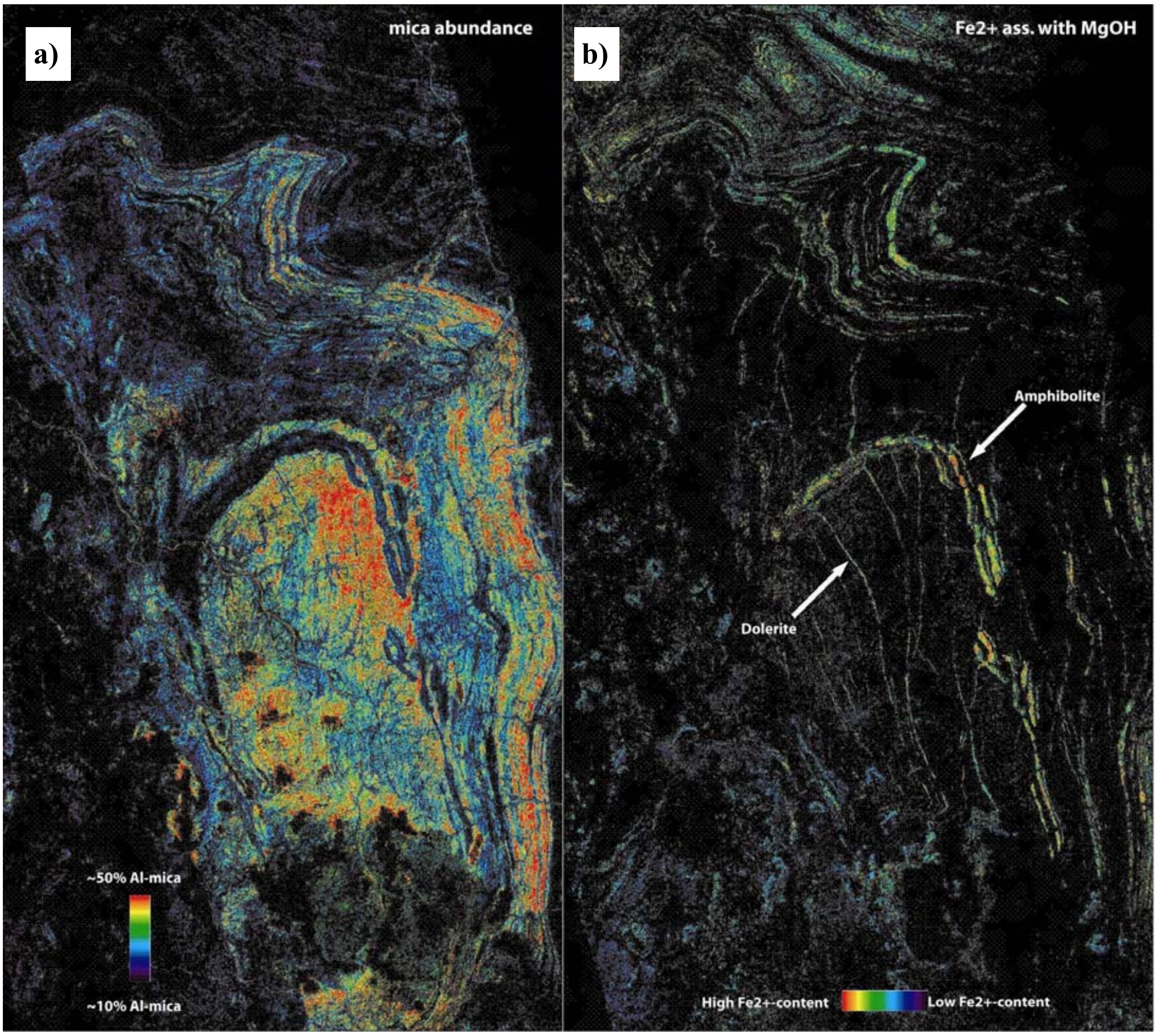


**Fig. 7. Hyperspectral images of the northern Block I (Cloncurry District): a) "mica abundance": Metasedimentary rocks of the Llewellyn Creek Formation shown in warm colours. Low accuracy especially around the SE-NW trending Snake Creek. , b) "$Fe^{2+}$ associated with MgOH": Amphibolite sills and dolerites dykes of the Soldiers Cap Group in warm colours. Low $Fe^{2+}$-content associated with MgOH indicated in the Corella Fm to the west of the Cloncurry Fault. Variable colours of the mafic units are presumably due to changes in the mineral composition of contained trioctahedral silicates. Folding of the Soldiers Cap Group in the northern Snake Creek Anticline and north of the Snake Creek Anticline evident from both geoscience products. Black is below threshold.**

The "Fe2+ associated with MgOH" image displays the distribution of the interlayered amphibolites sills and strata-discordant dolerite dykes (Fig. 7b). The various MgOH products show changes in the mineral assemblage and/or mineral composition of the mafic rock units. To the north of the Snake Creek Anticline the distinct folding of the amphibolites is accurately shown on these images.
The western to south-western part of the subsets shown in Fig. 7 consists mainly of calcsilicates of the Corella Formation, whose interpretation with the geoscience products remains problematic.

### *3.2 Camel Hill area*

The Camel Hill area is located about 20km south of Cloncurry. The dominating strata are the bedded and brecciated calcsilicates of the Corella Formation in the west separated by the NNW-SSE trending Cloncurry Fault from metasedimentary rocks and amphibolites of the Soldiers Cap Group in the east (Fig. 2, Fig. 4). Furthermore Oliver et al. (2006) described the occurrence of gabbros in the Corella Formation and calcsilicate breccia pipes "intruding" the Soldiers Cap Group or present as exotic breccias in the Soldiers Cap Group. Further characteristics of the Soldiers Cap Group are the NNW-SSE strike and interlayered amphibolites.

#### *3.2.1 geochemistry*

Semi-quantitative XRF analyses and qualitative XRD results of samples from the Camel Hill area are shown in Tab. 4 and Tab. 5 respectively. Further geochemistry on country rocks of this area can be found in Hingst (2002).

| rock type | micaschist | breccia pipe | meta-psammite | calcsilicate-breccia | altered gabbro or diabase | gabbro | calcsilicate-fels | epidoitised gabbro | calcsilicates, folded, scp-rich | heavily altered breccia, Cu-min | calcsilicate breccia, matrix rich |
|---|---|---|---|---|---|---|---|---|---|---|---|
| sample | 371P1 | 371P2 | 387P1 | 387P2 | 388P1 | 390P1 | 394P1 | 409P1 | 419P2 | 420P1 | 425P1 |
| **O** | 54,8 | 54,6 | 59,5 | 54,9 | 48,6 | 49,1 | 55,1 | 52,4 | 54,8 | 53,9 | 58,2 |
| **Na** | 0,307 | 2,090 | 0,363 | 5,790 | 2,840 | 2,280 | 2,270 | 2,560 | 0,631 | 1,790 | 3,870 |
| **Mg** | 1,110 | 2,510 | 1,430 | 0,458 | 2,980 | 2,800 | 2,460 | 1,960 | 1,780 | 2,320 | 0,512 |
| **Al** | 11,200 | 5,970 | 0,886 | 6,420 | 6,470 | 6,490 | 5,520 | 7,940 | 7,840 | 4,160 | 4,330 |
| **Al2** | 22,400 | 11,940 | 1,772 | 12,840 | 12,940 | 12,980 | 11,040 | 15,880 | 15,680 | 8,320 | 8,660 |
| **Si** | 22,20 | 22,10 | 6,02 | 20,40 | 21,20 | 20,00 | 27,30 | 18,50 | 25,40 | 26,80 | 20,50 |
| **P** | 0,155 | 0,329 | 0,106 | 0,156 | 0,107 | 0,070 | 0,094 | 0,074 | 0,131 | 0,055 | 0,078 |
| **S** | 0,028 | 0,018 | 0,006 | 0,008 | 0,006 | 0,021 | 0,060 | 0,004 | 0,008 | 0,008 | 0,006 |
| **Cl** | 0,109 | 0,056 | 0,038 | 0,021 | 0,369 | 0,618 | 0,032 | 0,290 | 0,020 | 0,860 | 0,044 |
| **K** | 5,060 | 3,900 | 0,383 | 0,065 | 1,080 | 0,536 | 1,310 | 0,687 | 4,900 | 0,032 | 0,035 |
| **Ca** | 0,293 | 5,450 | 30,200 | 8,720 | 4,800 | 6,190 | 2,220 | 8,050 | 0,826 | 1,450 | 11,300 |
| **Ti** | 0,486 | 0,269 | 0,054 | 0,293 | 0,960 | 1,150 | 0,272 | 0,377 | 0,371 | 0,443 | 0,186 |
| **V** | 0,010 | 0,014 | bd | bd | 0,055 | 0,060 | bd | 0,027 | 0,012 | 0,018 | 0,005 |
| **Mn** | 0,069 | 0,162 | 0,191 | 0,068 | 0,182 | 0,169 | 0,047 | 0,082 | 0,220 | 0,028 | 0,058 |
| **Fe** | 4,060 | 2,530 | 0,815 | 2,690 | 10,200 | 10,400 | 3,280 | 7,020 | 2,890 | 6,460 | 1,200 |
| **Cu** | bd | bd | bd | bd | 0,017 | 0,031 | bd | bd | bd | 2,490 | bd |
| **Rb** | 0,014 | 0,014 | | bd | 0,004 | bd | 0,003 | bd | 0,034 | bd | bd |
| **Sr** | bd | 0,003 | 0,033 | bd | 0,013 | 0,015 | bd | 0,055 | 0,010 | bd | bd |
| **Zr** | 0,020 | 0,010 | 0,004 | 0,015 | 0,008 | 0,007 | 0,024 | 0,005 | 0,018 | 0,005 | 0,010 |
| **Ba** | 0,084 | 0,058 | bd | bd | bd | 0,023 | bd | bd | 0,123 | bd | bd |
| **W** | 0,006 | bd | bd | bd | bd | 0,011 | 0,028 | 0,011 | bd | 0,038 | 0,010 |
| **Total** | 100,000 | 100,000 | 100,000 | 100,000 | 100,000 | 100,000 | 100,000 | 100,000 | 100,000 | 100,000 | 100,000 |

**Tab. 4. Semi-quantitative XRF analyses of samples from the Camel Hill area. All values in weight %. bd - below detection limit.**

| Camel Hill area | | | | fsp | | | | | clays | | | amphiboles | | | | | carb | | |
|---|---|---|---|---|---|---|---|---|---|---|---|---|---|---|---|---|---|---|---|
| | | | quartz | K-feldspar | plagioclase | *muscovite* | biotite | *chlorite* | *Illite* | *expanding clay* | *meionite (scapolite)* | *K-ferroedenite* | *actinolite* | *pargasite* | pyroxene | epidote | calcite | Calcite, magnesian | alunite |
| sample | rock type | unit | | | | | | | | | | | | | | | | | |
| 371P1 | micaschist | Pton | x | | | x | | x | | x | | | | | | | | | x |
| 371P2 | calcsilicate | Ptbr | x | x | x | x | | x | | | (x?) | x | | x | | | x | | |
| 374P1 | calcsilicate | Ptbr | x | | x | x | | | | | x | | | | | | x | | |
| 376P1 | micaschist | Pton | x | | | x | | | | | | | | | | | | | x |
| 378P1 | calcsilicatefels | Ptbr | x | | x | x | | | | | x | | | x | x | | x | | |
| 379P1 | calcsilicate | Ptbr | x | | x | x | | | | | x | | | | | | x | | |
| 382P1 | metapsammite | Pton | x | | x | x | | | x | | | x | | | | | | x | |
| 384P1 | calcsilicate | Ptkc_br | x | | x | x | | | | | x | | | | | | x | | |
| 387P1 | metapsammite | Ptkc | x | | x | | | | x | | | | x | | | | | x | |
| 387P2 | calcsilicatebreccia | Ptkc_br | (x) | | x | | | | | | | | x | | | | x | | |
| 388P1 | altered gabbro or diabase | Ptgi_g | | | x | x | | x | | | | x | | | (x) | | | | |
| 389P1 | gabbro, Fe-rich | Ptgi_g | | | x | | | | | | | | x | | | | | | |
| 390P1 | gabbro | Ptgi_g | | x | x | x | | x | | | | x | | | | | | | |
| 393P1 | calcsilicatefels, qtz-veining prominent | Ptkc_br | x | | x | | | x | | | x | | | | x | | x | | |
| 394P1 | calcsilicatefels | Ptkc_br | x | x | x | | | x | | | | | | | | | x | | |
| 396P1 | calcsilicatefels, qtz-veining prominent | Ptbr | x | x | | | | | | | x | | | | | | | | |
| 400P1 | calcsilicate, mg | Ptkc | x | x | x | | x | x | | | | | | | | | | x | |
| 404P1 | micaschist | Ptkc | | | | | | | | | | | | | | | | | |
| 405P1 | calcsilicate | Ptkc | x | | x | | x | x | | | | | | | | | | x | |
| 408P1 | calcsilcatebreccia | Ptkc_br | x | x | (x) | | | x | x | | | | x | | | | | x | |
| 409P1 | epidoitised gabbro | Ptgi_g | | | x | | | x | | | | | | x | | x | x | | |
| 415P1 | calcsilicates, bedded | Ptkc | x | | x | | | x | x | | x | | | | | | | x | |
| 418P1 | calcsilicate breccia | Ptkc_br | x | | x | | | x | | | | | | | | | x | | |
| 419P2 | calcsilicates, folded, scp-rich | Ptkc | x | x | x | x | | x | | | | | | | | | | | |
| 420P1 | heavily altered breccia, Cu-min | Ptkc_br | x | | x | | | x | | | | | | | | | (x) | | |
| 420P2 | dark rock associated with Cu-min | Ptkc_br | x | | x | | | x | | | | | | | | | | | |
| 425P1 | calcsilicate breccia, matrix rich | Ptkc_br | x | | x | | | x | | | | | | | | | x | | |

**Tab. 5. Qualitative XRD results of samples from the Camel Hill area. Minerals in italic are critical in the interpretation of the HyMap data. Rock units: Ptbr - Breccia Pipe, Ptgi_g - gabbros of the Saxby Suite, Ptkc - Cloncurry Formation, Ptkc_br - Corella Breccia, Pton - Soldiers Cap Group. Mineral occurrences: xx - percentage ≥ 80%, x - major component, (x) - minor component. Carb - Carbonates, fsp - feldspars.**

*3.2.2 PIMA analyses*

Reflectance spectra of PIMA analyses of selected samples from the Camel Hill area (Tab. 6) are shown in Fig. 8.

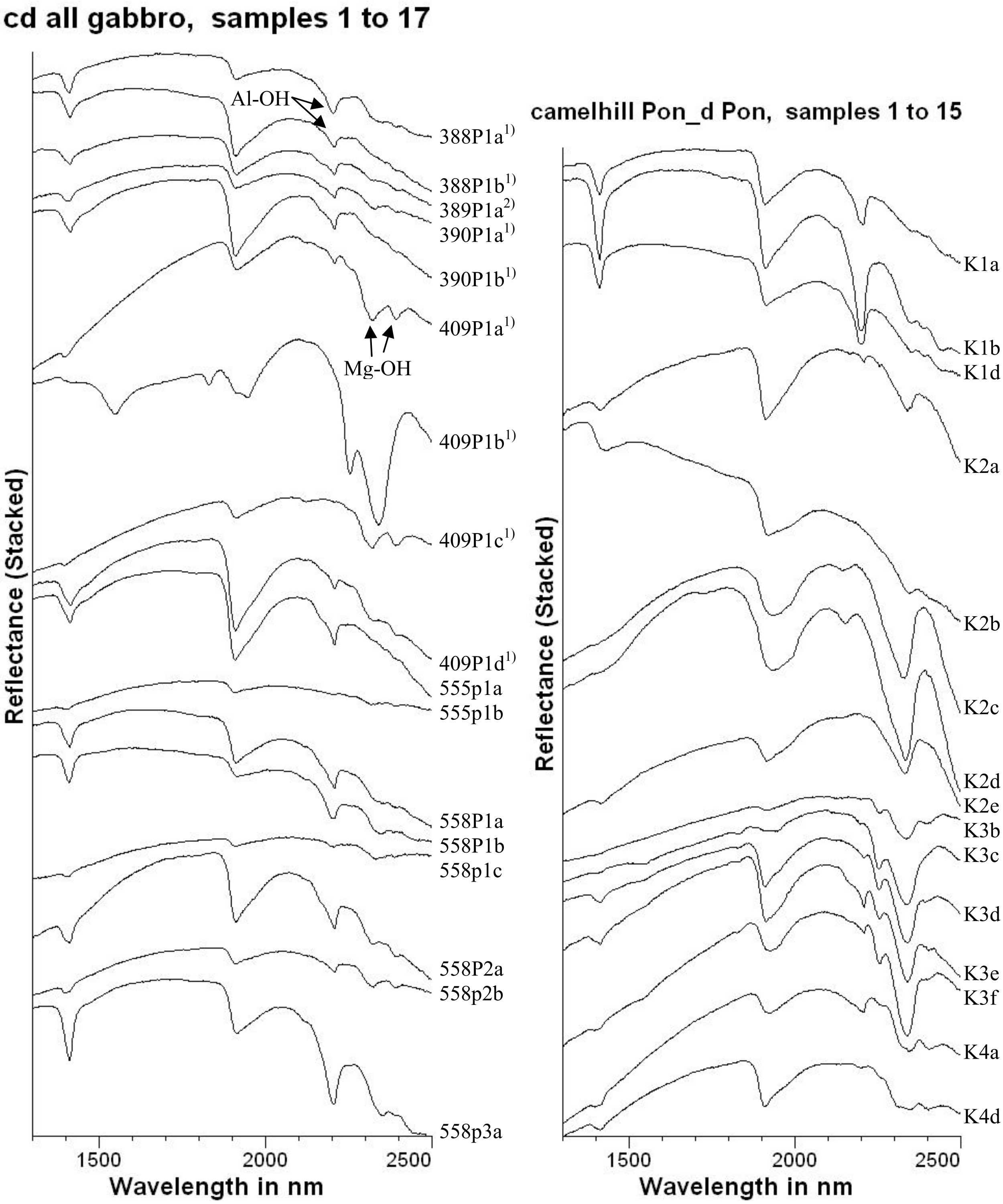


**Fig. 8. PIMA measurements of samples from the Camel Hill area. Left: Gabbros (ptgi_g) related to the Williams Naraku Suite. Right: Metasedimentary rocks (Pon) and interlayered amphibolites (Pon_d) of the Mount Norna Formation. 1) respective SSQ and interpretative results from XRD shown in Tab. 4 and Tab. 5. 2) respective interpretative results from XRD shown in Tab. 5.**

| sample | rock type | surface | cut | PIMA integration | spectra dominating minerals (acc. to TSG auxmatch or *own int.*) |
|---|---|---|---|---|---|
| 388P1a | altered gabbro or diabase | weathered | weathering surface | 1 | Ill, Act |
| 388P1b | altered gabbro or diabase | weathered, reddish | weathering surface | 1 | Ill, Hbl |
| 389P1a | gabbro, Fe-rich | weathered, reddish | weathering surface | 1 | Ill, Hbl |
| 390P1a | gabbro | weathered | weathering surface | 1 | Ill, Act |
| 390P1b | gabbro | weathered, red | weathering surface | 1 | Ill, Hbl |
| 409P1a | epidoitised gabbro | weathered | weathering surface | 1 | Hbl, Ill |
| 409P1b | epidoitised gabbro | fresh | break | 1 | Ep, Phl |
| 409P1c | epidoitised gabbro | fresh | break | 1 | Hbl |
| 409P1d | epidoitised gabbro | weathered, red | break | 1 | Hbl, Ill |
| 555P1a | gabbro | weathered, red, thick | break | 2 | Kln, Ill |
| 555P1b | gabbro | weathered | break | 4 | Hbl |
| 558P1a | gabbro, heavily scapolitised | weathered, reddish | weathering surface | 2 | Ill, Kln |
| 558P1b | gabbro, heavily scapolitised | weathered, whitish | weathering surface | 2 | Ill, Mg-Chl |
| 558P1c | gabbro, heavily scapolitised | slightly weathered | break | 2 | Ill, Act |
| 558P2a | gabbro, heavily scapolitised | weathered, red | weathering surface | 2 | Kln, Ill |
| 558P2b | gabbro, heavily scapolitised | weathered | weathering surface | 4 | Act, Ill |
| 558P3a | gabbro, large scp | weathered | weathering surface | 4 | Ill, Kln |
| K1a | micaschist | weathered, upper side | parallel S1 | 1 | Ill |
| K1b | micaschist | weathered, lower side | parallel S1 | 1 | Ill, Hbl |
| K1d | micaschist | fresh | | 1 | Ill, Hbl |
| K2a | carbonate breccia/vein | weathered | weathering surface | 1 | Cc, dry vegetation |
| K2b | carbonate breccia/vein | weathered, brown coating | weathering surface | 1 | Rbk, Cc |
| K2c | carbonate breccia/vein | fresh | break | 1 | *Mg-Cc* |
| K2d | carbonate breccia/vein | fresh | break | 1 | *Mg-Cc* |
| K2e | carbonate breccia/vein | weathering profile | weathering surface | 2 | *Mg-Cc* |
| K3b | amphibolite | fresh | break | 4 | Hbl, Ep |
| K3c | amphibolite | fresh | break | 4 | Ep, Phl |
| K3d | amphibolite | weathered, bright red | joint | 4 | Ep, Hbl |
| K3e | amphibolite | weathered, coating | weathering surface | 4 | Ep, Rbk |
| K3f | amphibolite | weathered | weathering surface | 4 | Ep, Rbk |
| K4a | amphibolite | weathered, red staining | weathering surface | 4 | Rbk |
| K4d | amphibolite | fresh, greenish | break | 4 | Hbl, Ep |

**Tab. 6. Description of samples shown in Fig. 8. Mineral abbreviations after Kretz (1983).**

### *3.2.3 hyperspectral imaging*

Most useful hyperspectral mineral maps in the Camel Hill area comprise "white mica abundance", "$Fe^{2+}$-content", "$Fe^{2+}$ associated with MgOH", the vegetation products and the false colour image. Parts of the Camel Hill area are characterised by dense vegetation, especially terpentine trees on top of amphibolites in the east and various bushes and trees on top of the Corella Breccia and the breccia pipes (see field pictures IMG_1868 - 1871, Appendix 8.3.1). Fig. 9 shows a "$Fe^{2+}$ ass. with MgOH" image from the southern central Camel Hill area. Variations of the abundance of ferrous iron associated with MgOH are largely due to variations of the amphibole and/or chlorite chemistry in the various mafic rocks. NNW-SSE striking amphibolites, interlayered in the Soldiers Cap Group, are shown in green to yellow colours, reflecting a higher abundance of ferrous iron associated with MgOH compared to the gabbro bodies, which appear in blue colours. The zoning of the southernmost gabbro body on this image is discussed in Laukamp et al. (2008a, 2008b). The variations of the chemical composition of tricoctahedral silicates in the mafic rocks are also displayed in the PIMA reflectance spectra (Fig. 8).

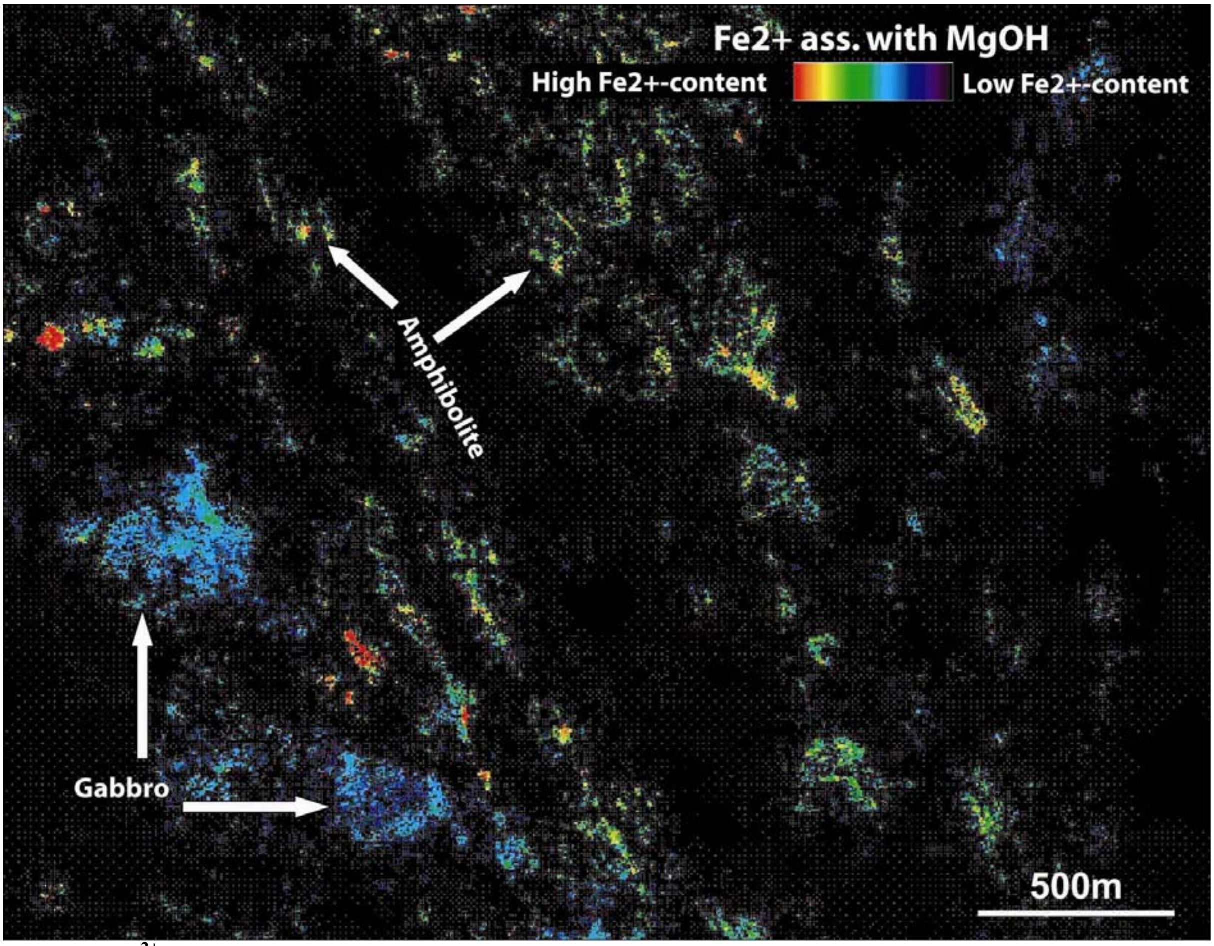


**Fig. 9. "$Fe^{2+}$ associated with MgOH"-map of the southern central Camel Hill area. NNW-SSE-trending amphibolites, interlayered in the Mount Norna Formation in green to orange colours. Gabbros of the Williams Naraku Suite in cool colours. Zoning of the southern gabbro body with increasing $Fe^{2+}$-content towards the rim. Red specks to the northeast and north of the gabbro bodies are occurrences of breccia pipes. Black is below threshold.**

### *3.3 Suicide Ridge area*

The Suicide Ridge area is located about 30km south of Cloncurry to the east of the Cloncurry Fault (Fig. 2, Fig. 4). The dominating units comprise the NNW-SSE striking Soldiers Cap Group, made of metasedimentary rocks and interlayered amphibolites and igneous bodies of the Saxby Granite in the south-western part of this area. The north-eastern side of the granite is surrounded by its carapace, which consists of calcsilicate hornfels. From this carapace a breccia pipe extends to the NE discordant to the Soldiers Cap Group. The Breccia Pipe consists mainly of actinolite, albite and calcite (Tab. 8), contains clasts made of gabbro and ironstone and is described by Bertelli (2007) and Oliver et al. (2006). A pegmatite of unknown relationship to the country rocks and paraconformal to the Soldiers Cap Group is located to the east of the breccia pipe. Substantial areas are covered by Mesozoic sandstones of the Gilbert River Formation.

### *3.3.1 geochemistry*

Semi-quantitative XRF analyses and qualitative XRD results of samples from the Suicide Ridge area are shown in Tab. 7 and Tab. 8 respectively.

| rock type | quartzite | micaschist | meta-quarzite | pegmatite | pegmatite | phyllite, micaschist | breccia | breccia | breccia | micaschist + sil | micaschist + sil | calcsilicate-hornfels | calcsilicate-hornfels | amphibolite | calcsilicate-hornfels | gabbro | gabbro | muskovite (pegmatite) |
|---|---|---|---|---|---|---|---|---|---|---|---|---|---|---|---|---|---|---|
| sample | 255S1 | 255S2 | 255S3 | 256S1 | 256S2 | 262S1 | 263S1 | 263S2b | 263S2c | 263S3a | 263S3b | 265S1 | 265S2 | 266S1 | 267S1 | 269S1a | 269S1b | 274S1 |
| O | 59,023 | 54,593 | 56,181 | 56,902 | 52,609 | 58,623 | 54,101 | 53,098 | 54,599 | 56,405 | 57,824 | 48,923 | 47,764 | 50,841 | 60,140 | 48,923 | 47,847 | 52,393 |
| F | bd | bd | bd | bd | bd | bd | bd | bd | bd | bd | bd | bd | bd | bd | bd | bd | bd | 0,434 |
| Na | 0,565 | 0,379 | 1,410 | 1,977 | 0,545 | 3,948 | 4,675 | 5,965 | 5,526 | 1,398 | 1,218 | 4,071 | 2,034 | 3,280 | 0,417 | 4,098 | 4,176 | 0,509 |
| Mg | 0,302 | 1,696 | 1,236 | 0,239 | 0,103 | 1,175 | 3,157 | 1,991 | 1,392 | 1,101 | 1,064 | 3,356 | 3,872 | 2,632 | 1,542 | 2,947 | 2,917 | 0,089 |
| Al | 1,702 | 12,485 | 6,465 | 7,450 | 15,076 | 8,133 | 5,558 | 7,284 | 6,114 | 12,043 | 10,265 | 7,648 | 7,047 | 7,959 | 0,554 | 7,330 | 7,447 | 17,638 |
| Si | 37,556 | 20,874 | 29,971 | 28,074 | 23,793 | 24,214 | 24,258 | 26,866 | 23,668 | 22,214 | 24,129 | 22,227 | 22,078 | 17,753 | 4,640 | 21,414 | 21,950 | 19,319 |
| P | 0,027 | 0,071 | 0,074 | 0,125 | 0,041 | 0,074 | 0,131 | 0,198 | 0,120 | 0,045 | 0,061 | 0,063 | 0,035 | 0,100 | 0,112 | 0,119 | 0,115 | 0,036 |
| S | 0,028 | bd | 0,005 | 0,004 | 0,006 | 0,005 | 0,006 | 0,008 | 0,010 | bd | 0,004 | 0,069 | 0,018 | 0,039 | 0,024 | 0,081 | 0,061 | 0,005 |
| Cl | 0,070 | 0,034 | 0,024 | 0,100 | 0,030 | 0,052 | 0,032 | 0,061 | 0,042 | 0,011 | bd | 0,059 | 0,059 | 1,323 | 0,091 | 0,217 | 0,200 | bd |
| K | 0,245 | 5,138 | 2,110 | 1,394 | 6,748 | 1,259 | 0,063 | 0,068 | 0,049 | 3,489 | 2,789 | 0,797 | 3,496 | 0,637 | 0,073 | 0,829 | 0,855 | 8,024 |
| Ca | 0,064 | 0,381 | 0,251 | 0,163 | 0,019 | 0,342 | 4,557 | 1,423 | 6,156 | 0,371 | 0,349 | 4,048 | 4,119 | 7,407 | 30,541 | 5,313 | 5,346 | 0,015 |
| Ti | 0,051 | 0,472 | 0,253 | 0,039 | 0,036 | 0,289 | 0,273 | 0,329 | 0,252 | 0,335 | 0,315 | 0,613 | 0,910 | 0,589 | 0,037 | 0,857 | 0,900 | 0,028 |
| V | bd | 0,012 | bd | bd | bd | bd | bd | 0,007 | bd | 0,010 | bd | 0,036 | 0,036 | 0,028 | bd | 0,033 | 0,033 | bd |
| Cr | 0,001 | 0,004 | 0,004 | bd | bd | 0,001 | bd | bd | bd | 0,004 | 0,003 | bd | bd | 0,003 | bd | 0,003 | 0,003 | bd |
| Mn | | 0,082 | 0,018 | 0,057 | 0,013 | 0,013 | 0,039 | 0,032 | 0,024 | 0,030 | 0,006 | 0,088 | 0,143 | 0,091 | 0,100 | 0,080 | 0,084 | 0,016 |
| Fe | 0,329 | 3,728 | 1,920 | 3,422 | 0,848 | 1,848 | 3,128 | 2,643 | 2,030 | 2,449 | 1,898 | 7,985 | 8,313 | 7,301 | 1,721 | 7,711 | 8,041 | 1,275 |
| Ni | bd | bd | bd | bd | bd | bd | bd | bd | bd | bd | bd | 0,004 | bd | bd | bd | 0,001 | bd | bd |
| Cu | bd | bd | bd | bd | bd | bd | bd | bd | bd | bd | bd | 0,004 | bd | bd | bd | bd | bd | bd |
| Zn | bd | bd | bd | 0,005 | bd | bd | bd | bd | bd | bd | bd | bd | bd | bd | bd | bd | bd | bd |
| Ga | bd | bd | bd | 0,003 | 0,008 | bd | bd | bd | bd | bd | bd | 0,002 | bd | 0,003 | bd | bd | bd | 0,013 |
| Rb | bd | 0,015 | 0,010 | 0,006 | 0,077 | 0,004 | bd | bd | bd | 0,005 | 0,005 | bd | 0,013 | 0,001 | bd | 0,003 | 0,003 | 0,189 |
| Sr | bd | bd | bd | bd | bd | 0,004 | bd | bd | bd | 0,003 | 0,003 | 0,013 | 0,015 | 0,015 | 0,023 | 0,015 | 0,013 | bd |
| Zr | 0,005 | 0,015 | 0,024 | bd | bd | 0,015 | 0,020 | 0,019 | 0,021 | 0,016 | 0,016 | 0,007 | 0,010 | 0,006 | 0,002 | 0,010 | 0,011 | bd |
| Nb | bd | bd | bd | bd | 0,014 | bd | bd | bd | bd | bd | bd | bd | bd | bd | bd | bd | bd | 0,028 |
| Ba | bd | 0,046 | 0,014 | bd | bd | 0,019 | bd | bd | bd | 0,073 | 0,053 | bd | 0,042 | bd | bd | 0,025 | bd | bd |
| W | 0,052 | | 0,050 | 0,043 | 0,041 | 0,013 | 0,021 | 0,025 | 0,020 | bd | bd | bd | bd | bd | bd | bd | 0,009 | bd |
| Total | 100,0 | 100,0 | 100,0 | 100,0 | 100,0 | 100,0 | 100,0 | 100,0 | 100,0 | 100,0 | 100,0 | 100,0 | 100,0 | 100,0 | 100,0 | 100,0 | 100,0 | 100,0 |

**Tab. 7. Semi-quantitative XRF analyses of samples from the Suicide Ridge area. All values in weight %. bd - below detection limit.**

| locality: Suicide Ridge | | | | fsp | | micas | | | | | | | amph | | | | | carb | | opaques | |
|---|---|---|---|---|---|---|---|---|---|---|---|---|---|---|---|---|---|---|---|---|---|
| sample | rock type | unit | quartz | *K-feldspar* | albite | *muscovite* | *Na-muscovite* | *clinochlore* | *talc* | *(Ca-)phillipsite* | *montmorillonite* | *meionite (scapolite)* | *actinolite* | *hornblende* | dopside | olivine | *tourmaline* | calcite | ankerite | hematite | magnetite |
| 255S1 | quartzite | Pon | x | | x | | | | | | | | | | | | | | | | |
| 255S2 | micaschist | Pon | | | | | x | x | | | | | | | | | | | | | |
| 255S3 | metaquarzite | Pon | x | x | x | x | | x | | | | | | | | | | | | | |
| 256S1 | pegmatite | pegmatite | x | x | x | x | x | | | | | | | | | | x | | | | |
| 256S2 | pegmatite | pegmatite | x | x | x | x | | | | | | | | | | | | | | | |
| 262S1 | phyllite, micaschist | Pon | x | | x | | x | | | | | | | | | | | | | | |
| 263S1 | breccia | breccia pipe | x | | x | | | | x | | | | x | | | | | x | | x | |
| 263S2b | breccia | breccia pipe | x | | x | | | | x | | | | x | | | | | x | | x | |
| 263S2c | breccia | breccia pipe | x | | x | | | | x | | | | | x | | | | x | | x | |
| 263S3a | micaschist + sil | Pon | x | | x | x | | | | | x | | | | | | | | | | |
| 263S3b | micaschist + sil | Pon | x | | x | x | | | | | x | | | | | | | | | | |
| 265S1 | calcsilicate-hornfels | carapace | | | x | | | x | | | | | x | | | | | x | | | x |
| 265S2 | calcsilicate-hornfels | carapace | | x | x | | | x | | | | | x | x | | | | x | | | (x) |
| 266S1 | amphibolite | Pon_d | | x | | | | x | | | | x | x | | | | | | x | | |
| 267S1 | calcsilicate-hornfels | clast in breccia pipe | x | | x | | | | | | | | | x | x | | | x | | | |
| 269S1 | gabbro | clast in breccia pipe | | x | x | | | | | x | | | | | | x | | | | | |
| 274S1 | muskovite | pegmatite | | | | x | | | | | | | | | | | | | | | |

**Tab. 8. Qualitative XRD results of samples from the Suicide Ridge area. Minerals in italic are critical in the interpretation of the HyMap data. Rock units: Pon - Soldiers Cap Group, Pon_d - amphibolites of the Soldiers Cap Group. Mineral occurrences: xx - percentage ≥ 80%, x - major component, (x) - minor component. Amph - amphiboles, Carb - carbonates, fsp - feldspars. Samples 255S2, 255S3, 263S1, 263S2b, 263S2c, 265S1, 265S2, 266S1 have been reported in Laukamp et al. (2008a).**

### *3.3.2 PIMA analyses*

Reflectance spectra of PIMA analyses of selected samples from the Suicide Ridge area (Tab. 9) are shown in Fig. 10

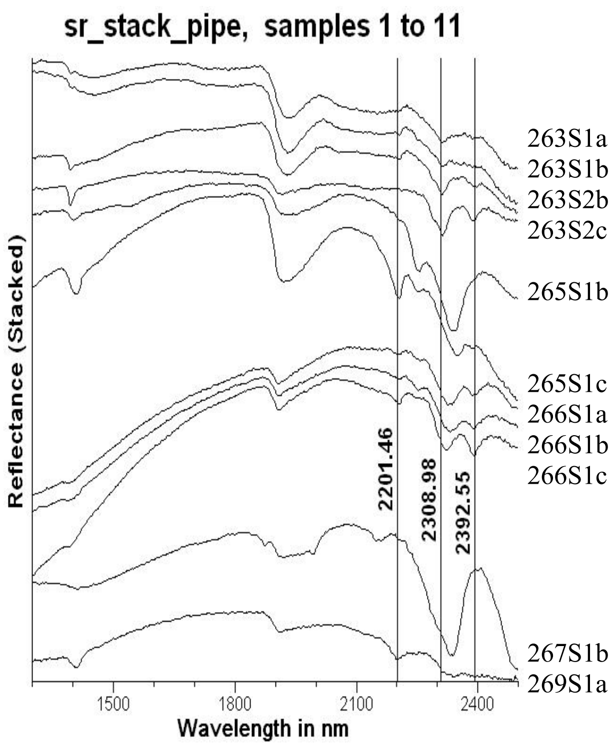


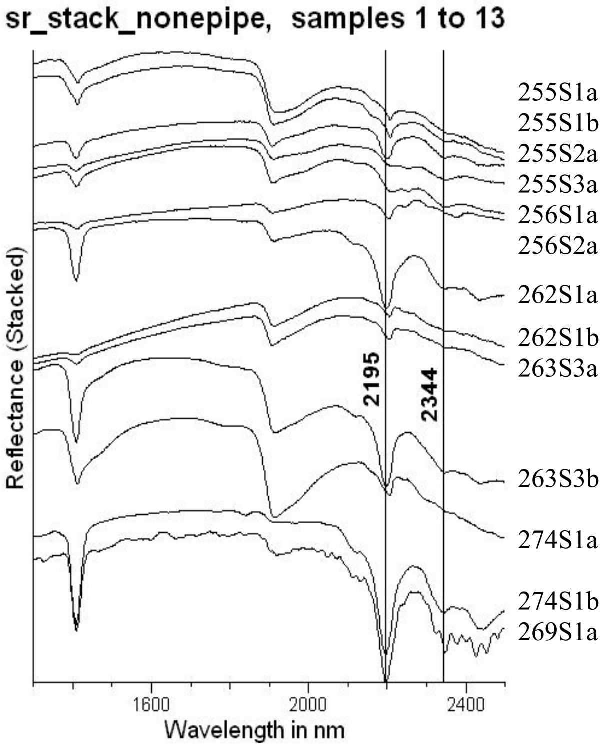


**Fig. 10. PIMA measurements of samples from the Suicide Ridge area. Left: Suicide Ridge breccia pipe, carapace of the Saxby Granite and amphibolites interlayered within the Mount Norna Formation. Right: Metasedimentary units of the Mount Norna Formation and pegmatite. For sample description see Tab. 9. Respective interpretative results from XRD shown in Tab. 8. Respective SSQ results from XRF shown in Tab. 7.**

| sample | rock type | surface | cut | spectra dominating minerals (acc. to TSG auxmatch or *own int.*) |
|---|---|---|---|---|
| 263S1a | calcsilicate breccia | weathered | weathering surface | *Mg-Cc, Alu* |
| 263S1b | calcsilicate breccia | weathered | weathering surface | *Mg-Cc*, Alu |
| 263S2b | calcsilicate breccia | weathered | weathering surface | Hbl, *Mg-Cc* |
| 263S2c | calcsilicate breccia | fresh | weathering surface | Hbl, Tr |
| 265S1b | carapace | weathered | perpendicular S0 | Mg-Chl, Ep |
| 265S1c | carapace | weathered | parallel S0 | Ill, *Mg-Cc* |
| 266S1a | amphibolite | weathered | parallel S1 | Hbl, Phl |
| 266S1b | amphibolite | weathered | perpendicular S1 | Hbl, Phl |
| 266S1c | amphibolite | weathered | parallel S1 | Hbl |
| 267S1b | calcsilicate breccia | weathered | weathering surface | *Mg-Cc* |
| 269S1a | gabbro | weathered | break | Ms, Hbl |
| 255S1a | quartz-vein | weathered | parallel S1 | Ms |
| 255S1b | quartz-vein | weathered | weathering surface | Ms |
| 255S2a | micaschist | weathered | weathering surface | Ms |
| 255S3a | metaquarzite | fresh | weathering surface | Int Chl, Ms |
| 256S1a | pegmatite | weathered | weathering surface | Ms, Fe-Tur |
| 256S2a | pegmatite | weathered | weathering surface | Ms |
| 262S1a | micaschist | weathered, upper side | parallel S1 | Ms, Mg-Chl |
| 262S1b | micaschist | weathered, lower side | parallel S1 | Ms |
| 263S3a | micaschist | weathered | weathering surface | Ms |
| 263S3b | micaschist | weathered | weathering surface | Ms |
| 274S1a | muscovite | | weathering surface | Ms |
| 274S1b | pegmatite | | weathering surface | Ms |

**Tab. 9. Description of samples shown in Fig. 10. PIMA integration: 1. Mineral abbreviations after Kretz (1983). Other minerals: Alu - alunite.**

#### *3.3.3 hyperspectral imaging*

Due to the grate variety of country rocks in the Suicide Ridge area numerous of the geoscience products can be used for classification of the mineral assemblages. Fig. 11a) shows the "water abundance relative to white mica abundance", which is an interpretation of the abundance of muscovite versus illite. It gives a rough estimation of the relative crystallinity of white micas in this area, but the accuracy is lowered by the assumption that all water in a given pixel in this image is associated with white mica (see HyMap product descriptions in Appendix 8.1.1). The Soldiers Cap Group is shown by light blue to red colours, depending on the respective lithologies. Warmer colours represent mainly mica schists, whereas cooler colours indicate metapsammites and metaquartzites, but may also be due to sericitisation of feldspars or other alumosilicates. Further uncertainties are related to the pegmatite, quaternary creek sediments and the Mesozoic sandstones of the Gilbert River Formation (Jurassic Mesa in Fig. 11), which cover large areas, especially in the western and most eastern part of the image. The pegmatite is characterised by red colours, presumably due to abundant fresh muscovite. PIMA analyses show that the reflectance spectra are dominated by muscovite (sample 256S2a, Fig. 10). However, a general trend to a higher crystallinity of white mica contained in the Soldiers Cap Group towards the west could possibly be observed in Fig. 11a). This might be related to an increasing metamorphic gradient towards the Saxby Granite in the west or just due to the various lithologies in the Soldiers Cap Group. Further characteristics of the lithologies of the Soldiers Cap Group can also be observed on other white mica mineral maps (e.g. "white mica abundance" in Fig. 7a, "white mica composition" in Appendix 8.1.3).
Fig. 11b) and Fig. 11c) are subsets of the area surrounding the Suicide Ridge Breccia Pipe, which doesn't appear on the white mica products, due to the lack of white mica in this calcsilicate breccia. Variations on both images are related to the occurrence of trioctahedral silicates and carbonates and compositional changes of these minerals in the various country rocks. The breccia pipe contains clinopyroxene (diopside) and K-feldspar as infill minerals together with albite, magnetite, and quartz (Oliver et al., 2006) and actinolite (Bertelli, 2007). However, no K-feldspar was detected in the qualitative XRD-analyses (Tab. 8) or thin sections during this study. Diopside was only detected in a calcsilicate-hornfels clast (Tab. 8). Breccia clasts are dominated by calcsilicates of the Corella Formation with rare fragments of the hosting Soldiers Cap Group (Bertelli, 2007). The Suicide Ridge Breccia Pipe contains a mineral assemblage similar to the amphibolites plus calcite, but shows adsorption at lower wavelengths in the "MgOH-composition"-map. This could be explained by the talc content or Mg-rich calcite, both indicated by XRD (Tab. 8). No talc was found in thin sections or PIMA spectra of the breccia pipe though. Therefore probably Mg-rich calcite causes especially on the shorter wavelength side the widening of the 2308 nm absorption feature, which is mainly due to trioctahedral silicates (PIMA spectra 263S2b, 263S2c Fig. 10).
In the "MgOH composition" image amphibolites of the Mount Norna Formation are highlighted in red. XRD-analyses reveal actinolite, clinochlore and meionite (Ca-scapolite) as major Mg and Ca-bearing minerals (Laukamp et al., 2008a; sample 266S1 in Tab. 8). Thin section analyses suggest that the high abundance of ferrous iron associated with MgOH shown in Fig. 11c) is either due to Fe-rich chlorites or actinolite. PIMA-analyses reveal that the reflectance spectra are dominated by an actinolite-type phase Fig. 10.
The Mount Norna quartzites show adsorption in similar wavelengths, which is less pronounced presumably because of a high muscovite-chlorite ratio in the micaschists (samples 255S2, 263S3 in Appendix 8.6: thin section list). High muscovite contents can disturb the mineral interpretation from the "MgOH-composition"-map, as these minerals absorb in the same range of wavelengths.

Fig. 12 allows the differentiation of major rock units in the Suicide Ridge area in one image by collating three different mineral abundance maps ("white mica abundance", $Fe^{2+}$ ass. with MgOH", "Kaolin abundance"). The metapsammites of the Llewellyn Creek Formation are shown in deep red colours, due to their high white mica content. Further metapsammites are part of the NW-trending Mount Norna Quartzites. Amphibolites, interlayered in the Mount Norna Quartzites, the strata discordant Suicide Ridge Breccia Pipe and dolerite dykes paraconform to the Llewellyn Creek Formation appear in bright green colours, due to their high content of trioctahedral silicates and/or carbonates.

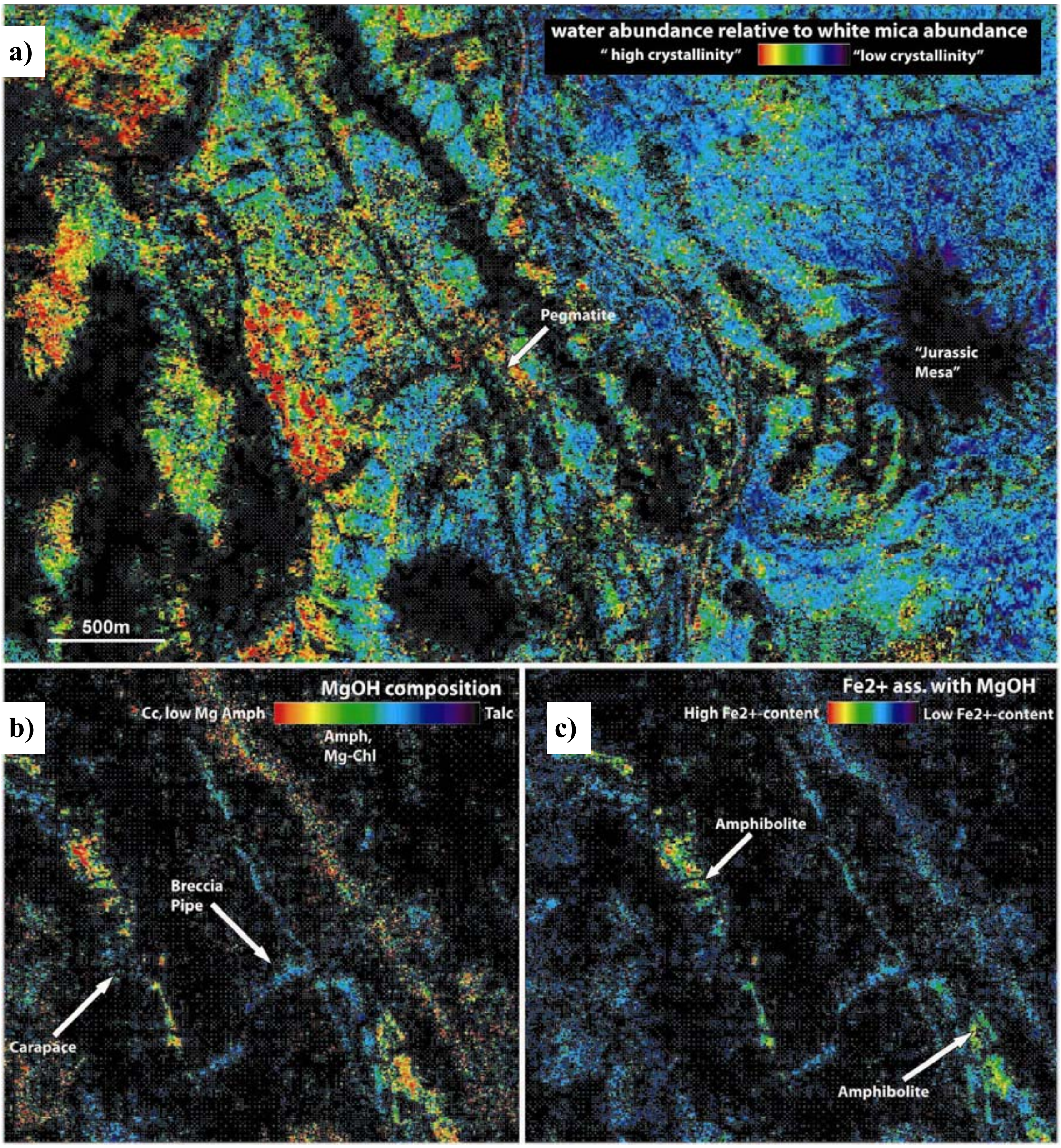


**Fig. 11. Hyperspectral images of the Suicide Ridge Breccia area: a) "water abundance relative to white mica abundance (in text referred to as "white mica crystallinity") showing the distribution of metasedimentary units of the Mount Norna Formation and a para-concordant pegmatite. b) "MgOH composition" showing the Suicide Ridge Breccia Pipe discordant to the NW-trending Mount Norna Formation. Yellow to red colours west and southeast of the breccia pipe represent amphibolites, interlayerd in the Mount Norna Formation. NW-trending feature in warm colours to the east of the breccia pipe are quartzites of the Mount Norna Formation. c) "$Fe^{2+}$ associated with MgOH": Suicide Ridge Breccia Pipe and Mount Norna Quartzites in blue. Amphibolites in green to red colours. Data from the blue area southwest of the amphibolites are disturbed by the Gilbert River Formation. Black is below threshold.**

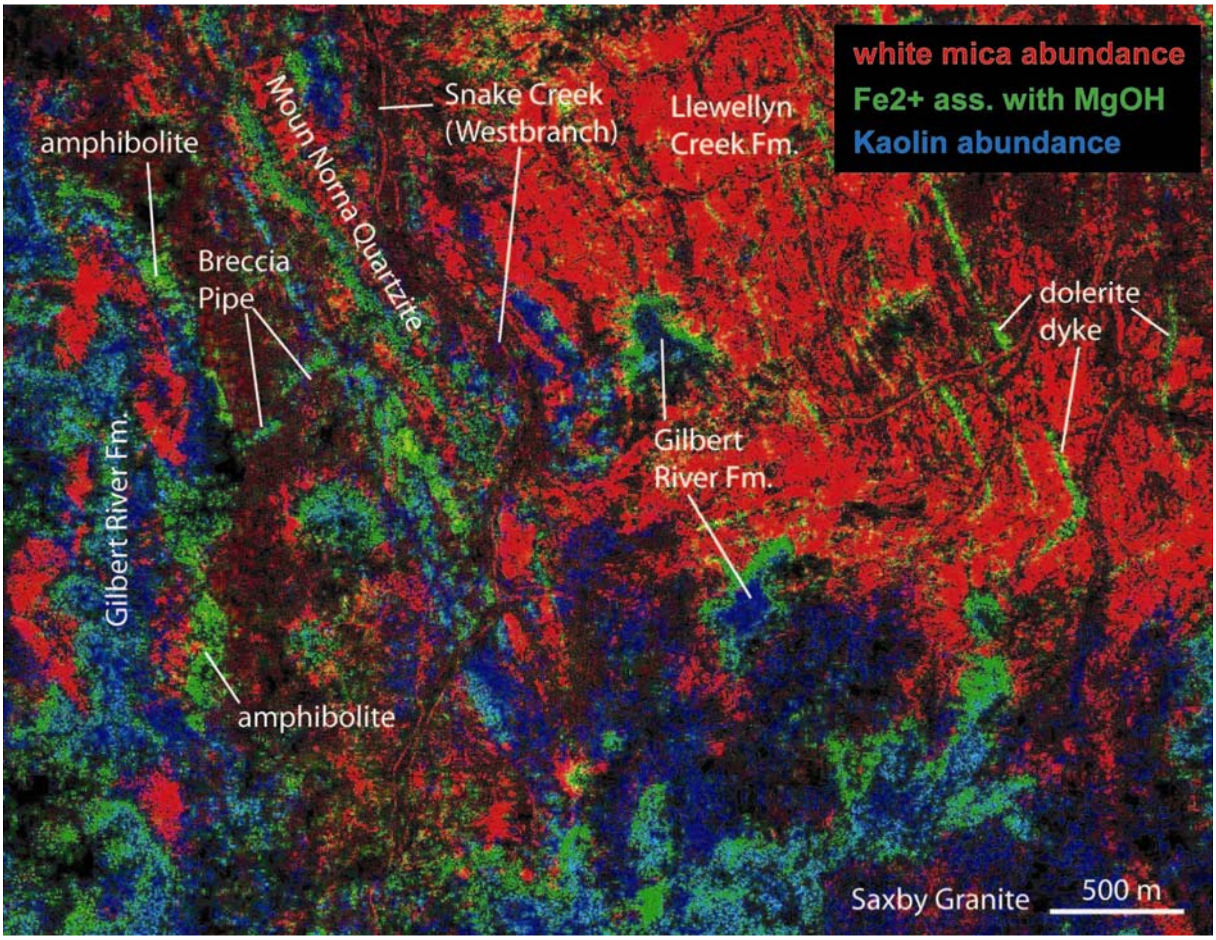


**Fig. 12. Combination image of three geoscience products from the Suicide Ridge area: red - "white mica abundance", green - "Fe2+ ass. with MgOH" and blue - "Kaolin abundance". The NW-trend of the Mount Norna Formation and the Llewellyn Creek Formation is clearly visible. Dolerite dykes in the east show folding of the Soliders Cap Group north of the Saxby Granite. The Suicide Ridge Breccia Pipe crosscuts the Mount Norna Formation. Especially in the west the Gilbert River Formation disturbs information about the Paleoproterozoic strata. Single occurences of these "Jurassic Mesas" are visible in the centre of the image, covering the Llewellyn Creek Formation.**

### *3.4 Tool Creek area*

The Tool Creek area is located about 15km SSE of Cloncurry. The dominant lithologies comprise metasedimentary successions and interlayered amphibolites of the Soldiers Cap Group (Fig. 2, Fig. 4). Several faults, which trend NNW, NE and ESE transpose the Soldiers Cap Group. A breccia pipe occurs at the junction of three main fault systems in the northwestern part and NNE-trending brecciated veins occur in the north-eastern part.

#### *3.4.1 geochemistry*

Semi-quantitative XRF analyses and qualitative XRD results of samples from the Cloncurry District are shown in Tab. 10 and Tab. 11 respectively.

| rock type | meta-psammite | phyllite | breccia vein, scapolite in clasts | breccia vein, scapolite in clasts | meta-psammite | meta-psammite | breccia vein, partly siderite-matrix | breccia vein, partly siderite-matrix | breccia vein, scapolite in clasts | breccia vein, scapolite in clasts | meta-psammite | graphitic schist | breccia pipe, scapolite |
|---|---|---|---|---|---|---|---|---|---|---|---|---|---|
| sample | 124S1 | 125S1 | 128S1b | 128S1c | 128S2d | 128S2b | 130S1a | 130S1b | 132S1 | 132S2a | 133S1 | 133S2 | 141S1 |
| O | 57,2 | 54,2 | 56,8 | 56,7 | 57,8 | 58,0 | 60,3 | 60,2 | 56,1 | 57,6 | 54,9 | 56,9 | 54,0 |
| Na | 0,083 | 0,087 | 5,01 | 4,35 | 1,78 | 2,95 | 0,104 | 1,64 | 3,73 | 5,46 | 0,563 | 3,22 | 0,090 |
| Mg | 0,369 | 0,542 | 1,44 | 2,35 | 2,43 | 2,55 | 6,15 | 4,32 | 0,219 | 1,38 | 0,422 | 0,028 | 0,667 |
| Al | 3,95 | 10,7 | 7,54 | 7,35 | 4,35 | 5,80 | 0,044 | 2,58 | 8,01 | 6,69 | 10,8 | 4,48 | 6,47 |
| Si | 30,5 | 27,1 | 21,1 | 19,0 | 18,9 | 17,4 | 0,093 | 6,40 | 29,2 | 19,4 | 27,3 | 34,2 | 25,7 |
| P | 0,092 | 0,047 | 0,069 | 0,047 | 0,162 | 0,146 | 0,006 | 0,047 | 0,073 | 0,047 | 0,032 | 0,071 | 0,096 |
| S | 0,068 | 0,006 | 0,029 | 0,019 | 0,047 | 0,049 | 0,004 | 0,005 | 0,006 | 0,008 | 0,009 | 0,158 | 0,010 |
| Cl | 0,034 | 0,031 | 0,051 | 0,057 | 0,081 | 0,031 | 0,136 | 0,110 | 0,029 | 0,037 | 0,023 | 0,016 | 0,017 |
| K | 0,045 | 4,88 | 0,579 | 0,912 | 0,908 | 0,945 | 0,009 | 0,244 | 1,33 | 0,094 | 4,31 | 0,350 | 8,52 |
| Ca | 4,55 | 0,188 | 4,78 | 6,07 | 8,20 | 8,10 | 21,6 | 15,5 | 0,537 | 6,81 | 0,053 | 0,296 | 0,485 |
| Ti | 0,148 | 0,345 | 0,617 | 0,700 | 0,830 | 0,765 | bd | 0,313 | 0,143 | 0,896 | 0,208 | 0,121 | 0,332 |
| V | | 0,007 | 0,034 | 0,042 | 0,023 | 0,028 | bd | 0,017 | bd | 0,023 | bd | bd | 0,008 |
| Mn | 0,347 | 0,039 | 0,104 | 0,086 | 0,248 | 0,183 | 0,723 | 0,554 | 0,018 | 0,061 | 0,007 | bd | 0,038 |
| Fe | 2,54 | 1,75 | 1,76 | 2,27 | 4,27 | 3,06 | 10,8 | 8,12 | 0,538 | 1,49 | 1,25 | 0,170 | 3,45 |
| Ga | bd | bd | 0,002 | bd | bd | bd | bd | bd | 0,002 | bd | bd | bd | bd |
| As | bd | bd | 0,008 | bd | bd | bd | bd | bd | bd | bd | bd | bd | bd |
| Rb | bd | 0,020 | bd | 0,004 | 0,003 | bd | bd | 0,002 | bd | bd | 0,015 | bd | 0,028 |
| Sr | 0,005 | bd | 0,007 | 0,008 | 0,004 | 0,006 | 0,005 | 0,006 | 0,004 | 0,004 | bd | 0,005 | bd |
| Y | bd | 0,003 | bd | bd | bd | bd | bd | bd | bd | bd | 0,003 | bd | bd |
| Zr | 0,013 | 0,022 | 0,008 | 0,009 | 0,011 | 0,012 | bd | 0,004 | 0,026 | 0,011 | 0,032 | 0,013 | 0,018 |
| Ba | 0,024 | 0,103 | bd | bd | bd | bd | bd | bd | bd | bd | 0,082 | bd | 0,026 |
| W | 0,053 | bd | 0,014 | 0,011 | 0,018 | bd | bd | bd | 0,017 | 0,010 | bd | 0,044 | 0,014 |
| Total | 100,0 | 100,0 | 100,0 | 100,0 | 100,0 | 100,0 | 100,0 | 100,0 | 100,0 | 100,0 | 100,0 | 100,0 | 100,0 |

**Tab. 10. Semi-quantitative XRF analyses of samples from the Tool Creek area. All values in weight %. bd - below detection limit.**

| Tool Creek Area | | | | micas | | clay minerals | | feldspars | | | | carbonates | | | scapolites | | | | |
|---|---|---|---|---|---|---|---|---|---|---|---|---|---|---|---|---|---|---|---|
| | | | quartz | *mica* | *phlogopite* | *kaolinite group* | *illite* | K-feldspar | Na-plagioclase | albite | low calcian albite | *dolomite* | *calcite* | *ankerite* | *meionite* | *Na-meionite* | *clinochlore-type phase* | *ferro-actinolite* | *hematite* |
| sample | rock type | unit | | | | | | | | | | | | | | | | | |
| 124S1 | meta-psammite | Pot | x | ~x | x | | | | | | | | | | | | | x | |
| 125S1 | phyllite | Pot | x | | | x | | | | x | | | | | | | | | |
| 128S1b | breccia vein, scapolite in clasts | Pot | x | x | | x | | | | | x | x | x | | | (x) | | | |
| 128S1c | breccia vein, scapolite in clasts | Pot | x | | | x | x | | | x | | x | | | x | | | | |
| 128S2d | meta-psammite | Pot | x | ~x | (x) | | | | x | | | | x | | | | | | |
| 128S2b | meta-psammite | Pot | x | ~x | (x) | | | | | x | | | x | | | | | | |
| 130S1a | breccia vein, partly siderite-matrix | breccia pipe | x | | | | | | | | | | | xx | | | | | |
| 130S1b | breccia vein, partly siderite-matrix | breccia pipe | x | x | | x | | | x | | | | x | x | | | x | | |
| 132S1 | breccia vein, scapolite in clasts | breccia pipe | x | | | | x | | | x | | | | | (x) | | | | |
| 132S2a | breccia vein, scapolite in clasts | breccia pipe | x | | | | x | | | x | | x | | | (x) | | | | |
| 133S1 | meta-psammite | Pot | x | x | | x | | | | x | | | | | | | | | |
| 133S2 | graphitic schist | Pot | x | x | | | | | | x | | | | | | | | | |
| 141S1 | scapolite | breccia pipe | x | x | | | | x | | | | | | | | x | | | x |

**Tab. 11. Qualitative XRD results of samples from the Tool Creek area. Minerals in italic are critical in the interpretation of the HyMap data. Rock units: Pot - Tool Creek Formation. Mineral occurrences: xx - percentage ≥ 80%, x - major component, (x) - minor component.**

### *3.4.2 PIMA analyses*

Reflectance spectra of PIMA analyses of selected samples from the Camel Hill area (Tab. 12) are shown in Fig. 13.

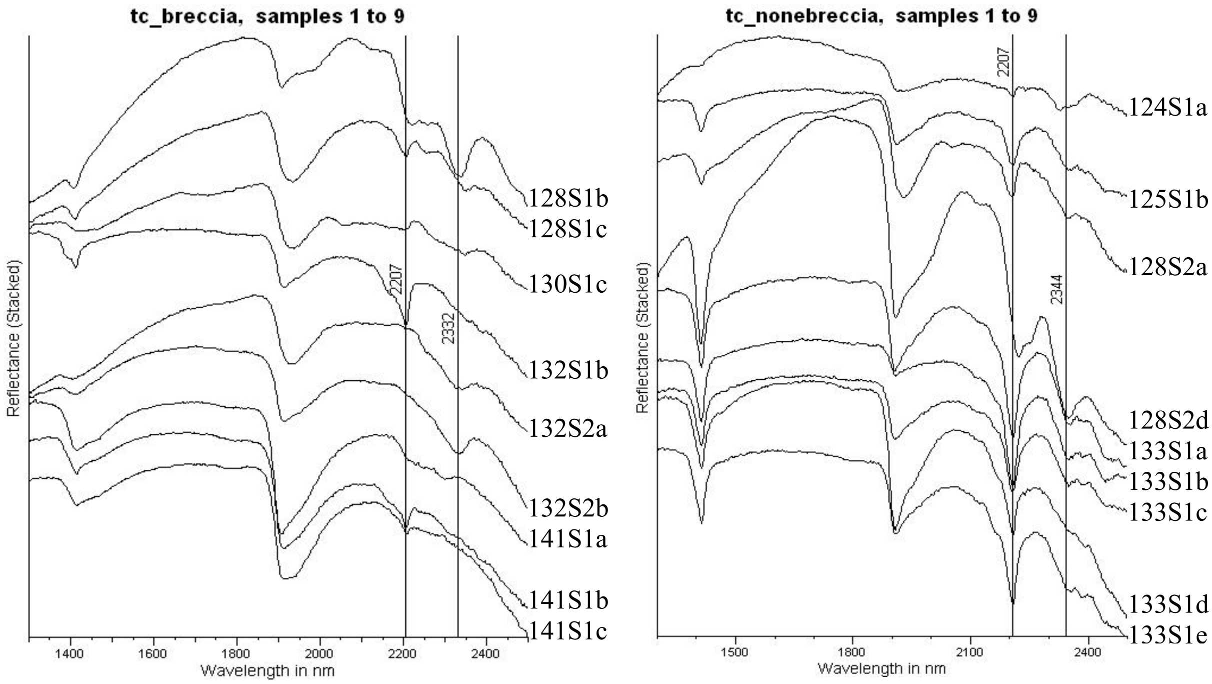


**Fig. 13. PIMA spectra of samples from the Tool Creek area. Left: Breccia pipe and breccia veins. Right: Metasedimentary units of the Mount Norna Formation. Sample description in Tab. 12. Respective interpretative results from XRD shown in Tab. 11. Respective SSQ results from XRF shown in Tab. 10.**

| sample | rock type | surface | cut | spectra dominating minerals (acc. to TSG auxmatch or *own int.*) |
|---|---|---|---|---|
| 128S1b | calcsilicate breccia | fresh | break | *Mg-Cc*, Ms |
| 128S1c | calcsilicate breccia | weathered | joint | *Mg-Cc*, Ms |
| 130S1c | calcsilicate breccia | | weathering surface | *Sd* |
| 132S1b | calcsilicate breccia | weathered | parallel S1 | Ill, *Mg-Cc* |
| 132S2a | calcsilicate breccia | weathered | break | *Mg-Cc*, Ep |
| 132S2b | calcsilicate breccia | fresh | break | *Mg-Cc* |
| 141S1a | calcsilicate breccia | weathered | break | *Mnt, Mg-Cc* |
| 141S1b | calcsilicate breccia | weathered | weathering surface | Ill, *Mg-Cc* |
| 141S1c | calcsilicate breccia | weathered | weathering surface | *Ill, Mg-Cc* |
| 124S1a | metapsammite | weathered | break | *Ms* |
| 125S1b | phyllite | weathered, upper side | parallel S1 | Ms, Bt |
| 128S2a | metapsammite | weathered, black | break | Ms |
| 128S2d | metapsammite | weathered | joint | Ph, Int Chl |
| 133S1a | metapsammite | weathered | parallel S1 | Ms, Fe-Chl |
| 133S1b | metapsammite | weathered | parallel S2 | Ms |
| 133S1c | metapsammite | weathered | joint, oblique, high angle | Ms |
| 133S1d | metapsammite | weathered, rough | oblique, low angle | Ms, Fe-Chl |
| 133S1e | metapsammite | weathered, "steps" | oblique, low angle | Ms, Bt |

**Tab. 12. Description of samples shown in Fig. 13. PIMA integration: 1. Mineral abbreviations after Kretz (1983). Other minerals: Ph - phengite.**

*3.4.3 hyperspectral imaging*

Two main groups of the geoscience products can be used to differentiate the metasedimentary rocks of the Soldiers Cap Group from the interlayered amphibolites. The occurrence of amphibolites is not only envisaged in the "MgOH content" (Fig. 14), but also on hyperspectral mineral maps showing the "MgOH composition", "Fe2+ ass. with MgOH" and "Fe3+ associated with MgOH". Even the distinct folding of the various layers can be recognised. Fig. 14 displays also variations of the mineral composition of the amphibolites, envisaged by a higher MgOH content in the southern amphibolites. The metasedimentary rocks of the Soldiers Cap Group are best shown on the white mica products (see Appendix 8.1.3).
The breccia pipe in the centre of the Tool Creek area is characterised by a low MgOH content (Fig. 14), and "MgOH composition" and abundance of ferrous iron associated with MgOH similar to the Suicide Ridge Breccia Pipe (see Appendix 8.1.3). The NNE-trending breccia veins in the north-eastern part of the Tool Creek Area are not displayed in any of the geological maps, which were available for this study (neither digital nor hardcopies) and they can't be found on any of the geoscience products. They have been found during the ground-truthing of the geoscience products in the Tool Creek area and samples, field photos and pima spectra are listed in the respective Appendix. Their relationship to the breccia pipes remained unclear until the finalisation of this study, but further studies are suggested, due to the observations of similarities in the field (mainly characteristics of clast components).

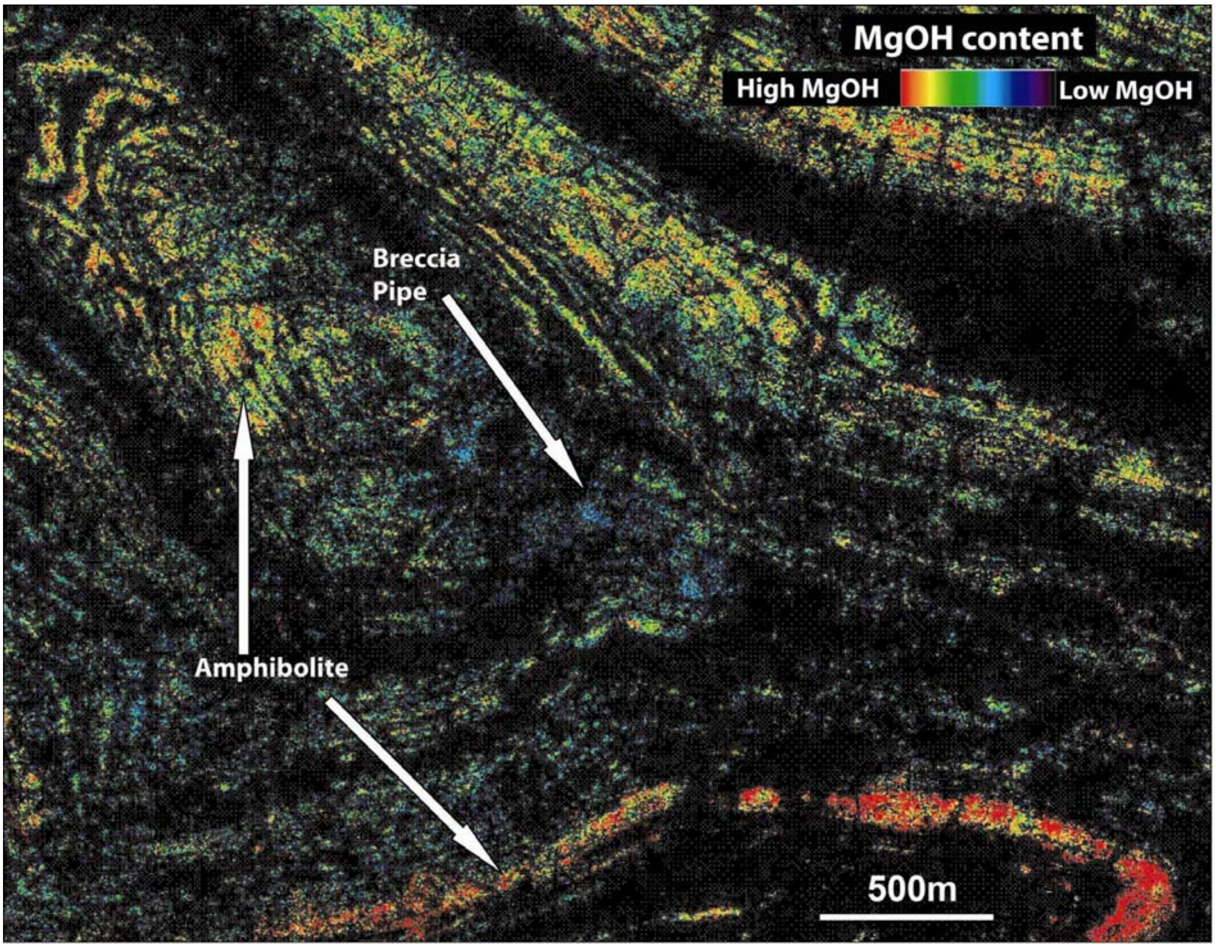


**Fig. 14. "MgOH content" of the central Tool Creek area showing amphibolites, interlayered in the Mount Norna Formation, in bluegreen, yellow and red colours. Variations in colour suggest variation in the mineral composition of contained minerals. Folding of the amphibolites is clearly visible. The breccia pipe is represented by cool colours, indicating a low MgOH content. Black is below threshold.**

### *3.5 Mount Angelay granite area*

The Mount Angelay area is located about 45km south of Cloncurry, on the western side of the Cloncurry Fault (Fig. 2). The dominating lithologies in this area comprise the metasedimentary rocks of the Doherty Formation and Corella Formation, the igneous suite of the Mount Angelay granites and its contact aureole to the metasediments. The Mount Angelay granite consists mainly of a non-foliated, partly porphyritic granite with biotite and/or hornblende and/or clinopyroxene (Blake, 1987) and was in more detail described in Mark (1999), Mark and Foster (2000) and Mark et al. (2005).

#### *3.5.1 geochemistry*

Semi-quantitative XRF analyses and qualitative XRD results of samples from the Mount Angelay area are shown in Tab. 13 and Tab. 14 respectively.

| rock type | coarse crystalline granite | schistose metadiorite in granite | schistose metadiorite in granite | breccia | coarse crystalline granite, shear zone | schistose granite | schistose granite | coarse crystalline granite | fine crystalline granite |
|---|---|---|---|---|---|---|---|---|---|
| sample | 196S1 | 196S2a | 196S2c | 197S1 | 200S1 | 201S1a | 201S1b | 204S1 | 215S1 |
| **O** | 61,5 | 57,8 | 57,7 | 62,3 | 59,2 | 60,6 | 59,7 | 60,8 | 60,6 |
| **Na** | 4,30 | 2,15 | 2,35 | 0,065 | 1,47 | 2,96 | 3,07 | 3,81 | 4,77 |
| **Mg** | 0,297 | 2,38 | 2,59 | 4,50 | 1,09 | 0,473 | 0,482 | 0,176 | 0,300 |
| **Al** | 6,36 | 5,75 | 5,99 | 0,522 | 6,75 | 6,51 | 6,47 | 5,99 | 8,51 |
| **Si** | 23,5 | 16,8 | 17,4 | 1,17 | 22,2 | 21,9 | 22,7 | 25,1 | 20,7 |
| **P** | 0,026 | 0,062 | 0,095 | bd | 0,114 | 0,144 | 0,111 | 0,052 | 0,064 |
| **S** | 0,005 | 0,006 | 0,023 | 0,012 | 0,007 | 0,014 | 0,004 | 0,006 | 0,053 |
| **Cl** | 0,100 | 0,300 | 0,153 | 0,008 | 0,088 | 0,117 | 0,185 | 0,115 | 0,090 |
| **K** | 1,95 | 0,764 | 0,875 | 0,125 | 5,43 | 3,41 | 3,63 | 2,39 | 0,939 |
| **Ca** | 0,740 | 4,71 | 4,46 | 31,0 | 1,12 | 1,13 | 1,21 | 0,751 | 2,37 |
| **Ti** | 0,237 | 0,587 | 0,698 | 0,026 | 0,202 | 0,455 | 0,372 | 0,139 | 0,121 |
| **V** | bd | 0,030 | 0,039 | bd | bd | bd | bd | bd | bd |
| **Mn** | 0,010 | 0,117 | 0,106 | bd | 0,026 | 0,034 | 0,020 | 0,008 | 0,013 |
| **Fe** | 0,898 | 8,48 | 7,40 | 0,257 | 2,04 | 2,11 | 1,91 | 0,596 | 1,36 |
| **Ga** | bd | bd | bd | bd | bd | bd | bd | bd | 0,002 |
| **Rb** | 0,005 | 0,003 | 0,004 | | 0,037 | 0,010 | 0,010 | 0,004 | 0,001 |
| **Sr** | 0,010 | 0,011 | 0,013 | 0,031 | 0,031 | 0,018 | 0,018 | 0,014 | 0,033 |
| **Y** | 0,003 | bd | bd | bd | 0,003 | 0,004 | 0,005 | 0,002 | 0,002 |
| **Zr** | 0,023 | 0,008 | 0,007 | 0,001 | 0,025 | 0,031 | 0,033 | 0,018 | 0,016 |
| **Nb** | 0,006 | bd | bd | bd | bd | 0,005 | 0,005 | bd | bd |
| **Ba** | 0,048 | 0,046 | 0,034 | bd | 0,274 | 0,116 | 0,107 | 0,060 | 0,019 |
| **W** | 0,019 | bd | bd | bd | 0,012 | 0,012 | 0,017 | 0,029 | 0,013 |
| **Total** | 100,0 | 100,0 | 100,0 | 100,0 | 100,0 | 100,0 | 100,0 | 100,0 | 100,0 |

**Tab. 13.Semi-quantitative XRF analyses of samples from the Mount Angelay area. All values in weight %. bd - below detection limit.**

| Mount Angelay area | | | | fsp | | | | | amph | | carb | | |
|---|---|---|---|---|---|---|---|---|---|---|---|---|---|
| | | | quartz | K-feldspar | microcline | albite | *muscovite* | *kaolin-type phase* | *chlorite* | *actinolite* | *pargasite* | *dolomite* | *calcite* | psilomelane |
| sample | rock type | unit | | | | | | | | | | | | |
| 196S1 | coarse crystalline granite | Pgia | x | x | | x | | | | | x | | | |
| 196S2a | schistose metadiorite in granite | Pgia | (x) | | | x | | x | | x | | | | |
| 196S2c | schistose metadiorite in granite | Pgia | | | | x | | | | x | | | | |
| 197S1 | post Isan breccia | regolith | | | | (x) | | | | | | (x) | xx | x |
| 200S1 | coarse crystalline granite, shear zone | Pgia | x | | x | x | x | | x | | | | x | |
| 201S1a | schistose granite | Pgia | x | | x | x | (x) | | | x | | | | |
| 201S1b | schistose granite | Pgia | x | | x | x | (x) | | | x | | | | |
| 204S1 | coarse crystalline granite | Pgia | x | | | x | - | | x | x | | | | |
| 215S1 | albitised granite? | Pgia | x | x | | x | x | x | | x | | | | |

**Tab. 14. Qualitative XRD results of samples from the Mount Angelay area. Minerals in italic are critical in the interpretation of the HyMap data. Rock units: Pgia - Mount Angelay granite. Mineral occurrences: xx - percentage ≥ 80%, x - major component, (x) - minor component. Amph - amphiboles, carb - carbonates, fsp - feldspars.**

### *3.5.2 PIMA analyses*

Reflectance spectra of PIMA analyses of selected samples from the Mount Angelay area (Tab. 15) are shown in Fig. 15.

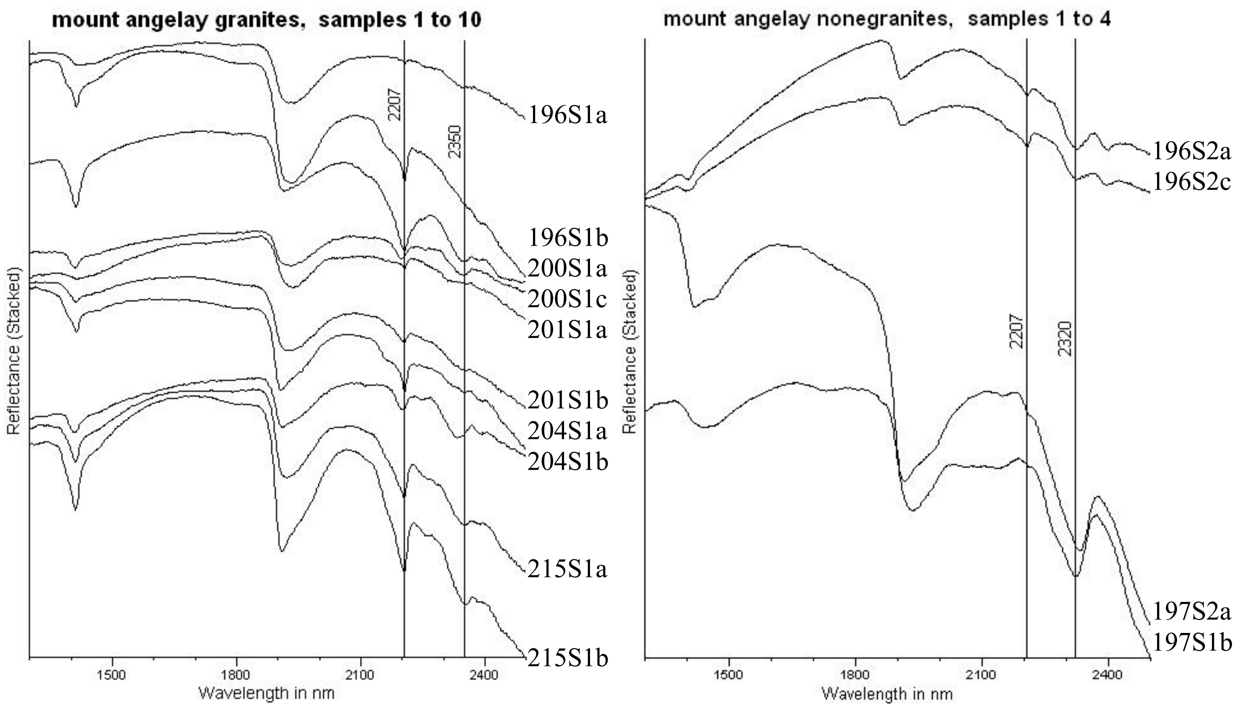


**Fig. 15. PIMA spectra of samples from the Mount Angelay area. Left: Mount Angelay Granite and calcsilicate breccias. Right: Diorite of the Mount Angelay granitoid and regolith. Sample description in Tab. 15. Respective interpretative results from XRD shown in Tab. 14. Respective SSQ results from XRF shown in Tab. 13.**

| sample | rock type | surface | cut | spectra dominating minerals (acc. to TSG auxmatch or *own int.*) |
|---|---|---|---|---|
| 196S1a | granite | fresh | break | Ill |
| 196S1b | granite | weathered | weathering surface | Hal, Alu |
| 200S1a | granite | weathered | weathering surface | Ms, Hal |
| 200S1c | granite | weathered | weathering surface | Ill, Int Chl |
| 201S1a | granite | weathered | weathering surface | Dc, Alu |
| 201S1b | granite | fresh | break | Hal, Ill |
| 204S1a | granite | weathered | weathering surface | Kln, Mnt |
| 204S1b | granite | weathered | weathering surface | Ill, Hbl |
| 215S1a | calcsilicate breccia | dark weathered | break | *Mg-Cc*, Ill |
| 215S1b | calcsilicate breccia | weathered | break | *Mg-Cc*, Ill |
| 196S2a | diorite | weathered | weathering surface | Hbl |
| 196S2c | diorite | red weathered | weathering surface | Hbl |
| 197S1a | regolith | fresh | break | Dol |
| 197S1b | regolith | weathered | weathering surface | Dol |

**Tab. 15. Description of samples shown in Fig. 15. PIMA integration: 1. Mineral abbreviations after Kretz (1983). Other minerals: Alu - alunite, Dc - dickite, Hal - halloysite.**

***3.5.3 hyperspectral imaging***

The Mount Angelay area was chosen to test the application of hyperspectral images for differing granite bodies in the Eastern Fold Belt from their carapace and for mapping of local variations in granite bodies. The Roxmere Pluton to the east of the Cloncurry Fault (Fig. 16) is described in Mark & Foster (2000).

The "MgOH composition" image shows occurrence of the Corella Formation to the west of the Cloncurry Fault (Fig. 16b). Warmer colours at the northern margin of the Mount Angelay Granite match with the occurrence of calcsilicate rocks and hornfels, which could represent contactmetamorph overprinted calcsilicates of the Corella Formation (samples 181S1, 182S1). The Roxmere Pluton is shown in blue colours in the "MgOH composition" image, which are either due to hornblende grains or chlorite. The green-yellow to red colours directly north of the Roxmere Pluton possibly show the extension of an actinolite-rich breccia (Mark & Foster, 2000). The circular pattern of rocks containing MgOH-bearing minerals possibly represents the occurrence of pod-like intrusions of amphibolites in the Doherty Formation, as described by Mark & Foster (2000).

The "mica composition" images envisages the N-S trending sillimanite-bearing psammitic metasedimentary rocks (Mark & Foster, 2000) of the Doherty Formation, which are bordered by the N-trending Cloncurry Fault on their western side, characterised by phengitic micas (Fig. 16c). The NE-trending occurrence of phengitic micas about 2 km to the west of the Cloncurry Fault might indicate another fault. The Cloncurry Fault is furthermore displayed by the "water content masked mica content", representing even the little amounts of white mica contained in the massive quartz veins along the Cloncurry Fault, and by the "opaques" image, the latter one due to the high silica amount in the fault zone. The culmination of Al-poor micas in the "mica composition" further to the west is due to alluvial plain deposits (Fig. 16c). The Roxmere Pluton and the Gilbert River Formation are not shown on the "mica composition" image and appear as black areas in the Doherty Formation.

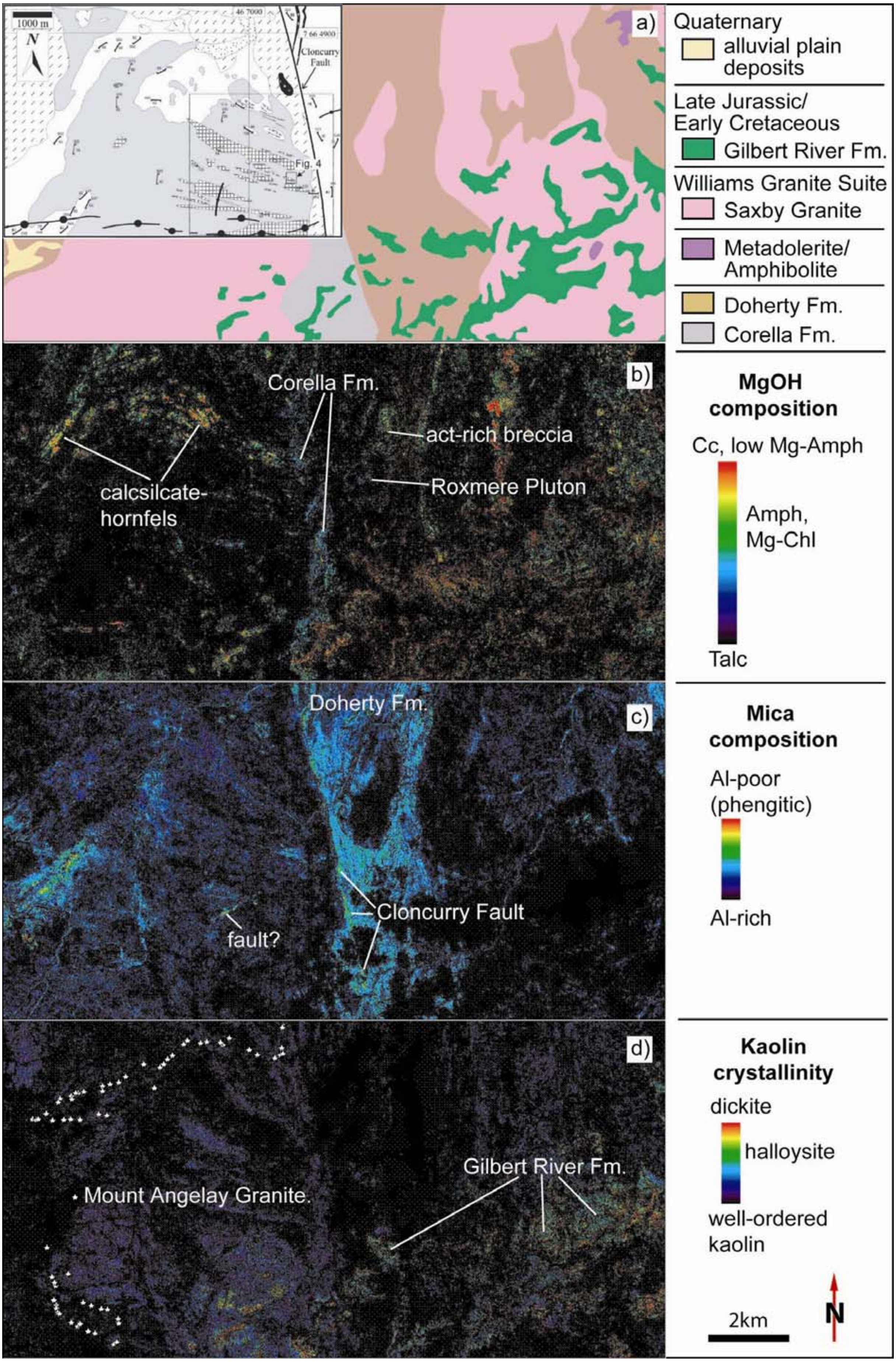

1000 m
N
Cloncurry Fault
Fig. 4
a)
Quaternary
alluvial plain deposits
Late Jurassic/ Early Cretaceous
Gilbert River Fm.
Williams Granite Suite
Saxby Granite
Metadolerite/ Amphibolite
Doherty Fm.
Corella Fm.
b)
Corella Fm.
act-rich breccia
Roxmere Pluton
calcsilcate-hornfels
MgOH composition
Cc, low Mg-Amph
Amph, Mg-Chl
Talc
c)
Doherty Fm.
Cloncurry Fault
fault?
Mica composition
Al-poor (phengitic)
Al-rich
d)
Mount Angelay Granite
Gilbert River Fm.
Kaolin crystallinity
dickite
halloysite
well-ordered kaolin
2km
N

**Fig. 16. Geological map (a) and hyperspectral images from the Mount Angelay area: b) "MgOH composition", c) "Mica composition", d) "Kaolin crystallinity". Black is below threshold. White points are sample points. act - actinolite. The subset in a) derives from Mark et al. (2005) (grey - hbl-bt-intrusions, crosshatched - leucocratic granite, /-pattern - Na-Ca altered cover sq 2-3, \-pattern - Na-Ca altered intrusions, white area - cover sq 2-3 rocks, black area - amphibolite, dotted pattern - Phanerozoic sedimentary rocks, dot-lines - tholeiitic dykes).**

The "kaolin crystallinity" image allows an estimation of the occurrence of granites in this area and even shows the E-W to WNW-ESE trending bodies of leucogranites west to the Cloncurry Fault (Fig. 16d). The granites are characterised by well-ordered kaolin. Though, the leucogranites are not distinguishable from the common Mount Angelay Granite in this geoscience product. A zoning of the Mount Angelay Granite is evident in the "water abundance masked white mica" and "white mica crystallinity" images, but these zones are not comparable to the subset of the geological map after Mark et al. (2005) shown in Fig. 16a). However, they possibly indicate slight variations in the crystal structure of white mica or just due to enhanced sericitisation of feldspars in distinct areas of the Mount Angelay Granite. Warmer colours in the "kaolin crystallinity" image indicate the occurrence of less ordered kaolin minerals like halloysite and dickite, which show the distribution of Mesozoic sandstones of the Gilbert River Formation (Fig. 16d).

### *3.6 Mallee Gap area*

The Mallee Gap area is located about 60km SSE of Cloncurry, covering strata on both sides of the Cloncurry Fault at the south-eastern extension of the Mount Angelay Granite (Fig. 2). The dominating units comprise the metasedimentary rocks of the Soldiers Cap Group and the Doherty Formation and calcsilicate breccias of the Corella Formation (Fig. 19). Igneous rocks in this area are represented by the Mount Angelay Granite and other undifferentiated granites of the Williams Granite Suite. Mesozoic Sandstones of the Gilbert River Formation cover partly the northern Mallee Gap area.
Albitisation of the Mount Angelay granite was described in DeJong (1995) and DeJong & Williams (1995).

#### *3.6.1 geochemistry*

Semi-quantitative XRF analyses and qualitative XRD results of samples from the Mallee Gap area are shown in Tab. 16 and Tab. 17 respectively.

| rock type | granite, albitised | granite | calcsilicate breccia (carapace?!) | calcsilicate | Cloncurry Fault | granite | carapace | calcsilicate |
|---|---|---|---|---|---|---|---|---|
| sample | 459P1 | 466P1 | 472P1 | 473P1 | 478P1 | 482P1 | 482P2 | 483P1 |
| O | 55,600 | 56,000 | 54,200 | 54,800 | 58,500 | 56,100 | 55,200 | 52,500 |
| Na | 6,200 | 6,690 | 5,580 | 4,190 | 0,029 | 5,980 | 0,259 | 6,170 |
| Mg | 0,168 | 0,280 | 2,770 | 0,737 | 0,061 | 0,192 | 0,036 | 1,530 |
| Al | 7,120 | 7,870 | 6,300 | 6,220 | 4,070 | 7,420 | 4,610 | 7,500 |
| Si | 29,700 | 27,300 | 25,000 | 30,000 | 36,400 | 29,000 | 27,300 | 23,800 |
| P | 0,030 | 0,034 | 0,098 | 0,099 | 0,007 | 0,017 | 0,017 | 0,170 |
| S | 0,016 | 0,017 | 0,033 | 0,015 | 0,015 | 0,004 | 0,008 | 0,012 |
| Cl | 0,067 | 0,077 | 0,048 | 0,085 | 0,033 | 0,070 | 0,037 | 0,050 |
| K | 0,182 | 0,358 | 0,112 | 1,900 | 0,375 | 0,461 | 0,033 | 0,081 |
| Ca | 0,475 | 0,712 | 2,820 | 0,755 | 0,027 | 0,265 | 7,490 | 3,350 |
| Ti | 0,052 | 0,077 | 0,273 | 0,214 | 0,022 | 0,068 | 0,053 | 0,296 |
| V | 0,002 | bd | bd | bd | bd | bd | bd | bd |
| Mn | 0,002 | 0,004 | 0,024 | 0,007 | bd | 0,003 | 0,050 | 0,050 |
| Fe | 0,452 | 0,579 | 2,680 | 0,873 | 0,427 | 0,433 | 0,479 | 4,520 |
| Ga | bd | 0,001 | 0,002 | bd | bd | bd | bd | bd |
| Se | bd | bd | bd | 0,001 | bd | bd | bd | bd |
| Rb | bd | bd | bd | 0,007 | bd | bd | bd | bd |
| Sr | 0,007 | 0,011 | bd | 0,004 | bd | 0,006 | 0,074 | bd |
| Zr | 0,007 | 0,007 | 0,019 | 0,016 | 0,011 | 0,006 | 0,006 | 0,012 |
| W | 0,054 | 0,033 | 0,015 | 0,056 | 0,053 | 0,033 | 0,052 | 0,012 |
| Total | 100,000 | 100,000 | 100,000 | 100,000 | 100,000 | 100,000 | 100,000 | 100,000 |

**Tab. 16. Semi-quantitative XRF analyses of samples from the Mallee Gap area. All values in weight %. bd - below detection limit.**

| locality: Mallee Gap | | | | fsp | | | | micas | | | | | | amph | | | | | | |
|---|---|---|---|---|---|---|---|---|---|---|---|---|---|---|---|---|---|---|---|---|
| | | | quartz | albite | sanidine | microcline | orthoclase | *muscovite* | *phlogopite* | *white mica* | *kaolinite* | *Ca-chlorite* | *meionite (scapolite* | *actinolite* | *Fe-tremolite* | *pargasite* | *hornblende* | epidote | calcite | *goethite v hematite* |
| sample | rock type | unit | | | | | | | | | | | | | | | | | | |
| 452P1 | calcsilicate | Pkd_br | | x | x | | | | | | | | | x | | | | | | |
| 453P1 | metapsammite | Pkd | | x | | x | | (x) | | | | | | | | x | | | | |
| 453P2 | calcsilicate | Pkd | | x | | | | | | | | | | | | x | | | | |
| 454P1 | micaschist | Pkd | x | x | | | x | x | | | | | | | | | | | | |
| 459P1 | granite, albitised | pgia | x | x | | | | | | | | | | x | | | | | | |
| 464P1 | granite, albitised | pgia | x | | | | | | x | x | x | x | | | x | | | | | |
| 466P1 | granite | pgia | x | x | | | x | | | | | | | | | | x | | | x |
| 467P1 | granite, albitised, heavily weathered | pgia | x | x | | | | | | | | | | | | | | | | |
| 472P1 | calcsilicate breccia (carapace?!) | Pkd_br | | x | | | | | | | | | | x | | | | (x) | | |
| 473P1 | calcsilcate | Pkd_br | (x) | x | | | x | | x | | | | x | | | | x | | | |
| 478P1 | Cloncurry Fault | Cloncurry Fault | xx | | | | | | | | x | | | | | x | | | | |
| 482P1 | granite | pgia | x | x | | | | | | | | | | | | | | | | |
| 482P2 | carapace | carapace | x | x | | | | | | | | | (x) | | | | | x | | |
| 483P1 | calcsilcate | Pkd_br | | x | | | | | | | | | | x | | | | | x | |
| 484P1 | granite, bright | pgia | x | x | | | | | | | | | | | | | | | | |
| 485P1 | granite | pgia | x | - | | x | | | | | | | | | | | | | | |
| 486P1 | granite, albitised | pgia | x | x | | | | | | | | | | | | | | | | |

**Tab. 17. Qualitative XRD results of samples from the Mallee Gap area. Minerals in italic are critical in the interpretation of the HyMap data. Rock units: pgia - Mount Angelay granite, Pkd - Doherty Formation, Pkd_br - breccias of the Doherty Formation. Mineral occurrences: xx - percentage ≥ 80%, x - major component, (x) - minor component. Fsp - feldspars, amph - amphiboles.**

### *3.6.2 PIMA analyses*

Reflectance spectra of PIMA analyses of selected samples from the Mallee Gap area (**Fehler! Verweisquelle konnte nicht gefunden werden.**, Tab. 18) are shown in Fig. 17 and Fig. 18.

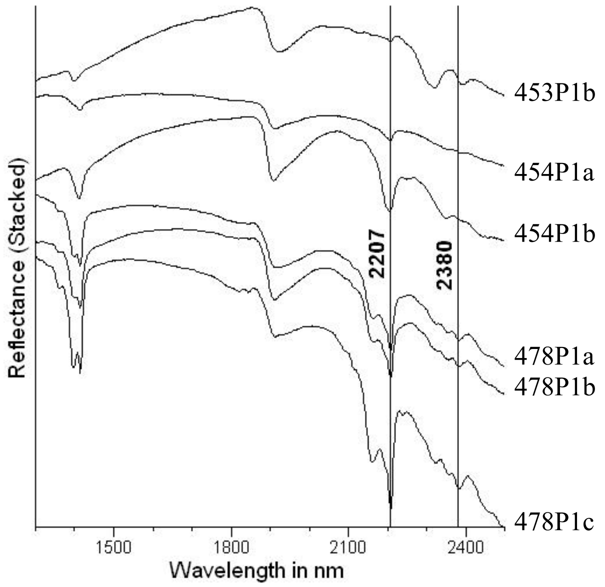


**Fig. 17. PIMA spectra of samples from metasedimentary rocks of Cover Sequence 3 and the Cloncurry Fault in the Mallee Gap area. Sample description in Tab. 18. Respective interpretative results from XRD shown in Tab. 17. Respective SSQ results from XRF shown in Tab. 16.**

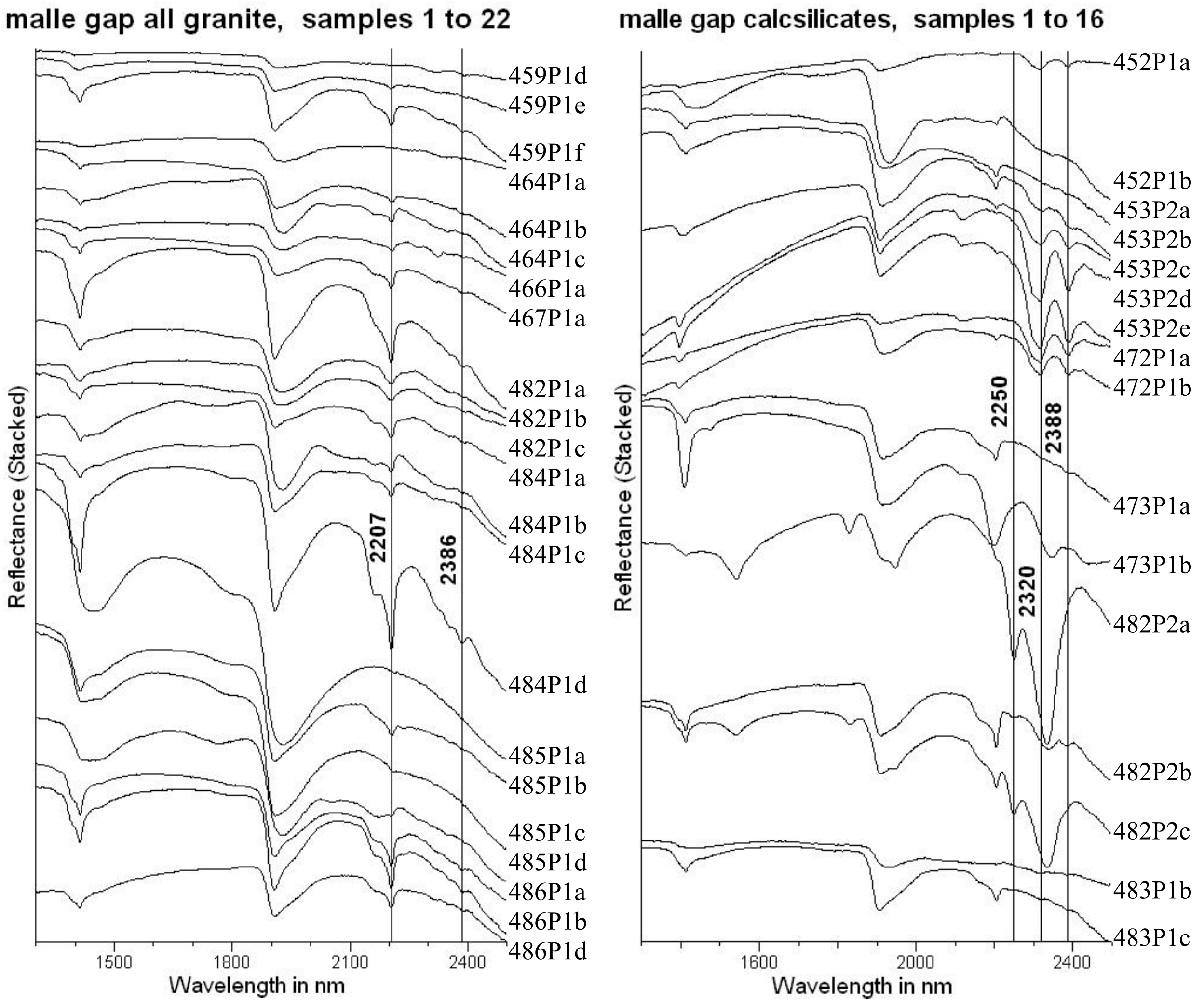


**Fig. 18. PIMA spectra of samples from the Mallee Gap area. Left: Mount Angelay Granite. Right: Carapace of the Mount Angelay Granite and calcsilicate rocks. Sample description in Tab. 18. Respective interpretative results from XRD shown in Tab. 17. Respective SSQ results from XRF shown in Tab. 16.**

| sample | rock type | surface | cut | spectra dominating minerals (acc. to TSG auxmatch or *own int.*) |
|---|---|---|---|---|
| 453P1b | metapsammite | weathered | break | Hbl |
| 454P1a | micaschist | weathered, lower side | parallel Sf | Hal, Ill |
| 454P1b | micaschist | weathered, upper side | parallel Sf | Ill |
| 478P1a | quartz (Cloncurry Fault) | fresh | break | Kln |
| 478P1b | | weathered | break | Kln |
| 478P1c | | weathered | internal weathering joint | Kln |
| 459P1d | granite | fresh | break | Hbl |
| 459P1e | granite | weathered | weathering surface | Hal |
| 459P1f | granite | weathered, orange stain | weathering surface | Hal |
| 464P1a | granite | fresh | break | aspectral |
| 464P1b | granite | weathered, white | weathering surface | Hal |
| 464P1c | granite | weathered, dark | weathering surface | Dc |
| 466P1a | granite | weathered | weathering surface | Hal |
| 467P1a | granite | weathered | weathering surface | Hal |
| 482P1a | granite | weathered, red stained | weathering surface | *Ms* |
| 482P1b | granite | fresh | break | *Ms* |
| 482P1c | granite | weathered | break | *Ms* |
| 484P1a | granite | fresh | break | *Ms* |
| 484P1b | granite | thick weathering crust, dark | break | aspectral |
| 484P1c | granite | thick weathering crust, bright | weathering surface | Hal |
| 484P1d | granite | weathered | weathering surface | Kln, Mnt |
| 485P1a | granite | fresh | break | aspectral |
| 485P1b | granite | weathered | internal weathering joint | *Ms* |
| 485P1c | granite | weathered | weathering surface | Mnt |
| 485P1d | granite | weathered, orange stain | weathering surface | Alu |
| 486P1a | granite | slightly weathered | break | Kln, Mnt |
| 486P1b | granite | weathered, orange stain | break | Kln, Mnt |
| 486P1d | granite | weathered | break | Hal |
| 452P1a | calcsilicate | fresh | break | Act |
| 452P1b | calcsilicate | weathered | break | aspectral |
| 453P2a | calcsilicate | weathered | break | Hal |
| 453P2b | calcsilicate | slightly weathered/fresh | internal weathering joint | Hbl, Hal |
| 453P2c | calcsilicate | weathered, deep red | break | Hbl, Mnt |
| 453P2d | calcsilicate | fresh | break | Hbl |
| 453P2e | calcsilicate | weathered | break (joint) | Act |
| 472P1a | carapace | fresh | break | Act |
| 472P1b | carapace | weathering coat | break | Act |
| 473P1a | calcsilicate | weathered | break | Hal |
| 473P1b | calcsilicate | fresh | break | Ms |
| 482P2a | carapace | slightly weathered | break | Ep |
| 482P2b | carapace | weathered | break | Kln, Ep |
| 482P2c | carapace | weathered, red stain | internal weathering joint | Ep, Hal |
| 483P1a | calcsilicate | fresh | break | aspectral |
| 483P1c | calcsilicate | weathered | internal weathering joint | Mnt, Kln |

**Tab. 18. Description of samples shown in Fig. 17 and Fig. 18. PIMA integration: 1. Mineral abbreviations after Kretz (1983). Other minerals: Alu - alunite, Dc - dickite, Hal - halloysite.**

### *3.6.3 hyperspectral imaging*

The Mallee Gap area can be split in three major domains. These are from west to east the Mallee Gap Granite and surrounding calcsilicate breccias of the Corella Formation, the NNW-SSE striking metasedimentary successions of the Soldiers Cap Group to the west of the Cloncurry Fault and metasedimentary units of the Soldiers Cap Group and calcsilicate breccias of the Corella Formation to the east of the Cloncurry Fault Fig. 19a). The western part is dominated by two granite bodies ("Mallee Gap Granite"), which are characterised by an "intermediate" ferrous iron content (Fig. 19b). The Mallee Gap Granite is shown as a single granite body on the geological map (Fig. 19a), but various geoscience products and field studies suggest the occurrence of two granite bodies, which are separated by a calcsilicate breccia. The calcsilicate breccias have a low spectral response in the wavelength combinations used for the geoscience products and interpretations are therefore difficult. However, the "MgOH composition"-image (Appendix 8.1.3) indicates a rim of calcsilicate rocks partly surrounding the southern Mallee Gap Granite, possibly containing Mg-rich carbonate minerals or talc. The genetic relationship of the whole range of calcsilicate breccias and the Mallee Gap Granite is unclear, but it might be possible to use the hyperspectral images to differ between the carapace of the Mallee Gap Granite and the calcsilicate breccias of the Corella Formation. Fig. 19c) ("white mica composition ") and Fig. 19d) ("mica content/water abundance" and "white mica crystallinity) highlight the rim of the northern Mallee Gap Granite, whereas data from the centre of this granite body are below the threshold. Based on field studies the rim of the northern Mallee Gap Granite is either intensively albitised and/or silicified. The "Kaolin content"-map shows a low Kaolin abundance in the centre of the granite and in the outer part of the albitised/silicified rim. PIMA analyses on samples from various altered and non-altered granites are shown in Fig. 18. Major differences in the reflectance spectra between the non-altered (e.g. 465P1a) and the altered granites (e.g. 459P1f) occur in the 2100 - 2250 nm wavelength range, suggesting variations in the white mica crystallinity.

The NNW-SSE striking metasedimentary successions and interlayered amphibolites of the Soldiers Cap Group are clearly visible in the "Fe2+-content" image and the white mica maps of Fig. 19. An increasing phengitic component in the white micas towards the Cloncurry Fault is accompanied by a decline of the white mica crystallinity. The Cloncurry Fault is consists of a several meters thick quartz vein in this area and is therefore not visible in any of the geoscience products.

The slopes of the Mesozoic Sandstones of the Gilbert River Formation are represented by a varying abundance of ferrous iron Fig. 19b and other components, showed on the various geoscience products. This may lead to obstructions with the interpretation of spectral information from the Soldiers Cap Group and the Corella Formation.

Fig. 20 shows a combination of three mineral group abundance maps, including the "white mica abundance", "Fe2+ associated with MgOH" and "Kaolin abundance". This image allows the direct comparison of the various lithologies and the determination of those dominant mineral species, which have distinct absorption features in the VNIR and SWIR. The Soldiers Cap Group in red is clearly visible due to its high whit mica content, as well as an interlayered amphibolite in green with its high content of trioctahedral silicates. Furthermore the zoning of the two Mallee Gap Granites is visible. The pink colours in the rim of the northern Mallee Gap Granite are related to the occurrence of both white mica and kaolin.

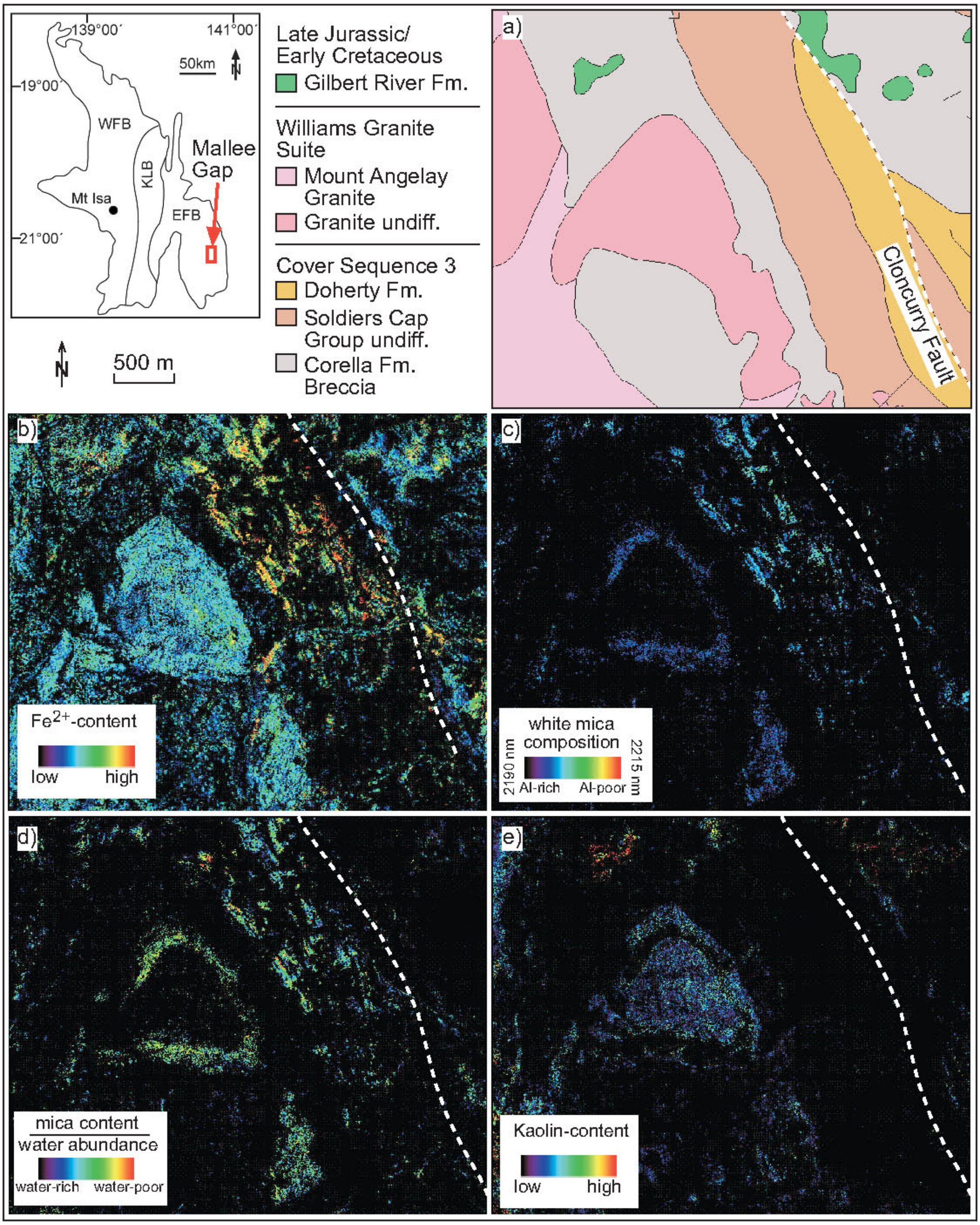


**Fig. 19. Hyperspectral mineral maps from the Mallee Gap area: b) "Fe2+-content": NW-trending Soldiers Cap Group in warm colours, Mallee Gap Granite in bright blue. c) "white mica composition": Inner part of the albitised rim of the northern Mallee Gap Granite characterised by Al-rich white mica. Albitisation of the southern Mallee Gap Granite is pervasive. Soldiers Cap Group characterised by more phengitic mica compared to the albitised Mallee Gap Granite. d) "water content masked white mica content": Inner part of albitised rim of the Northern Mallee Gap Granite shows low water content. e) "Kaolin-content": Core and outer part of the albitised rim of the northern Mallee Gap Granite highlighted by a low Kaolin content. Black is below threshold.**

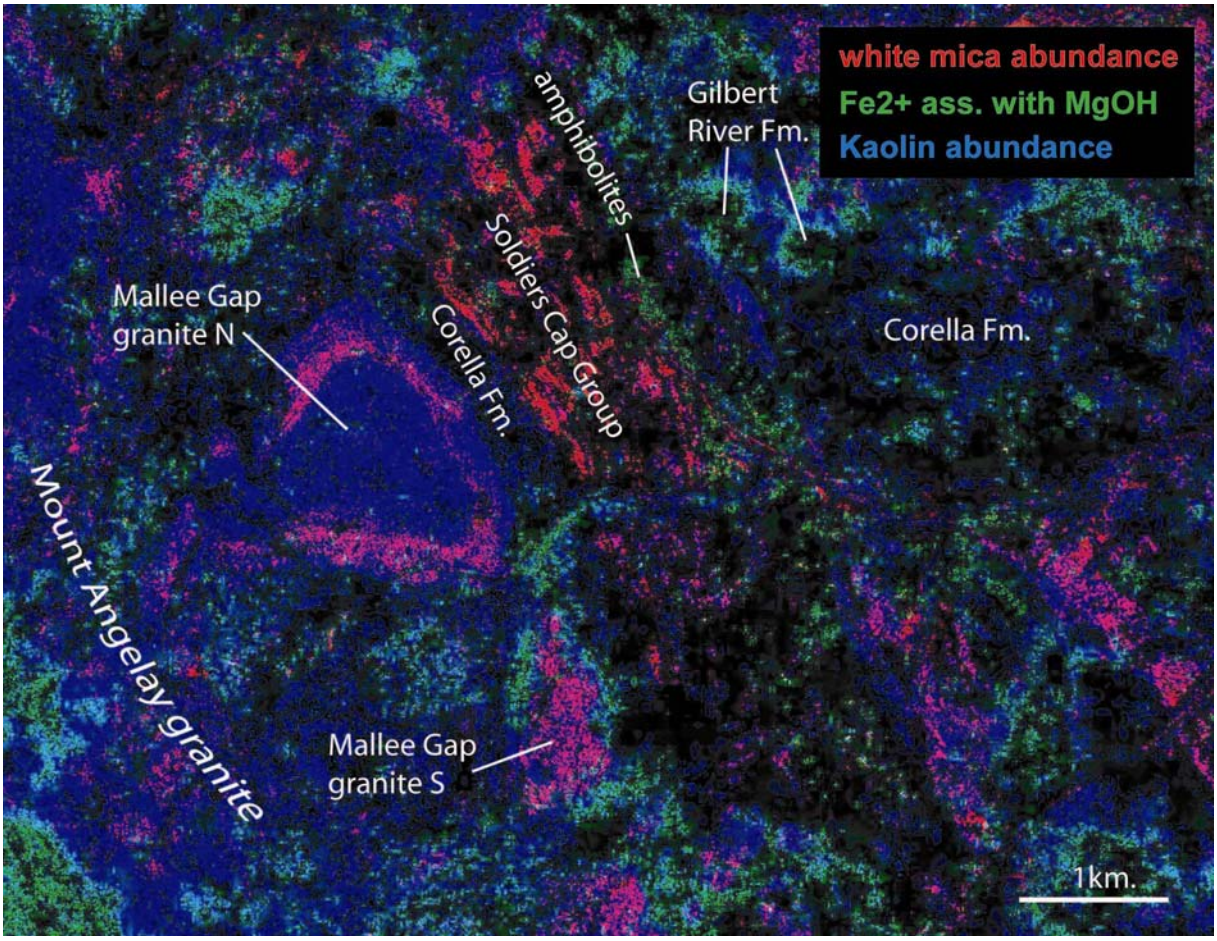


**Fig. 20. Combination image of three geoscience products from the Mallee Gap area: red - "white mica abundance", green - "Fe2+ ass. with MgOH" and blue - "Kaolin abundance". Zoning of the Northern Mallee Gap Granite clearly visible. The Corella Formation has a low spectral response in wavelength regions used for the three geoscience products. The Northwest trending Soldiers Cap Group seems to be confined to an area northeast of the northern Mallee Gap Granite.**

### *3.7 Starra area*

The Starra area is located about 80 to 100 km SSW of Cloncurry in Block H (Selwyn) (Fig. 2). The major country rocks are represented by the N-S striking metasedimentary successions of the Kuridala Formation, which contains interlayered metadolerite/amphibolites and iron stones (Fig. 22a). The ironstones consist of a series of discontinuous lenticular and sheet-like horizons of massive to schistose quartz-magnetite ± hematite rock hosted by various types of schists (Beardsmore, 1992). Field studies report graphite-rich schists in the eastern part of this area, which are typical for the Kuridala Formation in the Selwyn Range. The western part is framed by the peraluminous, muscovite-bearing Gin Creek Granite and the north-eastern part by the highly potassic Mount Dore Granite. The Kuridala Formation is highly strained along the N-S trending Mount Dore Fault and between the ironstones and the Gin Creek Granite. Quaternary alluvial plain deposits cover some area. Mine sites in this area are represented by red dots on the false colour image (Fig. 22b), on which also the extension of other man made features (e.g. mine dumps) is clearly visible. In the Starra area major Cu-Au deposits are hosted by Fe oxide rich units west of the Mount Dore Fault.

### *3.7.1 PIMA analyses*

Reflectance spectra of PIMA analyses of selected samples from the Starra area (Tab. 19) are shown in Fig. 21.

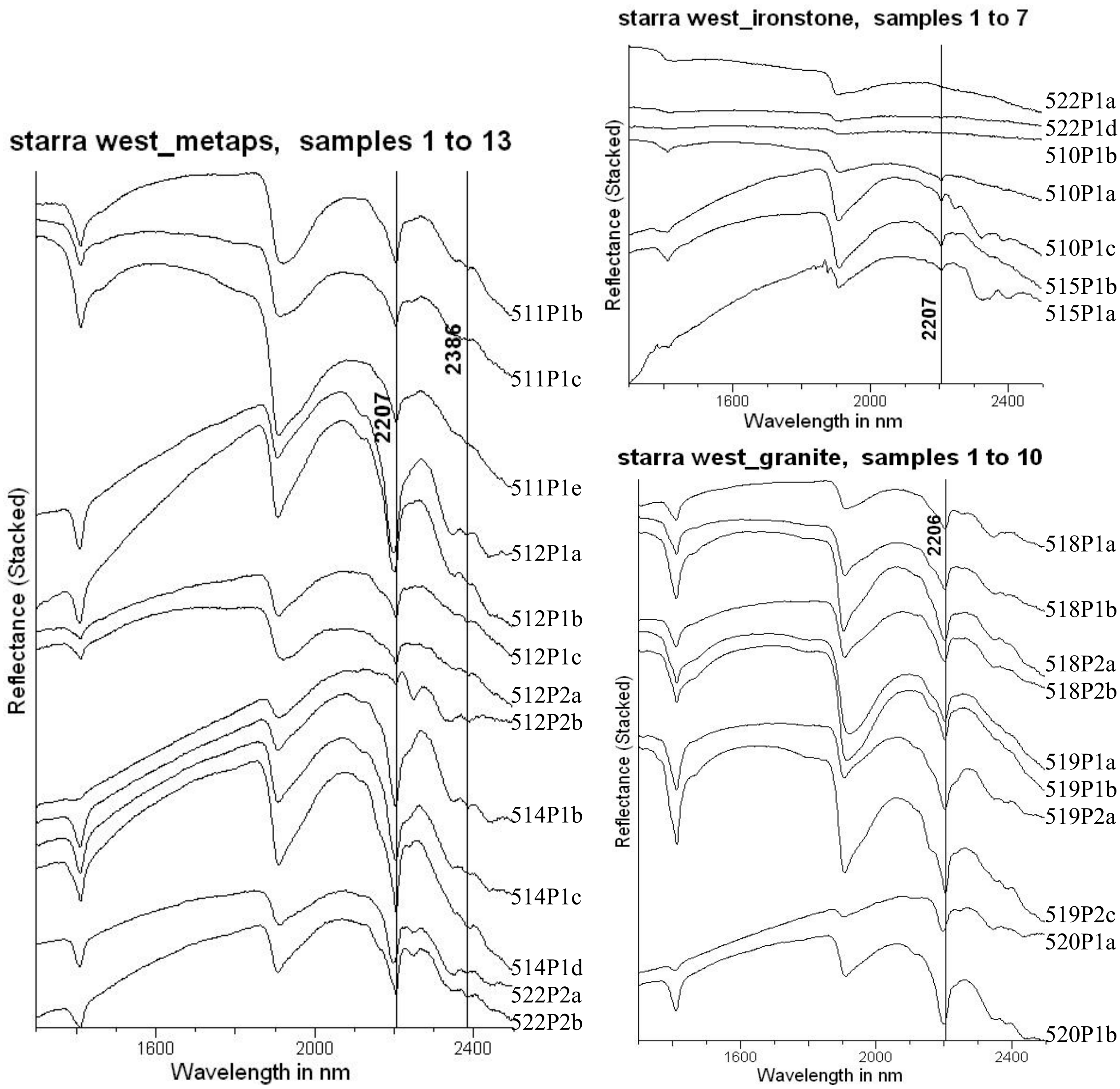


**Fig. 21. PIMA spectra of samples from the Starra area. Left: metasedimentary units of the Kuridala Formation. Top right: Ironstones and amphibolites. Bottom right: Gin Creek Granite. Sample description in Tab. 19.**

| sample | rock type | surface | cut | spectra dominating minerals (acc. to TSG auxmatch or *own int.*) |
|---|---|---|---|---|
| 511P1b | metapsammite | weathered, rough | break | Ms, Kln |
| 511P1c | metapsammite | weathered | break | Ms, Hal |
| 511P1e | metapsammite | fresh | break | Mnt, Ill |
| 512P1a | metapsammite | weathered | parallel S1 | Ill |
| 512P1b | metapsammite | weathered, red stain | parallel S1 | Ill |
| 512P1c | metapsammite | weathered | parallel S1 | Hal, Ill |
| 512P2a | metapsammite | weathered | parallel S1 | Hal |
| 512P2b | metapsammite | weathered | parallel S1 | Bt |
| 514P1b | metapsammite | fresh | oblique S1 | Ms, Hal |
| 514P1c | metapsammite | weathered | parallel S1 | Ms, Hal |
| 514P1d | metapsammite | weathered, red stain | parallel S1 | Hal, Ms |
| 522P2a | micaschist | slightly weathered | parallel S1 | Ill |
| 522P2b | micaschist | weathered, red stain | parallel S1 | Ill, Kln |
| 522P1a | ironstone | weathered | perpendicular S0 | aspectral |
| 522P1d | ironstone | weathered | oblique So (Sf?) | aspectral |
| 510P1a | ironstone | weathered, red stain | break | Hal, Hbl |
| 510P1b | ironstone | weathered | break | aspectral |
| 510P1c | ironstone | weathered, red stain | parallel S1 | Phl, Hal |
| 515P1a | amphibolite | weathered | parallel S1 | *Rbk* |
| 515P1b | amphibolite | weathered | parallel S1 | Ms |
| 518P1a | granite | weathered | break | *Ms* |
| 518P1b | granite | weathered | internal weathering joint | *Ms* |
| 518P2a | granite | weathered | break | *Ms* |
| 518P2b | granite | fresh | break | *Ms* |
| 519P1a | granite | weathered | break | *Ms* |
| 519P1b | granite | fresh | break | *Ms* |
| 519P2a | granite | weathered | break | Ms |
| 519P2c | granite | fresh, rough | break | *Ms* |
| 520P1a | granite | slightly weathered | parallel S1 | Ms |
| 520P1b | granite | weathered | parallel S1 | Ill |

**Tab. 19. Description of samples shown in Fig. 21. PIMA integration: 1. Mineral abbreviations after Kretz (1983). Other minerals: Alu - alunite, Hal - halloysite.**

### *3.7.2 hyperspectral imaging*

In comparison of the geological map, false colour image and the white mica products with the field observations a good accuracy of the white mica products can be stated. Mine dumps and mine sites are masked out and there are low interferences with man made features and data shown on these hyperspectral images (e.g. Fig. 22). However, man made feature interfere with other geoscience products, such as the kaolin content.

The white mica products in Fig. 22 highlight the petrographic differences between the Mount Dore Fault and the surrounding lithologies. The "white mica composition" image shows that the Al-content in white mica decreases from the Mount Dore Fault towards the Fe oxide units. To the west of the Fe oxide units a dominance of Al-rich white micas is evident in the Kuridala Formation. The chemical gradient from muscovite compositions along the fault towards phengitic micas towards the reducing rocks suggests a close relationship of the Mount Dore Fault to the Fe oxide hosted Cu-Au deposits and its importance as pathway for mineralising fluids.

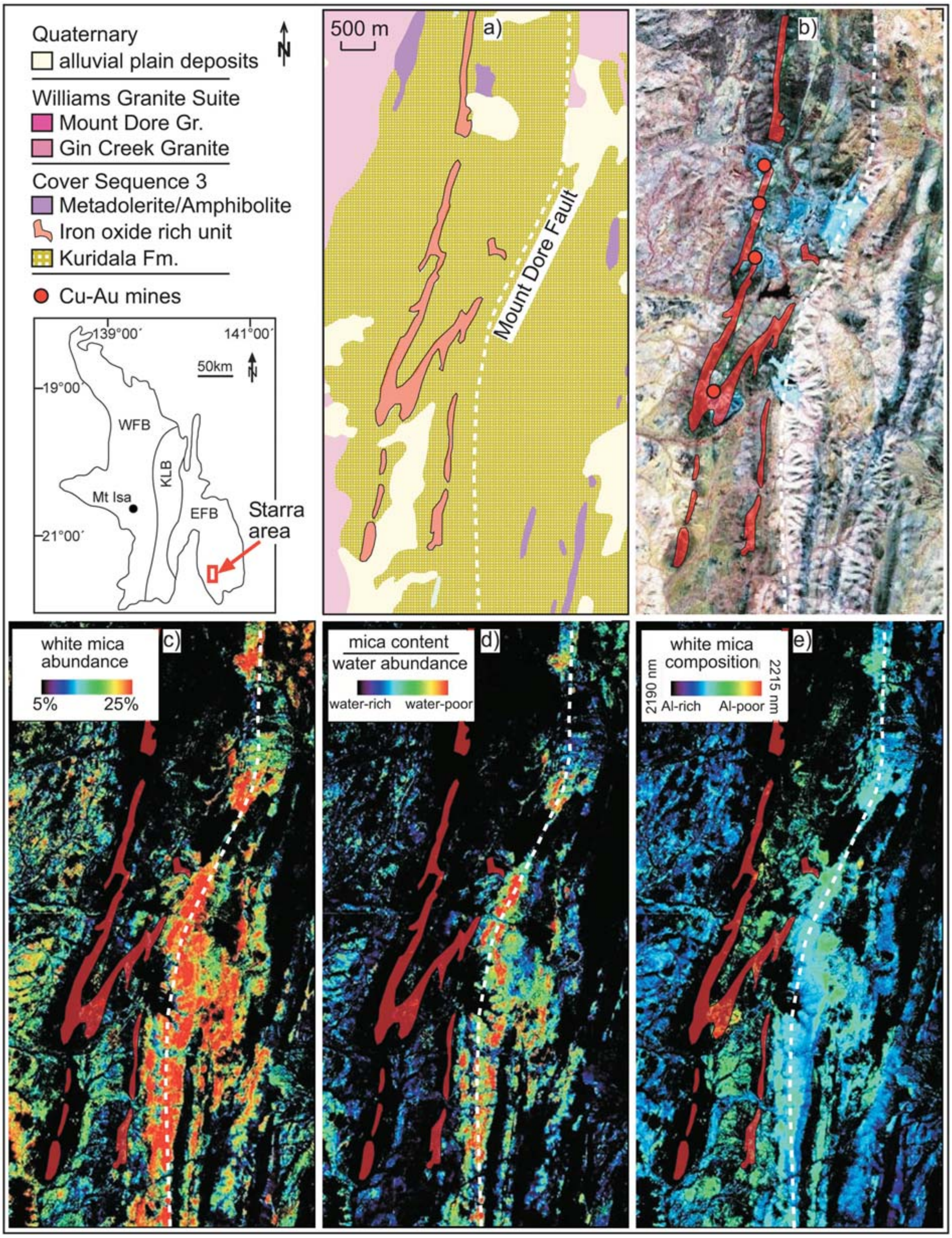


**Fig. 22. Geological map (a) and Hyperspectral mineral maps from the Starra area: b) "false colour image" showing the distribution of mine sites and tailings (in bright blue). c) "white mica abundance": High white mica abundance along the Mount Dore Fault indicated by red colours. d) "water content masked white mica content": High crystallinity of white mica along the Mount Dore Fault. e) "white mica composition": Gradual increasing phengitic composition of white micas away from the Mount Dore Fault. Black is below threshold.**

### *3.8 Mary Kathleen Fold Belt*

Data were collected from four key areas in the Mary Kathleen Fold Belt: "Corella N", "Corella S", "MKFB NE" and "Cameron Strain Shadow", which are covered by the HyMap swaths Block E and F (Fig. 3). The dominating lithologies of these areas comprise metasedimentary successions of the Argylla Formation, the Ballara Quartzites and the Corella Formation, and the Lime Creek Metabasalt Member. Especially in the western part of blocks E and F, intercalated amphibolites/metadolerites can be found in the Corella Formation. The listed lithologies are generally trending N-S to NE-SW (Fig. 3) and were intruded by the Wonga Batholith and the Lunch Creek Gabbro. The key areas are only to a minor part covered by Quaternary alluvial plain deposits.

#### *3.8.1 PIMA analyses*

Reflectance spectra of PIMA analyses of selected samples from the Mary Kathleen Fold Belt (Tab. 20, Tab. 21) are shown in Fig. 23 and Fig. 24.

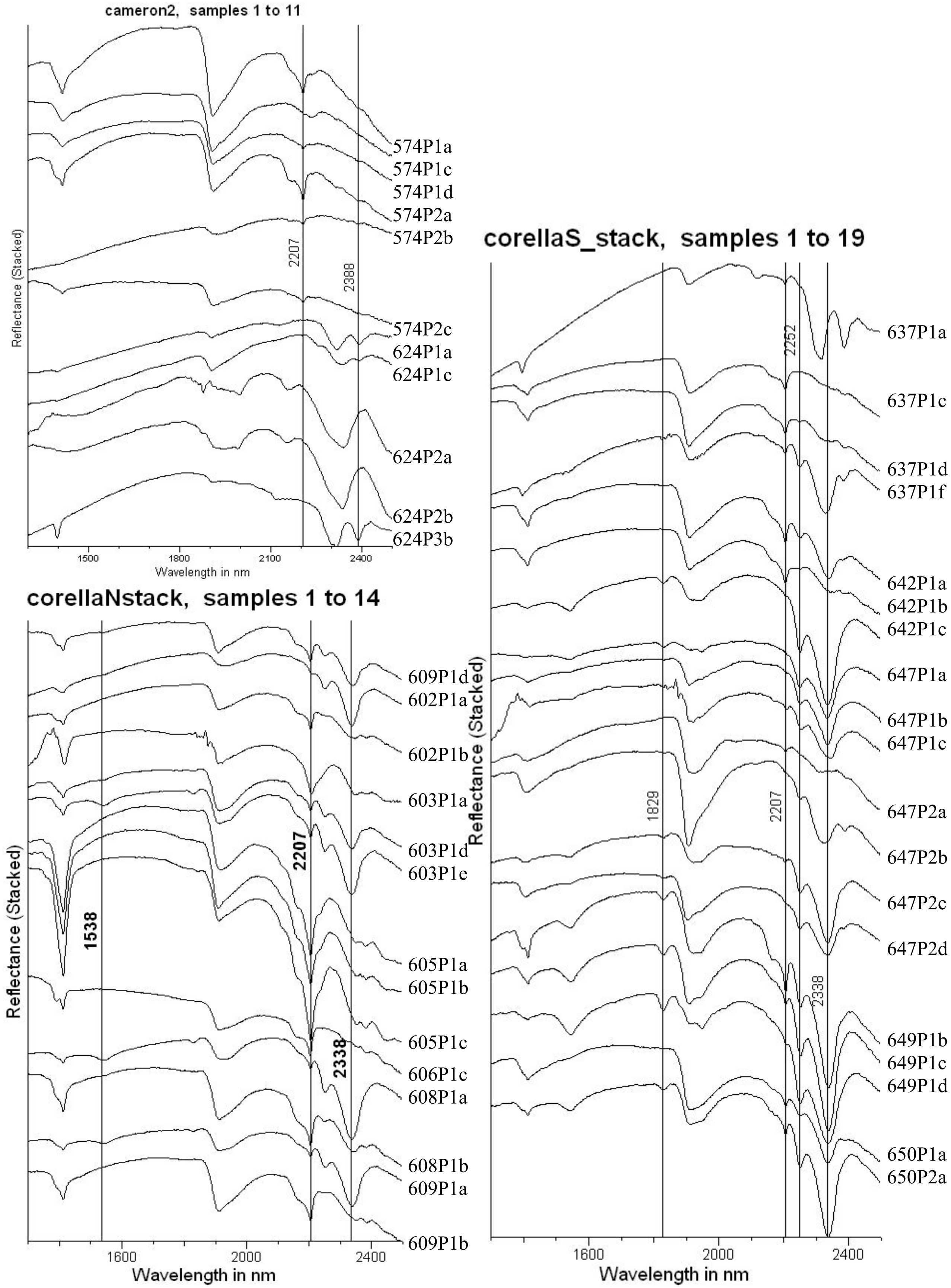


**Fig. 23. PIMA spectra of samples from the Mary Kathleen Fold Belt (top left: Cameron, bottom left: Corella N, right: Corella S area). Sample description in Tab. 20.**

| sample | rock type | surface | cut | PIMA integration | spectra dominating minerals (acc. to TSG auxmatch or *own int.*) |
|---|---|---|---|---|---|
| 574P1a | quartz-vein (Cameron Fault) | weathered, upper side | parallel S0 | 1 | Mnt, Kln |
| 574P1c | | fresh | perpendicular S0 | 1 | Mnt |
| 574P1d | | weathered | joint | 1 | Mnt, Kln |
| 574P2a | | weathered | weathering surface, rough | 1 | Hal |
| 574P2b | | weathered, black coating | weathering surface, rough | 1 | Hal |
| 574P2c | | fresh | break | 1 | Hal |
| 602P1a | calcsilicate | weathered, upper side | parallel S0 | 1 | Cc, *Bt* |
| 602P1b | calcsilicate | weathered, lower side | parallel S0 | 1 | Kln |
| 603P1a | micaschist | weathered, upper side | parallel S1 | 1 | Ms |
| 603P1d | calcsilicate | weathered, upper side | parallel S0 | 1 | *Mg-Cc*, Dc |
| 603P1e | calcsilicate | weathered, lower side | perpendicular S0 | 1 | *Mg-Cc*, *Bt* |
| 605P1a | micaschist | weathered | parallel S1 | 1 | Ms, Kln |
| 605P1b | micaschist | weathered | oblique S1 | 1 | Ms, Kln |
| 605P1c | micaschist | fresh | oblique S1 | 1 | Ms, Kln |
| 606P1c | micaschist | fresh | perpendicular S1 | 1 | Hal |
| 608P1a | regolith | weathered | weathering surface | 1 | Bt, *Mg-Cc* |
| 608P1b | regolith | weathered | weathering surface | 1 | Hal, *Bt* |
| 609P1a | calcsilicate | weathered, upper side | parallel S0 | 1 | *Mg-Cc*, *Bt* |
| 609P1b | calcsilicate | weathered, lower side | parallel S0 | 1 | Kln, Ill |
| 609P1d | calcsilicate | fresh | perpendicular S0 | 1 | *Mg-Cc*, Hal, *Bt* |
| 624P1a | amphibolite | fresh | break | 1 | Hbl |
| 624P1c | amphibolite | fresh | break | 4 | Hbl |
| 624P2a | amphibolite | fresh | break, rough | 1 | Cc |
| 624P2b | amphibolite | weathered joint | break, rough | 1 | *Mg-Cc* |
| 624P3b | amphibolite | fresh | break, rough | 4 | Act |
| 637P1a | calcsilicate | weathered, upper side | parallel S0, rough | 2 | Act |
| 637P1c | calcsilicate | weathered, soil | perp. S0, break | 2 | Hal |
| 637P1d | calcsilicate | weathered, lower side, red | parallel S0 | 2 | Hal |
| 637P1f | calcsilicate | weathered | perp. S0, break | 1 | Act, Phl, *Mg-Cc* |
| 642P1a | calcsilicate | weathered, upper side | oblique S0 | 1 | Hal, Cc |
| 642P1b | calcsilicate | weathered, some soil | oblique S0 | 1 | Hal, *Cc* |
| 642P1c | calcsilicate | fresh | perpendicular S0 | 1 | Bt, Cc |
| 647P1a | calcsilicate | weathered | joint | 1 | Bt, Cc |
| 647P1b | calcsilicate | weathered | joint | 2 | Bt, Cc |
| 647P1c | calcsilicate | weathered, some soil | joint | 1 | Cc, *Bt* |
| 647P2a | calcsilicate | weathered | parallel S0,weathering surface | 1 | *Mg-Cc* |
| 647P2b | calcsilicate | slightly weathered | parallel S0 | 1 | Mnt, *Mg-Cc* |
| 647P2c | calcsilicate | weathered | perpendicular S0, break | 1 | *Mg-Cc* |
| 647P2d | calcsilicate | break, partly white weathering coating | perpendicular S0, break | 1 | *Mg-Cc* |
| 649P1b | calcsilicate | weathered, upper side | parallel S0 | 1 | *Mg-Cc*, Dc |
| 649P1c | calcsilicate | weathered | perpendicular S0 | 1 | *Mg-Cc* |
| 649P1d | calcsilicate | fresh | perpendicular S0 | 1 | Bt, *Mg-Cc* |
| 650P1a | calcsilicate | weathered | break | 1 | *Mg-Cc* |
| 650P2a | calcsilicate | weathered | parallel S0 | 1 | *Mg-Cc* |

**Tab. 20. Description of samples shown in Fig. 23. Mineral abbreviations after Kretz (1983). Other minerals: Dc - Dickite, Hal - halloysite, Mg-Cc - Mg-rich calcite.**

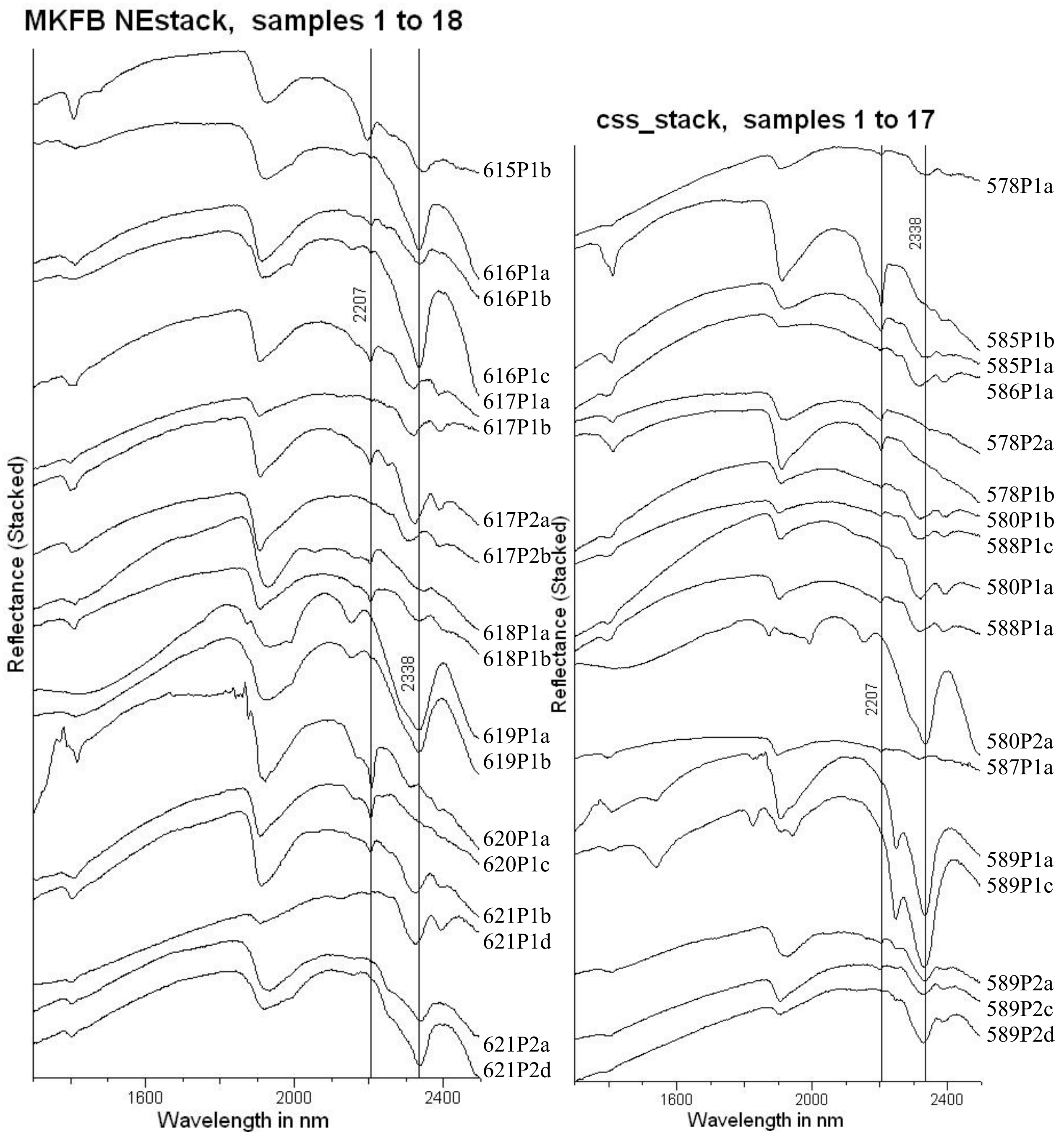


**Fig. 24. PIMA spectra of samples from the Mary Kathleen Fold Belt (MKFB NE and Cameron Strain Shadow areas). Sample description in Tab. 21.**

| sample | rock type | surface | cut | PIMA integration | spectra dominating minerals (acc. to TSG auxmatch or *own int.*) |
|---|---|---|---|---|---|
| 578P1a | metabasalt | weathered, upper side | parallel S0 | 1 | aspectral |
| 578P1b | metabasalt | weathered, lower side | parallel S0 | 1 | Hal, Non |
| 578P2a | metabasalt | weathered | weathering surface, rough | 1 | Ill |
| 580P1a | amphibolite | weathered, black coating | parallel S1 | 1 | Hbl |
| 580P2a | calcite | weathered, dark | weathering surface | 1 | Cc |
| 585P1a | metabasalt | weathered, red | joint | 2 | Ill, Act, *Cc* |
| 585P1b | metabasalt | weathered | parallel S1 | 2 | Hal |
| 586P1a | metabasalt | weathered, dark | oblique S1 | 1 | Hbl |
| 587P1a | metarhyolite | weathered | parallel S1 | 2 | aspectral |
| 588P1a | amphibolite | weathered, upper side | parallel S1 | 2 | Act, Mnt |

| | | | | | |
|---|---|---|---|---|---|
| 588P1c | amphibolite | fresh | perpendicular S1 | 2 | Hbl, Mnt |
| 589P1a | epidoisite | weathered, upper side | parallel S1 | 2 | Ep, Phl |
| 589P1c | epidoisite | fresh | perpendicular S1 | 1 | Ep, Phl |
| 589P2a | calcsilicate | weathered, dark | weathering surface | 1 | Hbl, Ep |
| 589P2c | calcsilicate | weathered | parallel S1 | 1 | Hbl, Mnt |
| 589P2d | calcsilicate | fresh | perpendicular S1 | 1 | Hbl, Cc |
| 615P1b | calcsilicate | weathered | parallel S1 | 1 | *Mg-Cc*, Ill |
| 616P1a | calcsilicate | weathered, upper side | parallel S1 | 2 | Cc |
| 616P1b | calcsilicate | weathered, lower side | parallel S1 | 1 | Cc, Hal |
| 616P1c | calcsilicate | weathered | oblique S1 | 1 | Cc, Phl |
| 617P2a | calcsilicate | weathered | | 2 | Hbl, Hal |
| 617P2b | calcsilicate | fresh | | 2 | Hbl, Mnt |
| 618P1a | calcsilicate | weathered, dark | joint | 2 | aspectral |
| 618P1b | calcsilicate | weathered, bright | joint | 1 | Hal, *Mg-Cc* |
| 619P1a | calcite | weathered, bright | cleavage | 2 | *Mg-Cc* |
| 619P1b | calcite | weathered, dark | cleavage | 2 | *Mg-Cc* |
| 620P1a | calcsilicate | weathered, deep red | joint | 1 | Kln |
| 620P1c | calcsilicate | fresh | break | 1 | Hal |
| 621P1b | calcsilicate | weathered, upper side | parallel S0, rough | 1 | *Mg-Cc* |
| 621P1d | calcsilicate | fresh | perpendicular S0 | 1 | Act, Rbk |
| 621P2a | metabasalt | weathered | parallel S1 | 1 | *Cc*, Ep |
| 621P2d | metabasalt | fresh | perpendicular S1 | 1 | Int Chl, Cc |

**Tab. 21. Description of samples shown in Fig. 24. Mineral abbreviations after Kretz (1983). Other minerals: Hal - halloysite, Non - nontronite.**

***3.8.2 hyperspectral imaging***

The MgOH products can be used to differentiate the various mafic intrusives and metasedimentary successions of the Corella Formation in the Mary Kathleen Fold Belt. The "MgOH composition" image for example indicates a high content of low Mg-amphiboles in metadolerites and amphibolites in the Cameron Strain Shadow area (Fig. 25). Blue to green colours of the Lime Creek Metabasalt Member in the same image, suggest Mg-rich trioctahedral silicates in the metavolcanic rocks. Clearly visible is the NE-trending offset of the county rocks along the Cameron Fault. The bright blue, NE-trending lens at the north-eastern end of the Cameron Fault represents phyllites and/or metavolcanic rocks enclosed in the Corella Formation (unit "Pkc2t" on geological map), characterised by a distinct MgOH composition. Considerable variations of the mineral assemblages and/or composition of the Corella Formation are envisaged in the Corella N and S areas (Fig. 25), which are presumably due to a varying Mg-content in carbonate minerals. Further compositional changes of the Corella Formation are indicated by the "$Fe^{2+}$ ass. with MgOH" (Fig. 25) and the "ferric oxide associated with MgOH" product (Appendix 8.1).
Other major lithologies of the Mary Kathleen Fold Belt, like the Wonga Batholith, are clearly visible in the "Al-smectite content" and "ferric oxide content" images (Appendix 8.1).

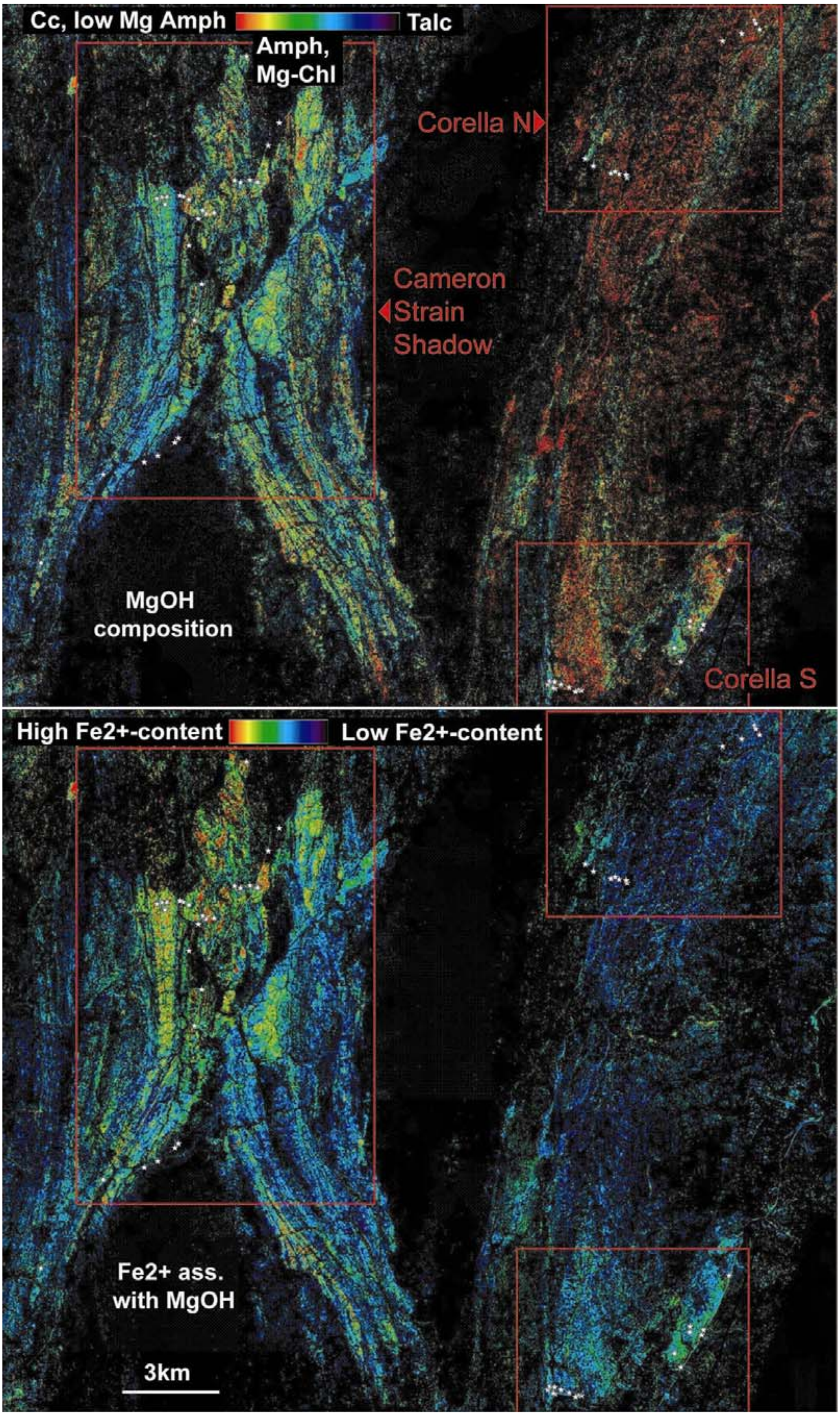


**Fig. 25. Hyperspectral mineral maps from the Mary Kathleen Fold Belt showing a) the "MgOH composition" and b) "ferrous iron associated with MgOH". In the eastern part of both images variations in the composition of the Corella Formation is evident. Black is below threshold. White stars are sample points (sample numbers available from MapInfo workspace in Appendix (8.1.3). For location of the areas see Fig. 3.**

### *4. Mapping of occurring rock units with spectral remote sensing data from the Eastern Fold Belt*

Mineral maps can be used to differentiate various lithologies based on their mineral composition. The "mica abundance" image outlines the distribution of metasedimentary rocks. The "Fe2+ associated with MgOH image" shows amphibolites interlayered in metasediments of the Soldiers Cap Group and discordant dolerites (Fig. 4, Fig. 7). For ground-truthing PIMA studies, XRD/XRF analyses and thin section studies were compared with the hyperspectral mineral maps. The digital geological map of the Camel Hill/Cloncurry Fault shown in Fig. 26 is based on interpretation of the hyperspectral data in combination with unpublished maps by T. Blenkinsop and N. Oliver. It is included as GIS-layers in the MapInfo Workspace (Appendix 8.1.3). Various white mica mineral maps help to identify metasedimentary lithologies, relative metamorphic overprint, pegmatite bodies and Jurassic Mesas (e.g. water abundance relative to white mica abundance from Soldiers Cap Group).

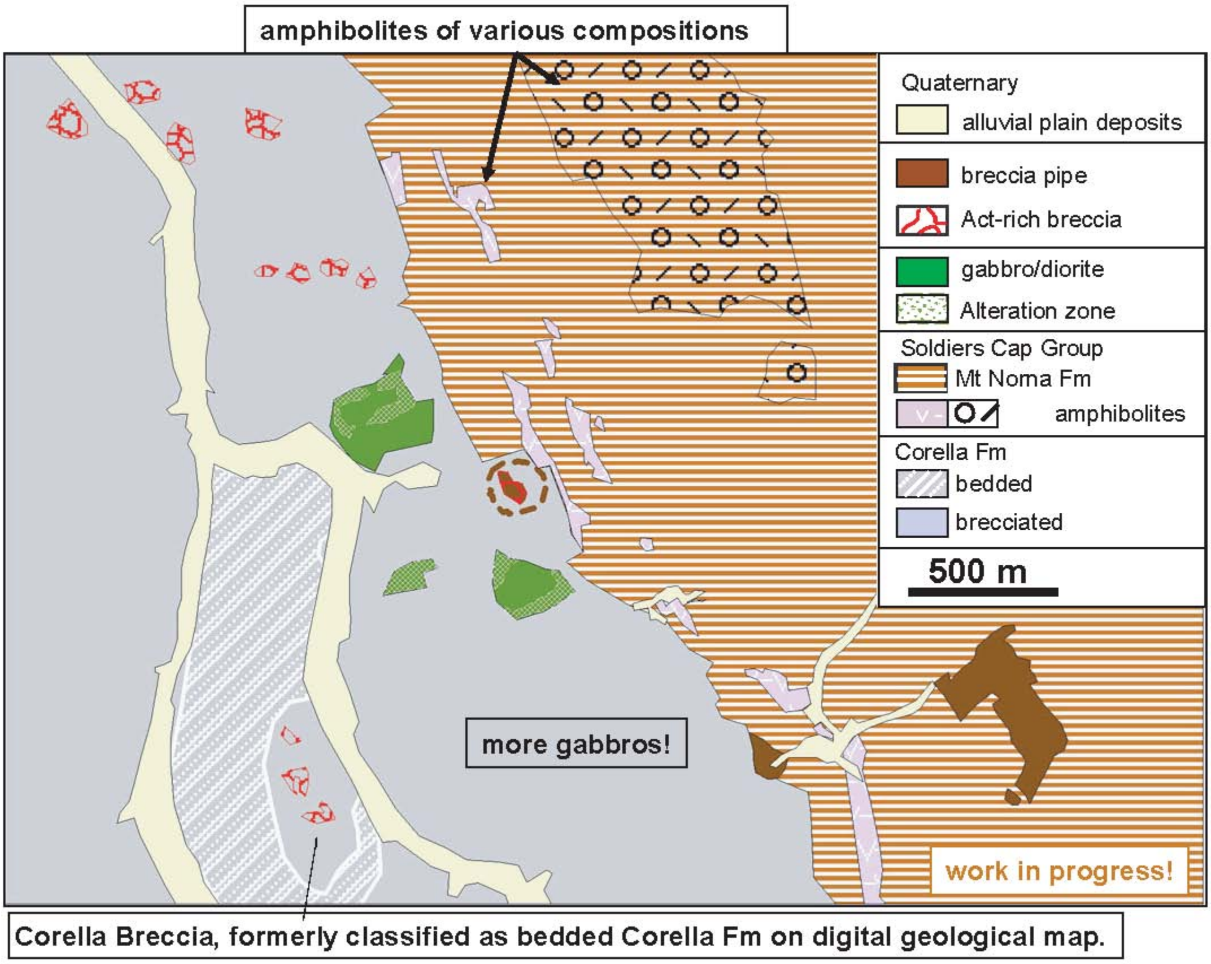


**Fig. 26. Preliminary geological map of the Camel Hill area, compiled from hyperspectral mineral maps in combination with unpublished maps by T. Blenkinsop and N. Oliver. The two different amphibolites haven't been mapped in this area before. Gabbro bodies in this area are not known from the published geological maps and their alteration zones have not been described before. A differentiation of bedded and brecciated Corella Formation is possible with the combination of various hyperspectral images. Actinolite-dominated breccia bodies appear on the "Fe2+ associated with MgOH" product.**

### *4.1 Calvert and Isa Superbasins*

The most abundant successions of the Calvert and Isa Superbasins in the studied areas are the Corella Formation and the Soldiers Cap Group (Fig. 2).
The spectral data of calcsilicates of the Corella Fm in the Cloncurry District are difficult to interpret. Only the bedded Corella Formation with interlayered metapelites and/or metapsammites can sometimes be distinguished from other successions of the Corella Formation. Substantial changes in the mineral assemblages of these rocks and the proximity of various mafic units, which partly contain similar mineral assemblages, lead to an inconsistent appearance in the geoscience products. However, in the Corella N and Corella S areas, distinct changes in the Corella Formation are evident (Fig. 25) and hyperspectral data from Blocks E and F would assist studies of the compositional changes in the calcsilicates.
The metapelites and metapsammites of the Soldiers Cap Group can be investigated with the various white mica products. Examples are presented in Fig. 7a, Fig. 11a, Fig. 12, Fig. 16c, Fig. 19c and d, and Fig. 20. Further studies of white mica crystallinity or alteration products of index minerals like kyanite or andalusite (e.g. north-western Snake Creek Anticline) could provide information about metamorphic facies. Distinguishing artefacts of primary mineral assemblages (e.g. pelite vs. psammite) from alteration minerals of metamorphic index minerals might be complicated. Furthermore, domains of intense albitisation in the Soldiers Cap Group could be visible in some of the white mica products (e.g. comparing Fig. 4 with Fig. 7; Laukamp, 2007a).
Mafic sills (e.g. amphibolites, metadolerites) interlayered in the metasedimentary units of the Isa Superbasins, and strata-discordant dykes of the Cloncurry District can be compared on the various MgOH products (Fig. 7b, Fig. 9, Fig. 11b and c). The variety of mineral assemblages and/or chemical compositions of trioctahedral silicates is exemplified in mafic sills located in the northern Snake Creek Anticline and the Tool Creek area. In some of the amphibolite layers of the northern and north-eastern Snake Creek Anticline, a primary zoning from mafic to felsic composition was observed (T. Blenkinsop, pers. comm.), which is confirmed by the "Fe2+ ass. with MgOH" and "MgOH composition" products.

### *4.2 Granitoids in the Eastern Fold Belt*

Vast areas of the Mount Isa Inlier consist of granitoid rocks, which intruded over time-span of at least 250 million years throughout the Paleoproterozoic. The importance of igneous bodies in the EFB is suggested by the close spatial relationship between IOCGs and intrusions, such as intra-ore intermediate dykes at the Mount Elliott Cu-Au deposit (Wang and Williams, 2001), pre- to syn-ore pegmatites at the Osborne Cu-Au deposit (Gauthier et al., 2001) and magmatic-hydrothermal mgt-rich mineralization within the Squirrel Hills Granite (Perring et al., 2000). Hyperspectral mineral maps can be used to differentiate various granite bodies in the Eastern Fold Belt (Fig. 2) and give therefore possible hints for exploration and determination of possible source rocks.
The two dominant granite bodies in the southern part of Block H (Selwyn), the Gin Creek Granite in the west and the Mt Dore Granite in the east (Fig. 2), for example, are quite distinct in their composition. The peraluminous Gin Creek Granite consists mainly of non-foliated, partly porphyritic biotite granites and weakly foliated tourmaline-muscovite leucogranites (Blake, 1987) and intruded during the Wongan event (1750 - 1730 Ma). The Mt Dore Granite is a non-foliated, partly porphyritic, biotite and hornblende-biotite granite with minor microgranites, aplites and pegmatites (Blake, 1987) and is part of the Williams-Naraku Suite, which intruded after the Isan peak metamorphism between 1550 - 1490 Ma (Rubenach et al., 2008, amongst others). In contrary to the Gin Creek Granite, the Mt Dore Granite has a high

K-content, which is typical for granitoids of the Williams-Naraku Suite (Mark & Foster, 2000) and can be easily recognised in radiometric images. These high K-values can be recognised in the white mica products as well (Appendix 8.1.3).
Another way to differentiate the granite bodies in the Mount Isa Inlier is based on the difference in their redox state (Belousova et al, 2001). Granitoids of the Williams Batholith are highly oxidised, whereas the Kalkadoon, Sybella and Naraku batholiths have lower $Fe_2O_3/FeO$ ratios. The lower redox state of the Mt Dore Granite is confirmed by high values of ferric oxide shown in the "ferric oxide abundance" image (Appendix 8.1.3) compared to a low ferric oxide content in the Wongan Gin Creek Granite.

#### *4.3 Breccia Pipes*

"MgOH composition-", “MgOH content-” and "$Fe^{2+}$ associated with MgOH”-maps enable us to separate metasediments and amphibolites from hydrothermal breccias (e.g. Suicide Ridge Breccia Pipe: Fig. 11) and various mafic units in the field area, based on their distinct amphibole and chlorite chemistry (e.g. Camel Hill area: Fig. 9).
Discordant breccia pipes and amphibolites S of Cloncurry contain various types of amphiboles. Different spectral responses are based on the $Mg/Mg+Fe^{2+}$-ratio and Tschermaks Substitution (e.g. Tool Creek: Fig. 14).

#### *4.4 Jurassic Mesa*

The clastic sediments of the Mesozoic Gilbert River Formation are covering the Paleoproterozoic strata in a horizontal way and quite often interfere with the interpretation of multi- and hyperspectral mineral maps in the Mount Isa Inlier. Recognition of these "Jurassic Mesas" is therefore essential, when exploring or mapping in this area.
Basically a good way to start is to look for the typical amoeboid or circular shapes of the Jurassic Mesas (Gilbert River Formation in green in Fig. 2). Jurassic Mesas are often distinguishable from other units by the extreme high content of ferric oxides and therefore well displayed in the "$Fe^{3+}$ abundance" image (Appendix 8.1.3). A typical Jurassic Mesa is shown in Fig. 27. The "false colour" image shows the amoeboid to circular shape and the embedded picture envisages the Paleoproterozoic units, which were protected from weathering by the Mesa. This results in relatively good outcrops of the Paleoproterozoic strata surrounding the Mesa. This is particular evident on the "mica abundance" image of the northern subset of Block I (Fig. 7), where the Jurassic Mesas cover metasedimentary successions of the Llewellyn Creek Formation. The signal of the weathering material on the slopes of the Mesas is virtually the same as for the well outcropping Llewellyn Creek Formation in the north-eastern Snake Creek Anticline. The sandstones themselves do not contain enough white mica and are therefore not visible in the "white mica abundance" image. When adding other geoscience products such as the "kaolin abundance", the Jurassic Mesas, containing kaolin, can easily be distinguished from the Llewellyn Creek Formation (Fig. 12). However, some of these Jurassic Mesas are covered with dense vegetation, which causes interferences with the kaolin "abundance" images. Furthermore, the "kaolin abundance" image is not applicable in areas, where the Gilbert River Formation covers granitoids, as the latter ones are often characterised by a medium kaolin content (Mallee Gap: Fig. 19). In these cases the mineral assemblage of the Jurassic Mesas has to be compared with the Paleoproterozoic units in detail.

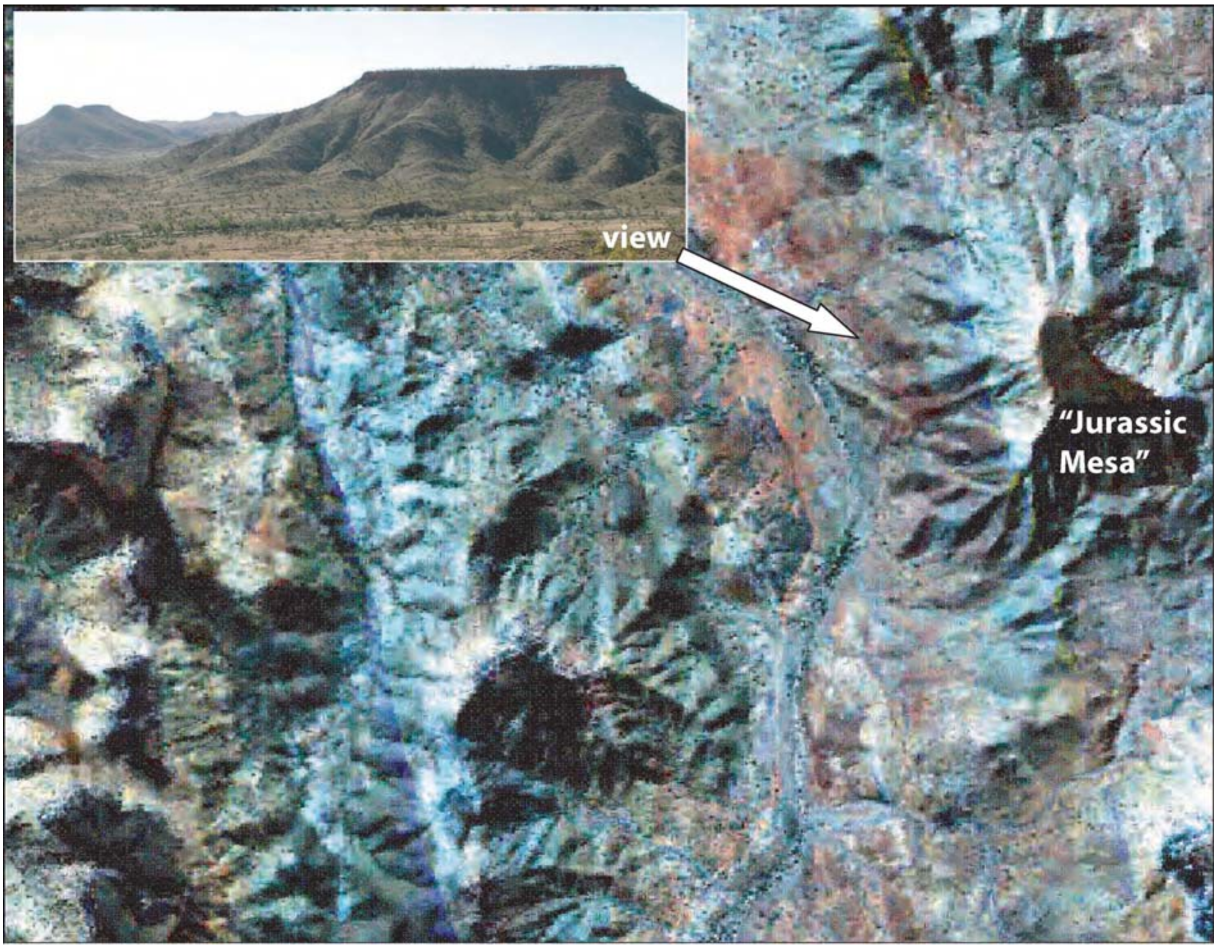


**Fig. 27. "False colour" image of the Suicide Ridge area, showing a Jurassic Mesa (lower side of "false colour" image: approximately 6km).**

#### *4.5 Cloncurry District HyMap interpretation sheet*

For some of the key areas in the Cloncurry District (Camel Hill, Suicide Ridge, Tool Creek) a spread sheet was constructed, listing the various Paleoproterozoic units, their typical mineral assemblage, their appearance in selected geoscience products and some interpretation from the hyperspectral mineral maps. An excerpt of the spread sheet is shown in Tab. 22 and the full list is enclosed in Appendix 8.7.

| mineral map | area | Soldiers Cap Group (metapsammites and/or micaschists) | Amphibolites | Corella Fm (Pkc) | Corella Breccia (Pkcbr) | Breccia Pipe Hem-staining | Carapace | Granites | Gabbros |
|---|---|---|---|---|---|---|---|---|---|
| mineral assemblage | Camel Hill (CH) | ± quartz, feldspar, *white mica, chlorite*, biotite, *clay minerals*, and, ky, sil, grt | **Ca-amphiboles (hornblende - tschermakite)**, plagioclase, ilmenite, ± quartz, almandine, **cummingtonite**, magnetite, titanite; **clinochlore**, *ankerite*, *meionite* | *calcite, scapolite*, k-feldspar, biotite, magnetite, titanite; minor alteration: **actinolite** (with lesser magnesio-hornblende, tremolite, Fe-act) | *calcite, scapolite*, k-feldspar, biotite, magnetite, titanite; local alteration: **actinolite** (with lesser magnesio-hornblende, tremolite, Fe-act) | < ~, see Hem-stained Breccia Pipes | - | - | plagioclase, *pyroxene*, **amphibole** (rim: more **chlorite, amphibole**, |
| | Suicide Ridge(SR) | | | | | cpx (dio), K-feldspar, albite, magnetite, quartz, **actinolite** (act. - Fe-act.); hematite, *calcite*, talc | cpx (dio), K-feldspar, ± albite, *calcite*, **clinochlore, actinolite** | **Mg-hornblende, Mg-edenite** | - |
| | Tool Creek | | | - | - | Breccia vein: qtz, ankerite-veins, dol, meionite, alb, ± kaolinite, chl. (Hem-stained Breccia Pipes) | - | - | - |
| MgOH content | Suicide Ridge | no signal | n.a. | no signal: few outcrops, vegetation | no signal: few outcrops, vegetation | low - medium (violett - green): cpx content higher than act content | low signal due to high cpx content, very low amph and chl content and less weathering | no signal | low (blue): low reflectance (dark rocks) |
| | Camel Hill | no signal | n.a. | | | no signal | - | - | |
| | Tool Creek | no signal | n.a. | | | no signal | - | - | - |
| MgOH composition | Suicide Ridge | no signal | high (red): Ca-amphiboles, clinochlore (Mg-rich chlorite); negligible influence of ankerite | no signal: few outcrops, vegetation | no signal: few outcrops, vegetation | low (blue - green): high amphibole content | low signal due to high cpx content, very low amph and chlorite content and less weathering | no signal | - |
| | Camel Hill | no signal | | | | no signal | - | - | core: medium (blue - green); rim: medium - high (green - yellow): various amph-composition. |
| | Tool Creek | no signal | medium - high: variations due to variable chemical compositions | | | no signal | - | - | - |

**Tab. 22. Cloncurry District HyMap interpretation sheet (excerpt).**

***5. Recommended HyMap and ASTER products for selected deposit types occurring in the Mount Isa Inlier***

Based on Roger Mustards database from the I2/3 report (Mustard et al., 2005: Cu-Au ± Iron-oxide deposits in the Mount Isa Inlier - training data set) the alteration styles of 93 deposits from the Mount Isa Inlier were compared, to compile a list of applicable HyMap and ASTER products for these deposits (Tab. 23). The general deposit models comprise hydrothermal and mesothermal vein, pipe and stockwork mineralisation, breccia hosted deposits and sediment hosted deposits, which were subdivided into detailed deposit models (Mustard et al., 2005). Suggestions for applicable HyMap and/or ASTER products were subdivided according to 1) type of alteration and mineral deposit form, 2) mineral deposit expression and 3) host rocks.

| Suggested HyMap and ASTER products for selected deposit types occurring in the Mount Isa Inlier (database includes about 93 deposits, based on R. Mustards database) | | | | | | |
|---|---|---|---|---|---|---|
| General Deposit Model | Detailed deposit model | type of alteration, mineral deposit form | | mineral deposit expression | host rocks | |
| | | suggested HyMap product | suggested ASTER product | suggested ASTER product | suggested HyMap products | suggested ASTER product |
| HYDROTHERMAL VEINS/PIPE/ STOCKWORK | PROTEROZOIC STRUCTURALLY-CONTROLLED COPPER-GOLD | **Ferrous iron and MgOH, MgOH content, MgOH composition, white mica content, white mica composition, white mica crystallinity, Al smectite content, Al smectite composition, kaolin content**, amphibole vs chlorite, opaques, ferric oxide content, hematite-goethite ratio | Ferrous iron abundance, **AlOH group abundance, AlOH group composition, ferrous iron abundance with MgOH**, MgOH abundance, MgOH composition, opaques group, ferric oxide abundance | **ferric oxide abundance, opaques group**, MgOH abundance, MgOH composition, | **Ferrous iron and MgOH, MgOH composition**, amphibole vs chlorite, epidote content, **white mica abundance, white mica composition,** opaques, ferric oxide content, hematite-goethite ratio | **ferrous iron abundance with MgOH group, MgOH group abundance, MgOH group composition, AlOH group abundance, AlOH group composition**, opaques group |
| HYDROTHERMAL VEINS/PIPE/ STOCKWORK | SHEAR ZONE-HOSTED HYDROTHERMAL | Al smectite content, Al smectite composition, kaolin content, MgOH content, MgOH composition, white mica content, white mica composition, white mica crystallinity, amphibole vs chlorite, Ferrous iron and MgOH, ferric oxide content, hematite-goethite ratio, opaques | advanced argillic group, AlOH group abundance, AlOH group composition, MgOH abundance, MgOH composition, ferrous iron abundance with MgOH, ferric oxide abundance, opaques group | **ferric oxide abundance, opaques group, CSIRO regolith ratios** | **Ferrous iron and MgOH, MgOH compositio**n, amphibole vs chlorite, epidote content, opaques, **white mica abundance, white mica composition** | **ferrous iron abundance with MgOH group, MgOH group abundance, MgOH group composition**, opaques group, **AlOH group abundance, AlOH group composition**, ferric iron abundance |
| HYDROTHERMAL VEINS/PIPE/ STOCKWORK | IRON-OXIDE CU-AU-U-REE | amphibole vs chlorite, **Ferrous iron and MgOH**, epidote content, **MgOH composition, opaques, ferric oxide and MgOH**, ferric oxide content, hematite-goethite ratio, **Al smectite content, Al smectite composition, kaolin content** | **ferrous iron abundance with MgOH, MgOH composition**, opaques group, ferrous iron abundance, **ferric iron abundance with MgOH**, ferric oxide abundance, **advanced argillic group, AlOH group abundance, AlOH group composition** | **CSIRO regolith ratios, ferric oxide abundance, opaques group** | **Ferrous iron and MgOH, MgOH composition**, amphibole vs chlorite, **white mica abundance, white mica composition**, opaques, epidote content | **AlOH group abundance, AlOH group composition, ferrous iron abundance with MgOH group**, opaques group, ferric iron content, **MgOH group abundance, MgOH group composition** |
| HYDROTHERMAL VEINS/PIPE/ STOCKWORK | CU+/-AG QUARTZ VEINS | lack info | lack info | lack info | **Ferrous iron and MgOH**, amphibole vs chlorite, **white mica abundance, white mica composition** | **ferrous iron abundance with MgOH group, AlOH group abundance, AlOH group composition** |
| HYDROTHERMAL VEINS/PIPE/ STOCKWORK | ROCK SILICA | n.c. | n.c. | n.c. | n.c. | n.c. |
| MESOTHERMAL VEINS/PIPE/ STOCKWORK | MESOTHERMAL VEINS METAMORPHIC-RELATED (SLATE BELT VEINS) | n.c. | lack info | lack info | n.c. | **AlOH group abundance, AlOH group composition, ferrous iron abundance with MgOH group** |
| BRECCIA HOSTED | BRECCIATED SEDIMENT-HOSTED COPPER | white mica content, white mica composition, white mica crystallinity, ferric oxide content, hematite-goethite ratio, opaques | **AlOH group abundance, AlOH group composition**, ferric oxide abundance, opaques group | **ferric oxide abundance, opaques group** | **Ferrous iron and MgOH, MgOH composition**, amphibole vs chlorite, **white mica abundance, white mica composition**, opaques | **ferrous iron abundance with MgOH group, MgOH group abundance, MgOH group composition, AlOH group abundance, AlOH group composition** |
| SEDIMENT-HOSTED DEPOSIT | SEDIMENT-HOSTED PB-ZN (BROKEN HILL TYPE) | n.c. | **MgOH abundance, MgOH composition**, ferrous iron abundance | **CSIRO regolith ratios** | n.c. | **ferrous iron abundance with MgOH group, AlOH group abundance, AlOH group composition**, opaques group |

**Tab. 23. Recommended HyMap and ASTER products for selected deposit types occurring in the Mount Isa Inlier. In bold are more important/applicable products for the respective type of deposit. n.n. - not covered; lack info - lack of information.**

## *6. Conclusion*

The workflow in Fig. 28 shows, how the multi- and hyperspectral data, derived from ASTER and HyMap imaging, have been used for this report and related studies. The product descriptions are very important and of great value for first-time users of the spectral images. They can be downloaded from the CSIRO webpage (www.em.csiro.au/NGMM). ASTER and HyMap data can only be used with a good knowledge of the regional geology of the examined area. Some of the spectral images (e.g. Amphibole & Chlorite mineralogy) are based on algorithms including wavelength absorption features, which are interfered by clouds or vegetation or can be related to more than one mineral species in the investigated material. The related high threshold results in unfeasible spectral images. Further restrictions of the remote sensing spectral techniques comprise wrong interpretations of the spectral images, caused by manmade features (e.g. mining activities) and vegetation. However, multi- and hyperspectral data can be a powerful tool for exploration, based on their numerous applications, such as the identification of various mineral assemblages, complementing geological maps and the detection of various alteration patterns.

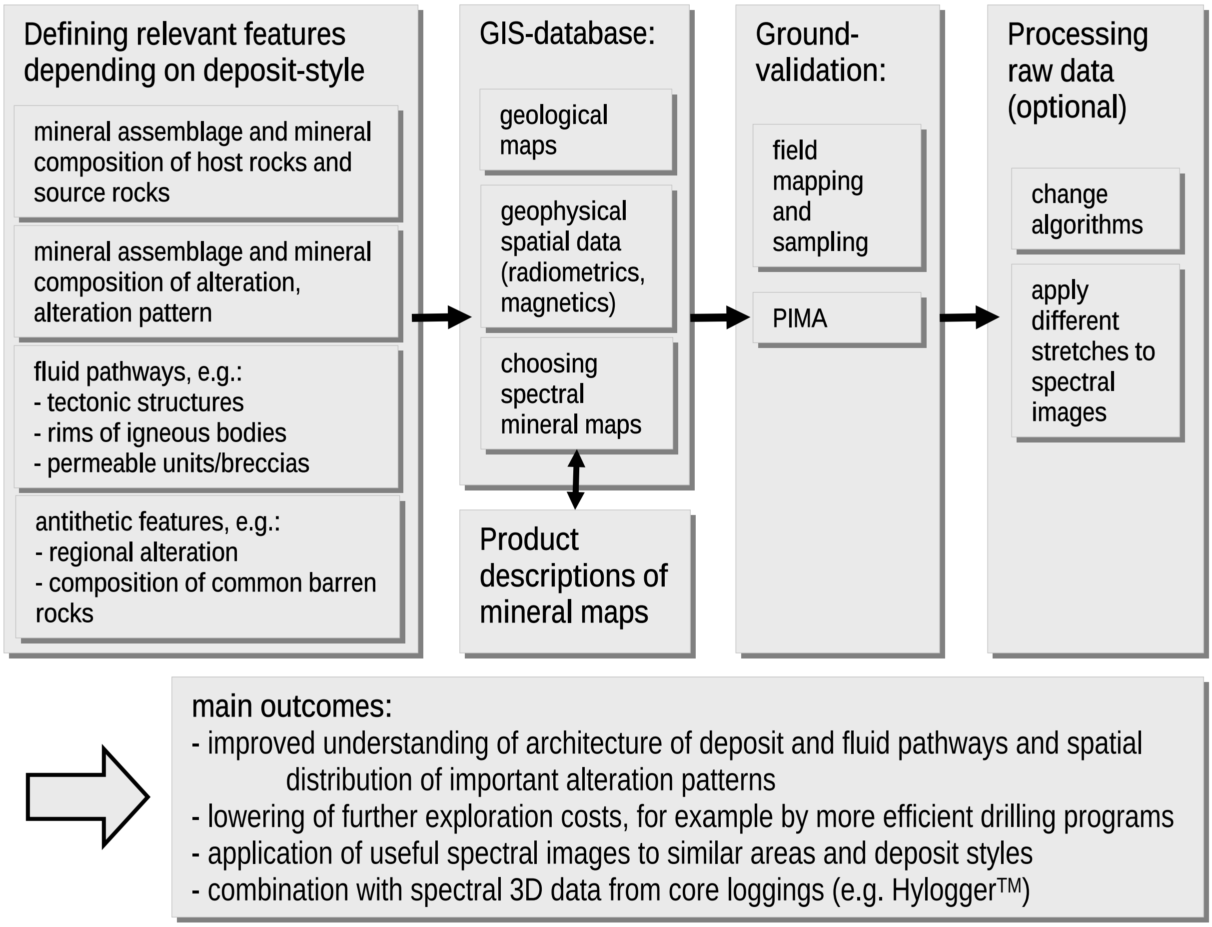


**Fig. 28. Workflow showing the application of multi- and hyperspectral images in combination with other geophysical spatial data and achievable outcomes.**

## *7. References:*

Beardsmore, T.J. (1992): Petrogenesis of Mount Dore-style Breccia-hosted Copper ± Gold mineralization in the Kuridala-Selwyn region of northwestern Queensland.- Unpublished Ph.D. thesis, Townsville, James Cook University of North Queensland.

Belousova, E.A., Walters, S., Griffin, W.L., O'Reilly, S.Y. (2001): Trace-element signatures of apatites in granitoids from the Mt Isa Inlier, northwestern Queensland.- Australian Journal of Earth Sciences, 48, 603-619.

Bertelli, M. (2007): Application of fluid inclusion microanalytical techniques to reduced IOCG deposits of the Cloncurry district - Unpublished Ph.D. thesis, Townsville, James Cook University of North Queensland, 302 pp.

Blake, D.H. (1987): Geology of the Mount Isa Inlier and environs, Queensland and Northern Territory.- Bureau of Mineral Resources Bulletin, 255.

Cudahy T.J., Caccetta, M., Cornelius, A., Hewson, R.D., Wells, M., Skwarnecki, M., Halley, S., Hausknecht, P., Mason, P. and Quigley, M.A., 2005. Regolith geology and alteration mineral maps from new generation airborne and satellite remote sensing technologies and Explanatory Notes for the Kalgoorlie-Kanowna 1:100,000 scale map sheet, remote sensing mineral maps. MERIWA Report No. 252, 114 pages.

De Jong, G., 1995, Post metamorphic alteration and mineralization in a highly deformed Proterozoic terrain; the eastern Selwyn Range, Cloncurry district, NW Queensland.- Unpublished Ph.D. thesis, Townsville, James Cook University of North Queensland, 302 p.

DeJong, G. & Williams, P.J. (1995): Giant metasomatic system formed during exhumation of mid-crustal Proterozoic rocks in the vicinity of the Cloncurry Fault, northwest Queensland.- Australian Journal of Earth Sciences, 42 281-290.

Gauthier, L., Hall, G., Stein, H.J., Schaltegger, U. (2001): The Osborne Deposit, Cloncurry District; a 1595 Ma Cu-Au skarn deposit..- Contributions of the Economic Geology Research Unit, 59, 58-59.

Hingst, R.J. (2002): Geology and geochemistry of the Cloncurry Fault, North-west Queensland, Australia.- Unpublished Bsc-honours thesis, Townsville, James Cook University of North Queensland, 57 pp.

King, P.L., Ramsey, M.S, Swayze, G.A. (2004): Infrared spectroscopy in geochemistry, exploration geochemistry, and remote sensing.- Mineralogical Association of Canada, Short Course Series Vol. 33, 284pp.

Kretz, R. (1983): Symbols for rock-forming minerals.- American Mineralogist, 68, 277-279.

Laukamp, C. (2007a): Recognition of hydrothermal footprints in the Eastern Fold Belt of the Mount Isa Inlier using geophysical-geochemical spatial data.- F6 quarterly report July-September, pmd*CRC, 4pp.

Laukamp, C. (2007b): Recognition of hydrothermal footprints in the Eastern Fold Belt of the Mount Isa Inlier using geophysical-geochemical spatial data.- EGRU Newsletter, Dec 2007, p. 20-22.

Laukamp, C. (2008): Report on the validation of spectral techniques for exploration in the Mount Isa terrane.- Enabling technology Final Report, Chapter 2.2.8, 5pp.

Laukamp, C., Cudahy, T., Thomas, M., Jones, M., Cleverley, J.S., Oliver, N.H.S. (2008a): Recognition of hydrothermal footprints in the Eastern Fold Belt of the Mount Isa Inlier using geophysical-geochemical spatial data. I7 final report, 18 pp.

Laukamp, C., Cudahy, T., Oliver, N.H.S., Cleverley, J.S. (2008): Detection of K-alteration in the Cloncurry District, NW Queensland, using Hyperspectral Mineral Maps.- AESC 2008, Perth, Australia, Program & Abstract Booklet, p.159-160.

Mark, G. (1999): Petrogenesis of Mesoproterozoic K-rich granitoids, southern Mt Angelay igneous complex, Cloncurry district, northwest Queensland.- Australian Journal of Earth Sciences, 46, 933-949.

Mark, G. & Foster, D.R.W. (2000): Magmatic–hydrothermal albite–actinolite–apatite-rich rocks from the Cloncurry district, NW Queensland, Australia.- Lithos, 51, 223-245.

Mark, G., Pollard, P.J., Foster, D.R.W., McNaughton, N., Mustard, R., (2005): Episodic syn-tectonic magmatism in the Eastern Succession, Mount Isa Block, Australia: implications for the origin, derivation and tectonic setting of potassic ‘A-type’ magmas. In: Blenkinsop, T.G. (Ed.), Final Report, Total Systems Analysis of the Mt Isa Eastern Succession, Predictive Mineral Discovery CRC, pp. 51–74.

Mustard, R., Blenkinsop, T., Foster, D.R.W., Mark, G., McKeagney, C., Huddelstone-Holmes, C., Partington, G., Higham, M. (2005): Critical ingredients in Cu-Au ± iron oxide deposits, NW Queensland: An evaluation of our current understanding using GIS spatial data modelling.- pmd*CRC I2+3 final report, 291-324.

Oliver, N.H.S., Rubenach, M.J., Fu, B., Baker, T., Blenkinsop, T.G., Cleverley, J.S., Marshall, L.J., Ridd, P.J. (2006): Granite-related overpressure and volatile release in the mid crust: fluidized breccias from the Cloncurry District, Australia. Geofluids, 6, 1-13.

Rubenach, M.J., Foster, D.R.W., Evins, P.M., Blake, K.L., Fanning, C.M. (2008): Age constraints on the tectonothermal evolution of the Selwyn Zone, Eastern Fold Belt, Mount Isa Inlier.- Precambrian Research, 163, 81-107.

Thomas, M. (2008): ASTER – HyMap Hyperspectral calibration report.- pmd*CRC I7 final report, 9pp.

Thomas, M., Laukamp, C., Cudahy, T., Jones, M. (2008): Flowpaths and Drivers: New spectral methods and products for resource and surface materials mapping in Queensland, Australia - methods and applications for industry.- In: Korsch, R.J. & Barnicoat, A.C. (eds.): New Perspectives: The foundations and future of Australian exploration, abstracts for the June pmd*CRC conference, Perth, Australia, p.99-105.

# *8. Appendix*

## *8.1 Spatial remote sensing product descriptions*

### *8.1.1 HyMap*

F6_final_report_disc1\Mount Isa Project Stage 1 HyMap Geoscience Product Descriptions.doc

### *8.1.2 ASTER*

F6_final_report_disc1\Mount Isa Project Stage 1 ASTER Geoscience Product Descriptions.doc

### *8.1.3 MapInfo workspace*

The MapInfo workspace contains:

- mineral occurrences in the Mount Isa Inlier
- GPS-data of sample points
- frames indicating field areas of publications, Bsc, Msc and PhD theses
- frames indicating the field areas
- HyMap swaths of the 2006 campaign
- layers of a preliminary geological map of the Camel Hill/Cloncurry Fault area (Fig. 26)
- combined digital geological map (from I7-project)
- tiles of geological maps covering the Mount Isa Inlier

F6_final_report_disc1\MapInfo_data\ efb_HyMap_database8.WOR

## *8.2 sample collection*

- sample list: F6_final_report_disc1*sample list.xls*
- gps-points: F6_final_report_disc1\F6_all_gps.xls

## *8.3 picture database*

### *8.3.1 field*

F6_final_report_disc2\pictures\field
For numbers of field images refer to sample list.

### *8.3.2 samples*

F6_final_report_disc1\pictures\samples
Sample images are named according to samples.

### *8.3.3 thin sections*

F6_final_report_disc1\pictures\thin sections
Thin section images are named according to samples.

### *8.4 PIMA database*

All original PIMA spectra can be found under: F6 final report > PIMA > all PIMA
The .tsg-files of figures showing reflectance spectra derived from PIMA can be found under: F6_final_report_disc1\PIMA

### *8.5 Original XRD/XRF results*

Samples analyses with semi-quantitative XRF and qualitative XRD are listed in Fig. 29. The original data (.pdf, .raw) are under: F6_final_report_disc1\XRD\"batch nr". XRD spectra interpreted by C. Laukamp are under: F6_final_report_disc1\XRD\"batch nr"\XRD cl int.

| sample nr. | area | batch | xrd | sample nr. | area | batch | xrd |
|---|---|---|---|---|---|---|---|
| 124S1 | Tool Creek | 8899 | | 204S1 | Mount Angelay | 8898 | |
| 125S1 | Tool Creek | 8899 | | 215S1 | Mount Angelay | 8898 | x |
| 128S1b | Tool Creek | 8899 | x | 255S1 | Suicide Ridge | 8899 | |
| 128S1c | Tool Creek | 8899 | | 255S2 | Suicide Ridge | 8899 | x |
| 128S2d | Tool Creek | 8899 | | 255S3 | Suicide Ridge | 8899 | x |
| 128S2b | Tool Creek | 8899 | | 256S1 | Suicide Ridge | 8899 | |
| 130S1a | Tool Creek | 8899 | | 256S2 | Suicide Ridge | 8899 | |
| 130S1b | Tool Creek | 8899 | x | 262S1 | Suicide Ridge | 8899 | |
| 132S1 | Tool Creek | 8899 | | 263S1 | Suicide Ridge | 8899 | x |
| 132S2a | Tool Creek | 8899 | | 263S2b | Suicide Ridge | 8899 | x |
| 133S1 | Tool Creek | 8899 | x | 263S2c | Suicide Ridge | 8899 | |
| 133S2 | Tool Creek | 8899 | x | 263S3a | Suicide Ridge | 8899 | |
| 141S1 | Tool Creek | 8899 | x | 263S3b | Suicide Ridge | 8899 | |
| 150S1 | Snake Creek | 8898 | | 265S1 | Suicide Ridge | 8899 | x |
| 150S2 | Snake Creek | 8898 | x | 265S2 | Suicide Ridge | 8899 | |
| 150S3 | Snake Creek | 8898 | | 266S1 | Suicide Ridge | 8899 | x |
| 150S4 | Snake Creek | 8898 | | 267S1 | Suicide Ridge | 8899 | |
| 150S5 | Snake Creek | 8898 | | 269S1a | Suicide Ridge | 8899 | |
| 150S6 | Snake Creek | 8898 | x | 269S1b | Suicide Ridge | 8899 | |
| 150S7 | Snake Creek | 8898 | | 274S1 | Suicide Ridge | 8899 | x |
| 151S1 | Snake Creek | 8898 | | 371P1 | Camel Hill | 9039 | x |
| 152S1 | Snake Creek | 8898 | | 371P2 | Camel Hill | 9039 | x |
| 152S2 | Snake Creek | 8898 | x | 387P1 | Camel Hill | 9039 | |
| 155S1 | Snake Creek | 8898 | | 387P2 | Camel Hill | 9039 | |
| 157S1 | Snake Creek | 8898 | | 388P1 | Camel Hill | 9039 | x |
| 162S1a | Snake Creek | 8898 | x | 390P1 | Camel Hill | 9039 | x |
| 162S1c | Snake Creek | 8898 | | 394P1 | Camel Hill | 9039 | |
| 163S1 | Snake Creek | 8898 | x | 409P1 | Camel Hill | 9039 | |
| 164S1a | Snake Creek | 8898 | | 419P2 | Camel Hill | 9039 | x |
| 164S1b | Snake Creek | 8898 | | 420P1 | Camel Hill | 9039 | x |
| 164S2 | Snake Creek | 8898 | | 425P1 | Camel Hill | 9039 | x |
| 164S3 | Snake Creek | 8898 | x | 459P1 | Mallee Gap | 9134 | |
| 196S1 | Mount Angelay | 8898 | x | 466P1 | Mallee Gap | 9134 | |
| 196S2a | Mount Angelay | 8898 | x | 472P1 | Mallee Gap | 9134 | |
| 196S2c | Mount Angelay | 8898 | | 473P1 | Mallee Gap | 9134 | |
| 197S1 | Mount Angelay | 8898 | | 478P1 | Mallee Gap | 9134 | |
| 200S1 | Mount Angelay | 8898 | | 482P1 | Mallee Gap | 9134 | |
| 201S1a | Mount Angelay | 8898 | | 482P2 | Mallee Gap | 9134 | |
| 201S1b | Mount Angelay | 8898 | | 483P1 | Mallee Gap | 9134 | |

**Fig. 29. Samples analysed with semi-quantitative XRF and qualitative XRD.**

### *8.6 thin sections*

F6_final_report_disc1\thin section list.xls

### *8.7 Cloncurry District HyMap interpretation sheet*

F6_final_report_disc1\cloncurry district datasheet1.pdf
F6_final_report_disc1\cloncurry district datasheet2.pdf

### *8.8 List of publications and workshops related to the F6 HyMap project*

<u>F6/I7 reports:</u>

Laukamp, C. (2007a): Recognition of hydrothermal footprints in the Eastern Fold Belt of the Mount Isa Inlier using geophysical-geochemical spatial data.- F6 quarterly report July-September, pmd*CRC, 4pp.

Laukamp, C. (2008): Report on the validation of spectral techniques for exploration in the Mount Isa terrane.- Enabling technology Final Report, Chapter 2.2.8, 5pp.

Laukamp, C., Cudahy, T., Thomas, M., Jones, M., Cleverley, J.S., Oliver, N.H.S. (2008a): Recognition of hydrothermal footprints in the Eastern Fold Belt of the Mount Isa Inlier using geophysical-geochemical spatial data. I7 final report, 18 pp.

Thomas, M. (2008): ASTER – HyMap Hyperspectral calibration report. pmd*CRC I7 final report, 9pp.

<u>Publications (peer-reviewed):</u>

Laukamp, C. (2007): Recognition of Hydrothermal Footprints in the Eastern Fold Belt of the Mount Isa Inlier Using Geophysical-Geochemical Spatial Data.- EGRU Newsletter, Dec 2007, p. 20-22.

<u>Abstracts for Conference Presentations:</u>

Thomas, M., Laukamp, C., Cudahy, T., Jones, M. (2008): Flowpaths and Drivers: New spectral methods and products for resource and surface materials mapping in Queensland, Australia - methods and applications for industry.- In: Korsch, R.J. & Barnicoat, A.C. (eds.): New Perspectives: The foundations and future of Australian exploration, abstracts for the June pmd*CRC conference, Perth, Australia, p.99-105

Laukamp, C., Cudahy, T., Oliver, N.H.S., Cleverley, J.S. (2008): Detection of K-alteration in the Cloncurry District, NW Queensland, using Hyperspectral Mineral Maps.- AESC 2008, Perth, Australia, Program & Abstract Booklet, p.159-160.

Cudahy, T., Jones, M., Thomas, M., Laukamp, C., Caccetta, P., Caccetta, M., Hewson, R., Verrall, M., Rodger, A. (2008): Next Generation Mineral Mapping in Queensland: Another piece to the precompetitive geoscience data puzzle.- AESC 2008, Perth, Australia, Program & Abstract Booklet, p.74.

Jones, M., Cudahy, T., Thomas, M., Laukamp, C., Hewson, R. (2008): Get closer to the Truth ... with Hyperspectral Mineral
Maps from Queensland.- AESC 2008, Perth, Australia, Program & Abstract Booklet, p.149.

Thomas, M., Laukamp, C., Cudahy, T., Jones, M. (2008): Exploration advances: New developments in spectral remote sensing in the Mount Isa region, Australia.- IGC Oslo, 6th-14th August 2008.

<u>Hyperspectral workshops:</u>

- Digging Deeper, Brisbane, Nov 2007
- Digging Deeper, Townsville, Nov 2007
- AESC, Perth, Jul 2008

*8.9 Figure captions:*

*8.10 Table captions:*